THERMAL DEGRADATION REACTIVITY OF CELLULOSE AND HEMICELLULOSE IN JAPANESE CEDAR AND JAPANESE BEECH WOOD CELL WALLS

JIAWEI WANG

Contents

List of Figures and Tables

Chapter 1

Introduction

1.1 Biomass as renewable energy

The large growth of the economy made a great development of human society. The global economic growth is around 3.0 percent in 2019 according to the forecast (IMF, 2019). However, beneath the large development of the world economy is much more energy consumption and demands. The global energy consumption in 2018 increased nearly twice the average of growth since 2010 (International Energy Agency (IEA), 2019). In most countries, large development is based on the extensive utilization of fossil fuels. As nonrenewable energy, the main forms of fossil fuels of petroleum, natural gas and coal were estimated to be finished in 52.5, 54.1 and 110 years, respectively, in 2014 (Kamel & Hamed, 1975). The contradiction between the energy shortage and the energy demands for development will be the normal state of the world economy last for decades in the future.

On the other hand, emissions produced from the utilization of fossil fuels are becoming more serious in recent years. CO_2, which is the major emission from fossil fuels, was reported to rise by 1.7% to 33 gigatonnes in 2018 (International Energy Agency (IEA), 2019). CO_2 emissions is the major greenhouse gases that generally exhausted into the air directly. This CO_2 emissions will increase its concentration in the atmosphere and further increase the heat that emit from atmosphere to the surface of earth. Then, the increased temperature will break the balance of the climate on the earth. For example, it makes the glaciers of the Antarctic and Arctic melt and increase the sea levels of the world. Above all, NO_x emissions are another kind of major product mainly produced by the engines. NO_x includes the released gas of NO and NO_2, which can lead to the formation of smog and fine particles (PM) being regarded as the major environmental problems produced from the transportation.

Besides the fuel production, the petroleum is one of the important sources for producing chemicals relating to the daily life. The petrochemicals mainly includes olefins and aromatic compounds. Ethylene, propylene and butadiene are the typical unsaturated aliphatic hydrocarbons produced by the fluid catalytic cracking of petroleum fractions. The aromatics are produced by the catalytic reforming such as benzene, toluene and xylenen. Moreover, other kinds of fossil energy is also used to producing chemicals. For example, methanol, as an organic solvent is produced from natural gas with steam in the industrial level. These chemicals construct our daily life since they can be further produced to plastic products, synthetic rubber and even the clothing items. The petrochemical industry meets the similar problems as the energy production such as the limited amount of the sources and environmental problems caused during the production and disposal.

To fix the above problems, researchers are looking for the alternatives to fossil energy. Renewable energy attracted much attention in recent years since it is friendly to the environment and its potentials. There are various kinds of renewable energies such as solar energy, geothermal heat energy and nuclear energy. Among them, biomass energy provides several advantages. It is carbon neutral since all of the energy is from the sun and the natures, so it does not produce extra CO_2 during the utilization. The amount of the biomass is quite large, around 550 gigatonnes of carbon exists on the earth, which has the potential to meet the demands as the petroleum industry. Moreover, it is composed of basic elements with C, H and O forming complex organisms that can produce chemicals as the petrochemical industry. Within the biomass, nearly 70% is included in the plants known as woody biomass (Bar-On, Phillips, & Milo, 2018). Even though it also has some disadvantages such as low heating values and its heterogeneous characteristic, which makes it difficult to handle. However, as the more attentions and developing technologies, these advantages could be fixed.

The utilization of biomass is associated with the development of human society. The woody biomass was used for combustion and construction in human society in the ancient time. However, as new technology develops, it should be used more efficiently in the modern world. By coping with new technologies, the energy and substance including in the biomass could be utilized as much as possible. The utilization of woody biomass

could be classified into two parts, the first is thermal conversion process that treats biomass with heat and the other is biochemical conversion that treats biomass with microorganism (United Nations Development Programme, 2000). Thermal process is one of the efficient ways to utilize the biomass. For example, gasification can produce flammable gas such as H_2, CH_4 and CO and further obtain energy by gas engine or turbine for power generation (Aznar, Corella, Delgado, & Lahoz, 1993; Puig-Arnavat, Bruno, & Coronas, 2010; Ruiz, Juárez, Morales, Muñoz, & Mendívil, 2013). The biochemical conversion includes fermentation and digestion, which produces biogas and ethanol.

However, the level for utilization of biomass is not high and balanced in the world. Approximately 10% of the global energy supply was covered by the biomass (Schill, 2013). In the developing countries, most of the biomass is utilized for cooking and heating by burning directly, which is considered as a low efficiency for utilizing the biomass. On the other hand, in developed countries, the fossil energy is much more convenient compared with biomass energy. This kind of problem is mainly caused by underdeveloped technologies for conversing biomass energy. Among them, the most important reasons is the wood is a complex structure and composed of several kinds component, the interactions among the content and the variation depend only on species and origin make it even harder to use biomass easily. Therefore, it is necessary to understand the details of the biomass itself and prompts the utilization of technology.

1.2 Major components from wood cell wall

Softwood and hardwood are the two major types of woody biomass. Softwood is generally used for construction and paper pulp. It is also known as gymnosperm trees or the wood of conifers. Typical softwood includes Douglas-fir, pinewood, spruce wood and cedar. On the other hand, hardwood is the wood from dicot trees or known as angiosperm trees. Hardwood usually has broad leaves grow in the tropical forests. Zelkova, walnut, ash, birch and beech are the common hardwood (Bond, Brian; Hamner, 2002). Both hardwood and softwood structure are composed of wood cells. The most important wood

cells are longitudinal tracheids and libriform fibres in softwood and hardwood, respectively.

The wood cells are composed several layers that are fabricated at different periods during the cell differentiation as shown in Fig. 1-1 (Plomion, Leprovost, & Stokes, 2001). Middle lamella is between wood cells to ensure the adhesion of the cells. Primary cell wall is a thin layer that mainly composed of pectin and a small amount of lignin and hemicellulose named as xyloglucan. When the cell grows to its definitive size, the most important layer of secondary cell wall is formed. The secondary cell wall is thick and can be divided into 3 layers, S1, S2, and S3. Among them, S2 layer is the thickest layer, which is composed of the most cellulose, hemicellulose and lignin. Among the three components, the composition of cellulose only varied slightly between hardwood and softwood. However, the hemicellulose and lignin have a significant difference in hardwood and softwood.

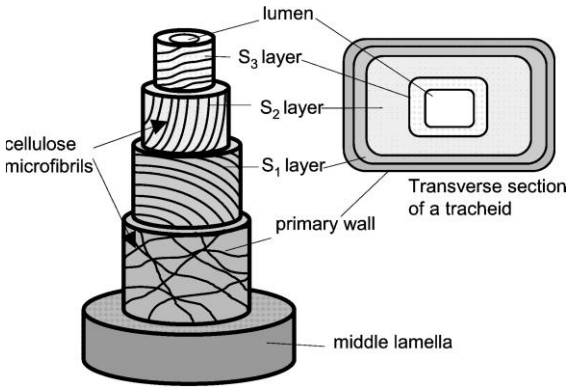

Fig. 1-1 Structure of primary and secondary wood cell walls divided into several layers

1.2.1 Contents in the primary cell wall

Primary cell walls are formed during the growth and typically are relatively thin, highly hydrated structures. The primary cell walls are comprised of 15-40% cellulose, 30-50% pectic polysaccharides and 20-30% xyloglucans, which were classified as cellulose, pectin and hemicellulose, respectively (Cosgrove & Jarvis, 2012). However, as

mentioned previously (Fig. 1-1), the primary wood cell wall much thinner than the secondary cell wall. In the present study, only major parts of pectin was discussed.

1.2.1.1 Pectin

Pectin is the major components from the primary cell wall. It is composed numerous kinds of monomers forming randomly. Generally, the pectin is formed by galacturonic acid-rich polysaccharides including homogalacturonan (HG), rhamnogalacturonan I (RG-I), and the substituted galacturonans rhamogalacturonan (RG-II). Among them, HG is a linear chain of 1, 4- linked α-D-galactopyranosyluronic acid groups. RG-I is composed of a backbone of repeating disaccharide of [-α-D-galactopyranosyluronic acid-1, 2- α-L-Rhamnose-1-4-]$_n$. The RG-II is the most complex pectin structure, which is composed of the HG backbone with several kinds of side chains. Besides, there are other substituted galacturonans know as xylogalacturonan (XGA) and apiogalacturonan (AP) whose amount was related to the parts of the wood. The pectin structure was easily methyl esterified of acetylated. Generally, it is believed that pectic polysaccharides covalently crosslinked the digestion by pectin-degrading enzymes are requires to isolate pectin monomers from each other and from cell walls, which showed in Fig. 1-2 (Mohnen, 2008; Ridley, O'Neill, & Mohnen, 2001).

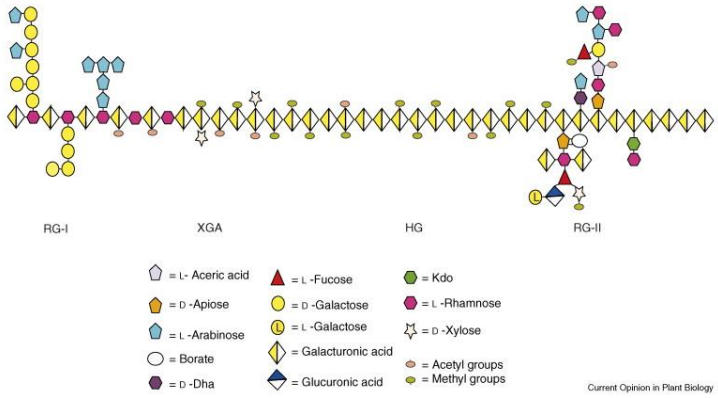

Fig. 1-2 Schematic structure of pectin

1.2.2 Contents in the secondary cell wall

As the wood cell wall grew up, a new layer is formed inside the primary cell wall, which is the most important layer of the cell in terms of mechanical strength. Most of the lignin, cellulose and hemicellulose from the wood were included in secondary wood cell wall. However, the contents and composition of them are different depending on the wood species, which will be described in detail in the later parts.

1.2.2.1 Cellulose

Cellulose is the most abundant organic compound comprises 40 to 50 wt% of the wood (Moon, Martini, Nairn, Simonsen, & Youngblood, 2011; Siró & Plackett, 2010). It is mainly composed of D-glucose linked together through an oxygen covalently bonded to C1 to one of glucose ring and C4 of the adjoining ring known as β-1, 4 glucosidic bonds as shown in Fig. 1-3. Moreover, the hydrogen bonds between hydroxyl groups and oxygens of the adjoining ring molecules make the linkage stable and results into the linear structure of the cellulose chain consisting of several hundreds to over thousands of linked glucose units. The interaction of hydrogen bonds between hydroxyl groups and oxygen connect the adjacent cellulose chains forming as large molecular weight microfibrils. Within the cellulose microfibrils regions, there are highly ordered regions and disordered parts, which are named as crystalline area and amorphous structure, respectively (Nishiyama, 2009). Regarding the cellulose crystalline area, it forms highly ordered cellulose with the degree of polymerization is evaluated around 5000 to 15000 (Gralén & Svedberg, 1943), which makes it hardly dissolve in normal organic solvent.

There are several kinds of crystalline cellulose, which are named as cellulose I, II, III (Mukarakate et al., 2016). Among them, cellulose I is the major cellulose crystalline produced by several kinds of organisms such as trees, plants and algae. According to the literature, the cellulose I can be converted to cellulose II or III by the regeneration process (O'Sullivan, 1997). However, the cellulose structure cannot be rearranged in the nature

condition. Moreover, the cellulose is similar in the characteristics of structure and composition for hardwood and softwood.

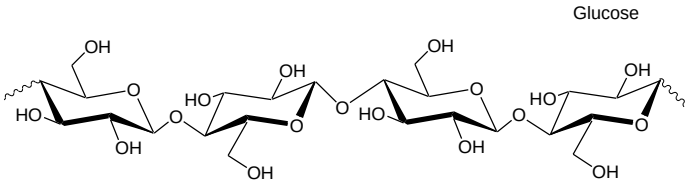

Fig. 1-3 Cellulose structure

1.2.2.2 Hemicellulose

Hemicellulose is a kind of relatively loosen structure compared with cellulose comprises 20-35 wt% of the wood (Alén, Kuoppala, & Oesch, 1996; X. Zhou, Li, Mabon, & Broadbelt, 2017). It can be easily extracted from the wood by the alkali solutions. Compared with cellulose, the degree of polymerization is much lower around 200 with heterogeneous structures that are different depending on the wood species. It is composed of several kinds of monosaccharides, which are D-xylose, D-glucose, D-mannose forming the main hemicellulose such as xylan and glucomannan. Above all, L-arabinose, D-galactose and some uronic acid units such as 4-*O*-methyl-D-glucuronic acid (4-*O*-MeGlcA) along with acetyl groups are typical side chains to form different kinds of hemicellulose (Werner, Pommer, & Broström, 2014).

In hardwood, the total amount of hemicellulose are 23-39 wt% from wood (Pettersen, 1984) including glucuronoxylan (20-35 wt%) and glucomannan are the major and minor hemicelluloses, respectively (Fig. 1-4 and Fig. 1-5). Xylan is composed of xylose chain with side chains of 4-*O*-MeGlcA and acetyl groups attach. The main chain is composed of xylose units linked through β-1, 4 bonds, which are attached at the position 2 of xylose by 4-*O*-MeGlcA and the C2 and/or C3 of the xylose by the acetyl groups. The molar ratios of xylose to glucuronic acid of 25:1, 20:1, 10:1, 6:1 have been reported in the literature (Cavalier et al., 2008; Scheller & Ulvskov, 2010; Shen, Gu, & Bridgwater, 2010a; Jinzhi Zhang, Chen, Wu, & Wu, 2014). On the other hand, as minor hemicellulose in hardwood, glucomannan comprises 3-4 wt%. The glucomannan is composed of D-

glucose and D-mannose linked through β-1, 4 bonds. The molar ratio of mannose: glucose is around 2:1 (Timell, 1967).

On the other hand, in softwood, galactoglucomannan are the major hemicellulose comprising 10-20 % of the wood and xylan are the minor hemicellulose comprising 5-15 % (Pettersen, 1984). Except for the main structure, glucomannan are partly attached by D-galactose through α-1, 6 bonds forming the galactoglucomannan showed in Fig. 1-6. Moreover, the acetyl groups attached to the galactoglucomannan chains at the C2 and C3 in mannose units rather than xylan in the softwood. As minor hemicellulose, arabinoxylan exists in the softwood without the side chains of acetyl groups but substituted by arabinose at C3 as compared with hardwood xylan showed in Fig. 1-7.

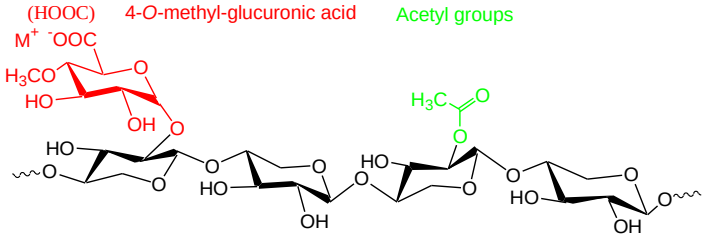

Fig. 1-4 Structure of xylan in hardwood

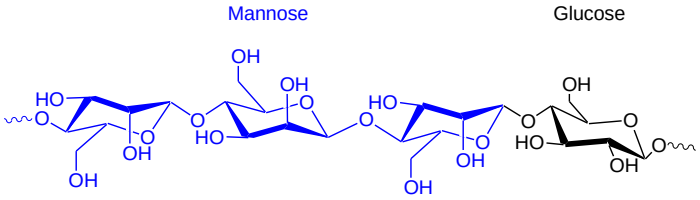

Fig. 1-5 Structure of glucomannan in hardwood

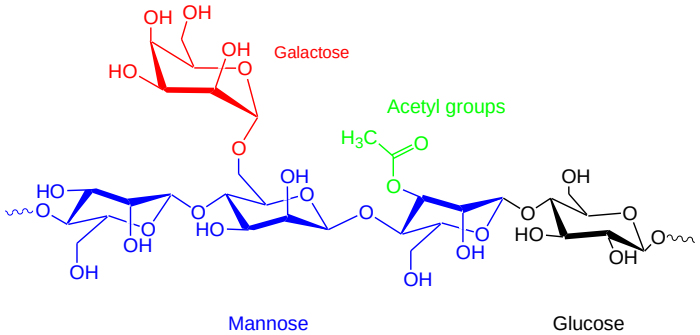

Fig. 1-6 Structure of galactoglucomannan in softwood

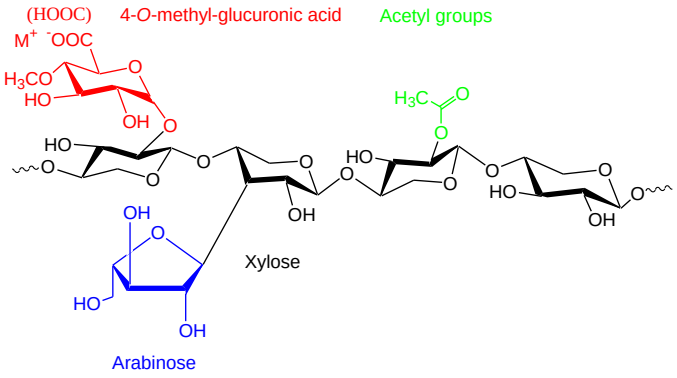

Fig. 1-7 Structure of arabinoxylan in softwood

1.2.2.3 Lignin

Lignin is another kind of polymer which provides the support of mechanical strength to the plant structure. It is regarded as the most abundant aromatic polymer in the nature that is mainly formed by the phenolic structures. There might be three kinds of classes based on the composition and structure composition, which are softwood, hardwood and grass lignin. Among them, the content of lignin is different in hardwood and softwood (19-24% for hardwood and 27-33% in softwood) (Adler, 1977; Pettersen, 1984; Timell, 1967).

Lignin is a kind of heterogeneous polymer that consists of aromatic based moieties by various kinds of various linkages such as C-C (condensed) and C-O-C (ether types) bonds. The β-ether is the most important that involves with most lignin units, which also helps resist the reaction of chemical and biochemical depolymerization (Pandey & Kim, 2011). Lignin are heterogeneous polymers derived from phenylpropanoid monomers, mainly the hydroxycinnamyl alcohols coniferyl alcohol (G-monomer), sinapyl alcohol (S-monomer) and p-coumaryl alcohol (H-monomer) illustrated in Fig. 1-8. These three types of structures of monomers would further form lignin polymers as guaiacyl (G), syringyl (S) and p-hydroxyphenyl (H) units. Softwood mainly comprises of G- and a small number of H-types, while hardwood includes both G- and S- types. Above all, grass lignin contains all of the three types.

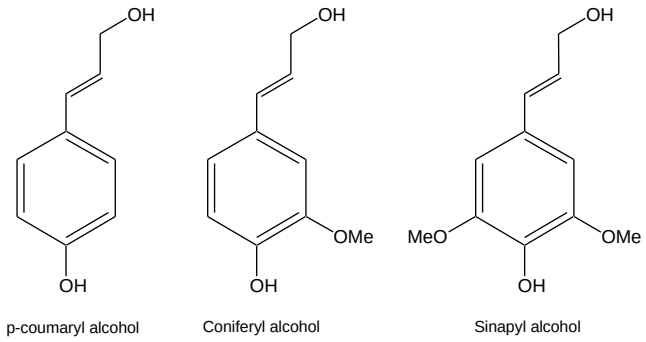

Fig. 1-8 Structure of the lignin monomers

1.2.3 Wood cell wall ultrastructure in the secondary cell walls from softwood and hardwood

The wood cell wall ultrastructure in the secondary cell walls is not fully understood. Generally, it is considered that cellulose microfibrils is covered by the lignin-hemicellulose matrix. However, as the contents of hemicellulose and lignin are different between softwood and hardwood as mentioned before, the wood cell wall ultrastructure might be different.

Terashima et al. proposed a wood cell wall ultrastructure based on Ginko, which is an old type of softwood. In this model, the cellulose microfibrils were covered tightly by glucomannan. Xylan and linin were on the surface of cellulose and glucomannan, which showed in Fig. 1-9 (Terashima et al., 2009). This structure were confirmed by other researchers since they found that cellulose and glucomannan had a strong binding in softwood (Åkerholm & Salmén, 2001; Kumagai & Endo, 2018). However, a recent report showed that xylan bound to cellulose microfibrils by the method of solid state NMR in spruce, which is a softwood (Terrett et al., 2019).

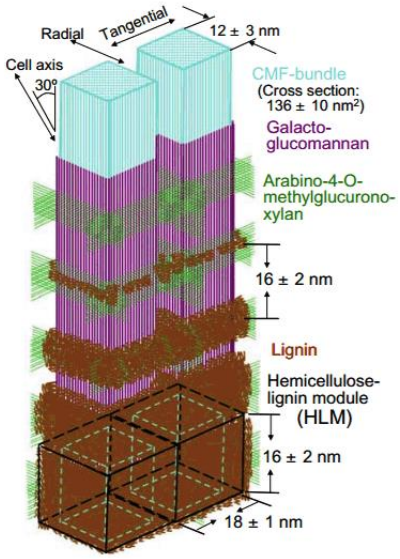

Fig. 1-9 Schematic picture of a model for the arrangement of cellulose, xylan and lignin in the secondary cell walls of softwood

On the contrary, hardwood cell walls exhibited differently comparing with that from softwood. As the major hemicellulose, xylan is reported to bind with cellulose. Dammström reported that xylan and cellulose had a strong association by the dynamic FT-IR analysis on the aspen, which is a hardwood as shown in Fig. 1-10 (Dammström, Salmén, & Gatenholm, 2009). Simmons et al. reported the evidence for xylan binding to cellulose by solid-state NMR that the xylan flattens a three-fold helical screw in solution into a two-fold helicoidal screw to bind to cellulose (Simmons et al., 2016).

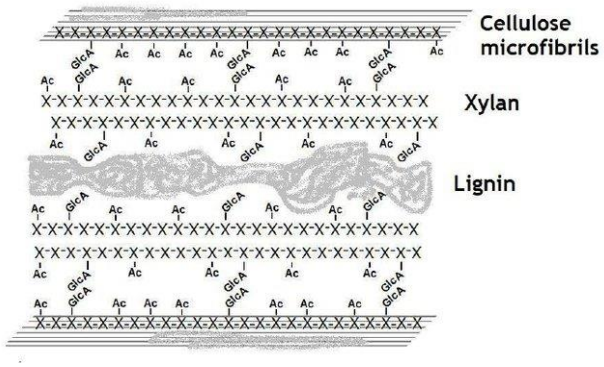

Fig. 1-10 Schematic picture of a model for the arrangement of cellulose, xylan and lignin in the secondary cell walls of hardwood

Besides, the interaction between lignin and carbohydrate known as lignin-carbohydrate complex (LCC) are also reported to commonly exist in the wood cell walls. The LCC linkages known as Cγ-ester with 4-O-MeGlcA, benzyl ether, and phenyl glycoside are reported in softwood and hardwood cell walls (Balakshin, Capanema, Gracz, Chang, & Jameel, 2011; Du et al., 2014; Takahashi & Koshijima, 1988b; Tarasov, Leitch, & Fatehi, 2018; Yuan, Sun, Xu, & Sun, 2011). These different interactions may further affect the thermal degradation behavior in softwood and hardwood.

1.3 Thermal conversion process

Thermal-chemical and bio-chemical processes are the two major process regarding the conversion of biomass into useful product. Bio-chemical process mainly produce liquid fuel by treating the biomass with several kinds of microorganisms, which has a high selectivity but a low reactivity. However, thermal-chemical conversion process has a higher reactivity but a lower selectivity comparing with bio-chemical process. The thermal-chemical conversion process is able to convert the biomass by several kinds of process. Its high reactivity makes thermo-chemical process receive much attention in recent years. Among the conversion processes, pyrolysis is considered as a good way to utilize the biomass by heating under the circumstance in the absence of oxygen and air. The technology of pyrolysis develops a lot since it can not only produce useful organic chemicals but also produce the fuels in solid, liquid and gas phases.

According to the different pyrolysis condition such as heating rate, residence time and pyrolysis temperature, pyrolysis could be divided into fast pyrolysis, slow pyrolysis. The product derived from pyrolysis are different depending on the different pyrolysis conditions, which provides fast and slow pyrolysis with advantages and disadvantages, respectively.

1.3.1 Fast pyrolysis

Fast pyrolysis is conducted by treating the biomass with a high heating rate (larger than 10-200 ℃/s) and short residence time (less than 1s) under relatively lower temperature range. The pyrolysis liquid, which is also called bio-oil is the major product from pyrolysis and its yield is up to 75 wt% (Akhtar & Saidina Amin, 2012). The bio-oil could be further utilized as fuel for the transportation or the electric-production system. However, there are limits for the fast pyrolysis. As the fast pyrolysis needs high heating rate and short residence time, the fast pyrolysis is quite sensitive to the conditions such as temperatures and the size of the particles. Temperature plays a key role in the fast pyrolysis. Generally, the conversion rate of biomass increases as the temperature increases since more energy inputs. At lower temperature that less than 300 ℃, the conversion efficiency is around 0-20% according to the weight loss curves (Fisher, Hajaligol, Waymack, & Kellogg, 2002). The final pyrolysis temperature has a significant effect on the oil and composition of liquid. According to the literatures, 500-550 ℃ range was suitable to obtaining the maximum liquid yield (Akhtar & Saidina Amin, 2012). On the other hand, the particles size also affects the pyrolysis behavior a lot. The small particles usually makes heat transfer easier and enhances the bio-fuel production. However, there is still a contradiction between the particles and the bio-fuel production since the smaller particle needs more energy for the grinding.

1.3.2 Slow pyrolysis

Different with fast pyrolysis, slow pyrolysis is conducted with lower heating rate and longer residence time (from hours to days). It has sufficient time for the heat to access into the samples and complete the pyrolysis reaction, which makes slow pyrolysis accept a large range of the particle size (5-50mm) (Kloss et al., 2012). Slow pyrolysis is also called carbonization and has been utilized for hundreds of years to improve the fertilizer in the soil.

During the slow pyrolysis process, the organic materials evaporate partly at lower temperature. As the temperature increases, several kinds of reaction takes place including dehydration, depolymerization, isomerization, aromatization, decarboxylation and

charring, which produces gaseous product and condensable products (Collard & Blin, 2014; Lange, 2007; Vamvuka, 2011). After slow pyrolysis, most of the carbons exist in the solid phase. In the heat-treated residue, it includes unreacted carbohydrate, condensable product and char. These product could be further utilized into the industry. To efficiently use the product derived from slow pyrolysis, the mechanism of the reaction should be understood.

1.3.3 Primary pyrolysis and secondary pyrolysis in the thermal conversion process

Primary and pyrolysis and secondary reactions of the primary products are the two basic steps for the thermal conversion process. In the primary pyrolysis process, the volatiles and char are produced and these products are further pyrolyzed to produce final products in the secondary reactions in gas, liquid and solid phase.

These two steps are different depending on the thermal process. In gasification process, the secondary reaction of primary-pyrolysis product take place extensively to increase the gaseous product yield. To enhance the secondary reaction of primary tar and char, steam and air are utilized as gasifying agents. This also indicate the importance of the tar and char from primary pyrolysis step since the gas composition could be converted by using some kind of agents such as steam, which promotes the production of H_2.

On the other hand, the secondary reaction prohibits the yield of bio-fuel since it enhance the product of gaseous product from the primary pyrolysis product. The heating time of the volatile products is limited in 2s to avoid much secondary reaction and ensure the as much as the bio-fuel product. Regarding the slow pyrolysis, as the bio-char is the major product, it is necessary to avoid the secondary reactions but enhance the primary steps. However, as there are many unknown factors, slow pyrolysis is an efficient way to understand the inte raction between each kind of component.

1.3.3.1 Cellulose

Among the three kinds of major component in the wood cell wall, cellulose is relatively utilized extensively comparing with the other two polymers due to its homogeneous structure. TG analysis is an efficient way to evaluate the pyrolytic behavior of the wood components. The TG analysis of isolated cellulose and cellulose from wood were investigated by many researchers that the decomposition generally started from 300 ℃ to 400 ℃. In this temperature range, the highest decomposition rate took place between 330 and 370 ℃ (Biswas et al., 2017; Shen, Gu, & Bridgwater, 2010b; Yang, Yan, Chen, Lee, & Zheng, 2007). At lower temperature (<300 ℃), dehydration reactions mainly contributes to the weight loss in the TG curves. The dehydration reactions are also considered as a main factor to the char yield. The intermolecular dehydration result in the formation of extra covalent bonds leading to a higher molecular-weight compounds and promotes the aromatic product that contributes to the char yields.

As the temperature increases, the glycosidic bond becomes quite active and several reactions takes place in the meantime (Wang, Guo, Liang, Zhou, & Luo, 2012). The active glycosidic bonds lead to the depolymerization forming condensable product such as anhydro-oligosaccharides and anhydro-saccharides. Among them, levoglucosan is the dominant product that yields up to 60% (Patwardhan, Dalluge, Shanks, & Brown, 2011; Worasuwannarak, Sonobe, & Tanthapanichakoon, 2007). Besides, other low molecular weight (MW) product can be divided into (1) furan product, such as 5-hydroxymethylfurfural (5-HMF), furfural, furfuryl alcohol, (2) carboxylic acid product, such as formic acid, acetic acid and glycolic acid, (3) gaseous product such as carbon monoxide and carbon dioxide (Alén et al., 1996; T. Hosoya, Kawamoto, & Saka, 2007b).

1.3.3.2 Hemicellulose

As discussed before, hemicelluloses have heterogeneous structures and are only constituted by an amorphous phase (Saha, 2003; Shen, Gu, & Bridgwater, 2010b). Moreover, the side chains including in the hemicellulose makes it different with characteristics of cellulose pyrolysis.

Due to the amount and process of extraction, only a few studies concentrate on the pyrolytic behavior of glucomannan and a large amount of studies on the xylan pyrolysis. Generally, the isolated hemicellulose are regarded as the sample for investigating the pyrolysis. According to the TG/DTG curves, xylan and glucomannan mainly occurs in the temperature range 200-350 ℃ (Lv & Wu, 2012; Peng & Wu, 2010). For the glucomannan, the major pyrolysis behaviors take place around 310 ℃ and forms only one big peak in the DTG curves. However, the xylan shifted slightly to lower temperature forming a peak with another small shoulder forming around 260 ℃. This indicates that the xylan and glucomannan may act differently during the pyrolysis.

At lower temperature (xylan: 150-240 ℃, glucomannan: 150-270 ℃), the dehydration and cleavage of weak linkages takes place. Similar with cellulose, the dehydration reacts within the polysaccharides. At this temperature range, the side chains are not as stable as the main chains for both xylan and glucomannan. For the xylan, methanol is the major product from the fragmentation of the methoxy groups of the 4-*O*-methyl-α-D-glucuronic acid. In the meantime, formic acid is produced due to the function of hexuronic acids. The acetyl groups in both xylan and glucomannan contributes to the production of acetic acid (Lv & Wu, 2012; Peng & Wu, 2010; Z. Wang, Cao, & Wang, 2009).

With temperature increases (xylan: 240-320 ℃, glucomannan: 270-350 ℃), the depolymerization takes place. At this temperature range, the glycosidic linkages between monomer units become quite unstable and leads to the formation of different anhydro-sugars. For the glucomannan, levoglucosan and levomannosan and levogalactosan derives from glucose, mannose and galactose, respectively. These compounds could be further converted to more stable furan related products. Regarding the xylan pyrolysis, furfural is a dominant furan related product, while 4-hydroxy-5,6-dihydro-2H-pyran-2-one (having a molecular mass of 114) is a compound frequently utilized as a marker of xylan pyrolysis (Ohnishi, Kato, & Takagi, 1977; Patwardhan, Satrio, Brown, & Shanks, 2009; Ponder & Richards, 1991).

Moreover, as the xylan includes uronic acid units (mainly 4-*O*-methyl-α-D-glucuronic acid units), the uronic acid units could exist as two forms, which are

substituted by alkali and alkaline metal cations forming metal uronate and the other ones are in the acid phase. Pyrolytic behavior could be influenced by the different kinds of units. Generally, after the demineralization process, it enhances char yield of xylan and glucomannan (T. Hosoya et al., 2007b). And the metal cations may also work as base catalyst to affect the product and the thermal behaviors.

1.3.3.3 Lignin

Pyrolysis of lignin occurs in a wider temperature range than the cellulose and hemicellulose from 200 ℃ to 600 ℃ due to its variety of chemical functions differ in thermal stability. It shows several peaks in the DTG curves. The main conversion step of lignin takes place from 200 ℃ to 450 ℃ with the main peak forming around 350 ℃ (Shen, Gu, Luo, Wang, & Fang, 2010; Wang et al., 2009). As the temperature increases, the secondary reaction of the primary pyrolysis product occurs at 550-600 ℃.

The primary pyrolysis occurs at the temperature range from 200 ℃ to 450 ℃, in which several kinds of reactions take place. At the beginning of the pyrolysis (from 180 ℃), the release of volatile compounds mainly results from the propyl chains and some linkages between monomer units (Jakab, Faix, Till, & Székely, 1995). When the carbon Cγ includes in carbonyl and carboxyl groups, it leads to the formation of CO and CO_2, respectively. Besides, the most common linkage of β-O-4 in lignin decomposes from 240 ℃ (Nakamura, Kawamoto, & Saka, 2008). The reorganization of the chemical groups from the cleavage of ether linkages also produce the gaseous product such as CO, CO_2 and H_2O.

When the temperature increased higher than the 400℃, the second pyrolysis reactions occurs. The C-C bonds within and between alkyl chains becomes unstable and the cracking occurs, which increases the yield of monomers. At this temperature range, besides the small chain compounds that have been released in the previous steps, other low molecular weight also forms such as CH_4, acetaldehyde and acetic acid (Candelier et al., 2011).

1.4 Objectives of this research

According to the previous description, it is necessary to clarify the thermal behaviors of the hemicellulose and cellulose in wood at the primary pyrolysis stage. However, the studies describing the detailed information about the catalytic effect of 4-*O*-MeGlcA in the xylan pyrolysis and wood pyrolysis between hardwood and softwood is quite limited. So this thesis focus on the thermal reactivities of hemicellulose and cellulose in hardwood and softwood cell wall ultrastructure.

In chapter 2, the acid and base catalytic effect of 4-*O*-MeGlcA and its sodium urnoate were evaluated in the isolated xylan pyrolysis. Further, the thermal reactivities of hemicellulose and cellulose were compared for Japanese beech and Japanese cedar wood for understanding the different wood cell wall structure in chapter 3. In chapter 4, the effect of acid and base catalytic effect of 4-*O*-MeGlcA was investigated in the original and demineralized Japanese beech wood to understand the effect in the wood cell wall. Finally, the thermal reactivities of hemicellulose and cellulose in Japanese beech and cedar wood after delignification ball-milling process were analyzed to understand its effect on the wood cell wall ultrastructure, in chapter 5 and chapter 6, respectively.

In chapter 7, concluding remarks about the effect of wood cell wall structure on the reactivities of hemicellulose and cellulose were described.

Chapter 2

The effect of uronic acid moieties on xylan pyrolysis

2.1 Introduction

Hemicellulose is a major component of lignocellulosic biomass and comprises 20-40% of woody biomass by weight (McKendry, 2002). The chemical composition of hemicellulose varies depending on the wood species; xylan is the major component of hardwood, whereas the glucomannan concentration is much greater than that of xylan in softwood (Asmadi, Kawamoto, and Saka 2017; Fengel and Wegener 1979; Jacobs and Dahlman 2001; Timell 1967; Wang et al. 2015). In both materials, acetyls group and 4-*O*-methyl-D-glcuronic acid (4-*O*-MeGlcA) are present on the hemicellulose glycan chains, but in different manners. Specifically, acetyl groups are attached to xylan in hardwood but to glucomannan in softwood, and the concentration of acetyl groups in softwoods is typically lower than in hardwoods (Shen, Gu, & Bridgwater, 2010a; Sims, Craik, & Bacic, 1997; Sims, Munro, Currie, Craik, & Bacic, 1996; X. Zhou, Li, Mabon, & Broadbelt, 2016). The 4-*O*-MeGlcA groups are bonded at the C_2 locations of xylose units along the xylan main chains through α-1→2 linkages in both types of wood, but to a greater extent in hardwoods (Gírio et al., 2010; Jacobs & Dahlman, 2001). Part of the chemical structure of xylan is illustrated in Fig. 2-1, in which 4-*O*-MeGlcA moiety exists as the acid form. These differences in the chemical compositions of these two types of woods can affect their pyrolysis behaviors, although the correlation is not well understood at present.

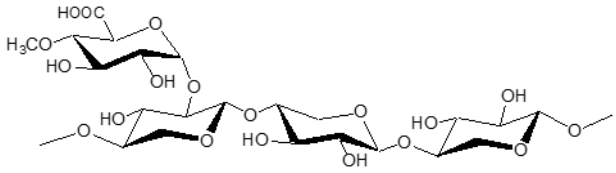

Fig. 2-1 Part of chemical structure of xylan. (Uronic acid: acid type)

During pyrolysis, hemicellulose is less stable than cellulose; the thermal degradation of hemicellulose occurs in the temperature range of 220 to 315 °C, while cellulose devolatilization becomes significant at temperatures between 300 and 350 °C (Sanchez-Silva, López-González, Villaseñor, Sánchez, & Valverde, 2012; Yang et al., 2007, 2006; Zhou et al., 2015). Although both polysaccharides generate similar volatile products, including anhydrosugars, aldehydes, ketones, acids, and noncondensable gases, xylan produces furanoic and pyranoic compounds in greater yields (Asmadi, Kawamoto, and Saka 2010; Branca, Di Blasi, and Galgano 2016; Le Brech et al. 2016; Eom et al. 2011, 2012; Evans and Milne 1987; Hosoya, Kawamoto, and Saka 2007a; Katō 1967; Ralph and Hatfield 1991; Shafizadeh, McGinnis, and Philpot 1972; Šimkovic et al. 1988; Wang et al. 2013). Furfural is a typical furanoic compound obtained from xylan pyrolysis, while 4-hydroxy-5,6-dihydro-2H-pyran-2-one (having a molecular mass of 114) is a pyranoic compound frequently utilized as a marker of xylan pyrolysis (Miyazaki, 1975; Patwardhan et al., 2009; Ponder & Richards, 1991).

The presence of minerals (typically alkali and alkaline earth metals) is one of the most important factors affecting the pyrolysis behavior of hemicellulose and cellulose (Asmadi et al., 2017; Kawamoto, Yamamoto, & Saka, 2008; Müller-Hagedorn, Bockhorn, Krebs, & Müller, 2003; Ponder & Richards, 1991; Shafizadeh et al., 1972; Shen, Gu, & Bridgwater, 2010b; Shimada, Kawamoto, & Saka, 2008; Tsuchiya & Sumi, 1970; Varhegyi et al., 1988; Yang et al., 2006). In general, the anhydrosugars yield decreases but the char yield increases in the presence of such substances. The effects of minerals may also be different during cellulose and xylan pyrolysis, because xylan contains carboxylic acids such as 4-*O*-MeGlcA. DeGroot (DeGroot, 1985) reported that the ion-exchange capacity of 4-*O*-MeGlcA in xylan explains the mineral content of cottonwood, and determined that the uronic acid groups are complexed with metal cations to form metal uronates. Based on an analysis of ten wood species, Asmadi et al. (Asmadi et al.,

2017) confirmed that the mineral content in the wood exhibited a linear relationship with the 4-*O*-MeGlcA concentration. Patwardhan et al. (Patwardhan, Brown, & Shanks, 2011) and Giudicianni et al. (Giudicianni, Gargiulo, Grottola, Alfè, & Ragucci, 2018) also reported that the uronic acid moieties in commercially-available xylan mainly exist as salts with sodium cations.

With regard to the effects of metal uronates and uronic acid on the xylan pyrolysis products, both furfural (Giudicianni et al., 2018; Patwardhan, Brown, et al., 2011) and anhydrosugars (Ohnishi et al., 1977; Patwardhan, Brown, et al., 2011) yields are reported to increase upon the removal of minerals from xylan. Asmadi et al. (Asmadi et al., 2017) examined the yields of glycolaldehyde and hydroxyacetone (both fragmentation products) as well as acetic acid from the pyrolysis of original and demineralized wood samples as a means of assessing the base catalysis effect of metal uronates, because the fragmentation and hydrolysis of acetoxy esters are enhanced under basic conditions. However, there is currently very little information available in this field of study.

Thermogravimetric (TG) analysis is an effective means of assessing the thermal behaviors of xylan and similar materials. Xylan pyrolysis proceeds via two different mechanisms at different temperatures, resulting in the appearance of two peaks in differential thermogravimetric (DTG) curves as discussed later. It has been proposed that the lower temperature peak can be ascribed to the decomposition of side units (4-*O*-MeGlcA and acetyl groups), whereas the higher temperature peak is due to cracking of the xylan main chain (Giudicianni et al., 2018; Sanchez-Silva et al., 2012; Shen, Gu, & Bridgwater, 2010b; H. Zhou et al., 2015). However, there is insufficient experimental evidence to conclusively accept this hypothesis.

In the present study, the decomposition behaviors of 4-*O*-MeGlcA moieties and xylan main chains during TGA were evaluated by pyrolysis experiments using commercial beech wood xylan and samples of this same material demineralized, at temperatures between 220 and 340 °C under N_2. These trials were followed by char methanolysis to recover unreacted 4-*O*-MeGlcA and xylose. The effects of the presence of uronic acid and metal uronate moieties on xylan pyrolysis were assessed by analyzing

the various specimens using pyrolysis-gas chromatography-mass spectrometry (Py-GC-MS).

2.2 Material and methods

2.2.1 Materials

Beech wood xylan was purchased from Megazyme (Wicklow, Ireland) and utilized as the so-called original xylan, without any further purification. Demineralized xylan was prepared according to a literature procedure (Asmadi et al., 2017; T. Hosoya et al., 2007b). In this process, a quantity of xylan (1 g) was dispersed in 30 mL of a 0.05 M solution of HCl in methanol. After stirring for 24 h at room temperature, the suspended material was removed by filtration and washed with methanol until the filtrate became neutral. This procedure was repeated twice and the resulting product was dried in an oven at 105 °C for 24 h. This treatment decreased the mineral content from 5 wt% in the original material to 0.1 wt%, as determined by incineration of original and demineralized xylan samples at 600 °C in air for 2 h.

2.2.2 Characterization of xylan

The molar ratio of xylose to 4-*O*-MeGlcA (xylose/4-*O*-MeGlcA ratio) in the xylan main chains was determined using proton (^{1}H) nuclear magnetic resonance (NMR) spectra acquired from the xylan (Fig. 2-2) in D_2O with a Bruker AC-400 (400 MHz) spectrometer. The C_1-H signals of free xylose and xylose in which 4-*O*-MeGlcA is attached at C_2 appeared as two doublets at J = 6.7 Hz, δ = 4.48 ppm and J = 6.4 Hz, δ = 4.63 ppm, respectively, in agreement with literature values (Gabrielii, Gatenholm, Glasser, Jain, & Kenne, 2000). The latter signal was shifted to a lower magnetic field value due to the electron-withdrawing character of the carboxylic acid group. The C_1-H signal assigned to 4-*O*-MeGlcA was observed at 5.29 ppm as a broad singlet. Based on the peak areas of these signals, the xylose/4-*O*-MeGlcA molar ratio was determined to be 7.7, and a similar value has previously been reported in the literature (Shen, Gu, & Bridgwater, 2010a).

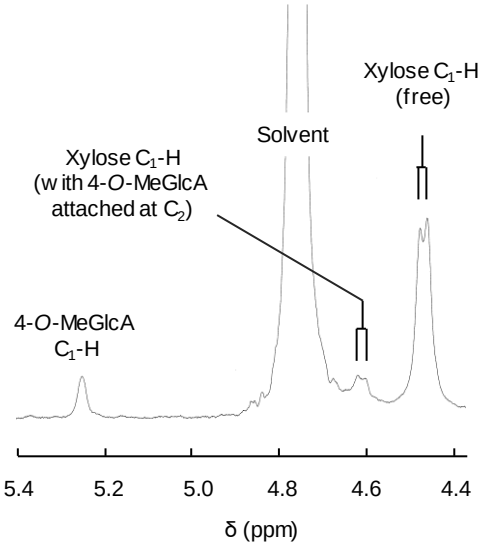

Fig. 2-2 An expanded view of the 1H-NMR spectrum of commercial beech wood xylan in D_2O

The carboxylic acid peak in the infra-red (IR) spectrum of such materials shifts from approximately 1700 to 1600 cm^{-1} following the transition to a salt with a metal cation. Fig. 2-3 demonstrates that the spectrum of the original xylan clearly exhibits this characteristic shift relative to the spectrum acquired from the demineralized xylan, confirming the presence of carboxylate groups in the original material. Investigations via scanning electron microscopy with energy dispersive X-ray analysis (SEM-EDXA) confirmed that the primary cation was Na^+ along with a lesser amount of Ca^{2+} (Fig. 2-4, which shows the spectrum acquired from the original xylan after incineration at 600 °C in air for 2 h).

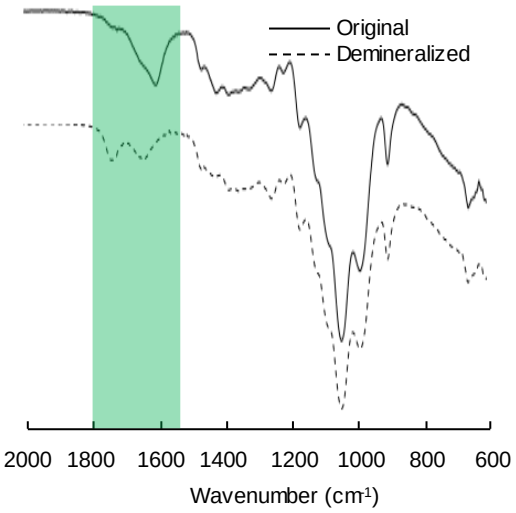

Fig. 2-3 The IR spectra of the original and demineralized xylans

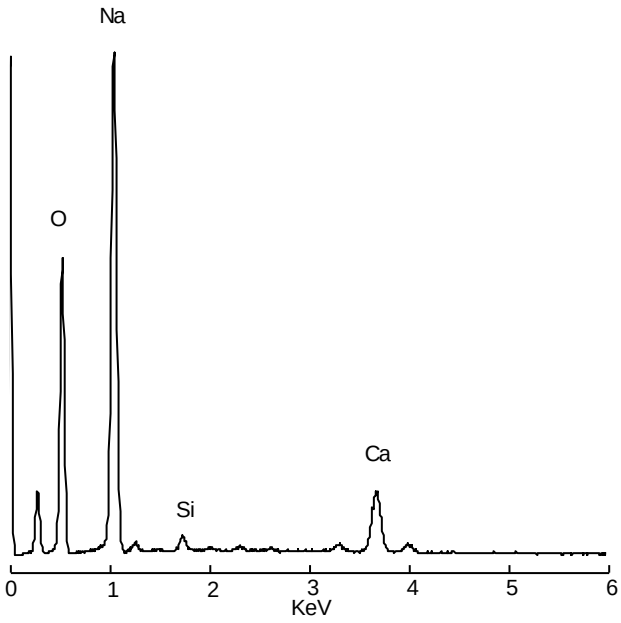

Fig. 2-4 SEM-EDXA results obtained from the original xylan after incineration in air at 600 ºC for 2h

2.2.3 TG

TGA was conducted with a TGA-50 instrument (Shimadzu, Kyoto, Japan), with either the original or demineralized xylan (1 mg) placed in a platinum pan. The sample

was heated from room temperature to 500 °C at a rate of 10 °C/min under a N_2 flow of 10 mL/min.

2.2.4 Pyrolysis and char analysis

The experimental set up used in this work is illustrated in Fig. 2-5. The apparatus consisted of a quartz glass tube (internal diameter 15 mm, length 400 mm, wall thickness 1.5 mm) held in a cylindrical furnace (Asahi-Rika Seisakusho, Chiba, Japan). A sample of the original or demineralized xylan (20 mg) was placed in a ceramic boat and the tip of a fine thermocouple (0.25 mm in diameter, type K, Shinnetsu, Ibaraki, Japan) was placed in the sample layer without contacting the bottom of the ceramic boat. The thermocouple was connected to a thermologger (AM-8000, Anritsu Corporation, Kanagawa, Japan) to allow measurement of the sample temperature during the pyrolysis experiments. After a 10 mL/min flow of N_2 was supplied for 5 min (using an SEC-400MK3 mass flow controller, Horiba, Kyoto, Japan) to replace the air inside the tube, the sample was heated to the set temperature (from 220 to 340 °C in 20 °C intervals) at 10 °C/min (the same rate as applied during TGA) using a digital temperature controller (AMF-1P, Asahi-Rika Seisakusho, Chiba, Japan). When the desired temperature was achieved, the cover of the cylindrical furnace was immediately opened and the quartz glass tube was cooled by a flow of air.

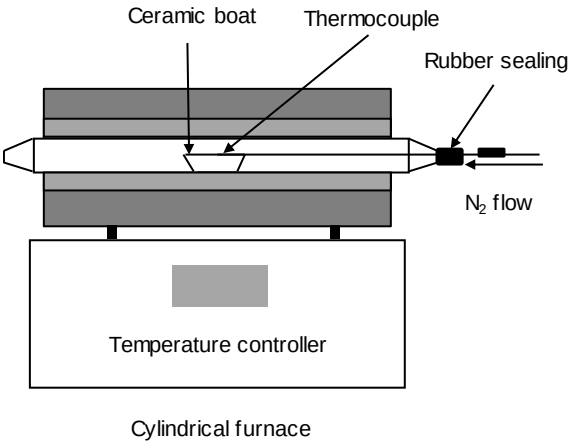

Fig. 2-5 The experimental setup

The char fraction obtained from each sample was subjected to methanolysis (Bertaud, Sundberg, & Holmbom, 2002; Bleton, Mejanelle, Sansoulet, Goursaud, & Tchapla, 1996; Li, Kisara, Danielsson, Lindström, & Gellerstedt, 2007) to determine the recoveries of unreacted xylose and 4-*O*-MeGlcA moieties, using a previously reported methanolysis procedure (Huang, Indrarti, Azuma, & Okamura, 1992). In this process, the ceramic boat containing the char fraction was soaked in a 2 M solution of HCl in methanol within a sealed glass tube. The glass tube was sealed and then heated at 60 °C for 16 h to complete the methanolysis reaction, after which the reaction mixture was neutralized with pyridine. A portion of the filtrate was dried under vacuum after the addition of glucitol as an internal standard and then silylated by adding pyridine, hexamethyldisilizane (HMDS) and trimethylchlorosilane (TMCS) in conjunction with stirring and heating at 60 °C for 30 min. The trimethylsilyl derivatives were analyzed by gas chromatography–mass spectroscopy (GC-MS) using a QP 2010 Ultra mass spectrometer (Shimadzu Corporation, Kyoto, Japan). The instrumental conditions consisted of: column; Agilent CPSil 8CB (length: 30 m, diameter: 0.25 mm), injector temperature; 260 °C, column temperature; 100 °C (2 min), 4 °C/min to 220 °C, 220 °C (2 min), 15 °C/min to 300 °C, 300 °C (2 min), carrier gas; helium, flow rate; 1.0 mL/min. The signals originating from xylose and 4-*O*-MeGlcA were assigned based on the associated mass spectra and retention times as compared with literature data (Bertaud, Sundberg, and Holmbom 2002; Bleton et al. 1996; HA and Thomas 1988; Sundberg et al. 1996).

2.2.5 Py-GC-MS

Py-GC-MS analysis was conducted using a portable Curie-point injector (JCI-22, Japan Analytical, Tokyo, Japan) coupled to the GC-MS instrument described in Section 2.4. A 0.1 mg sample of xylan was pyrolyzed at 590 °C for 5 s. Different types of pyrofoils were also utilized for the pyrolysis trials at various temperatures, including 255, 280, 315, 386 and 423 °C. The GC and MS conditions were similar to those noted in Section 2.4 except for the column temperature program, which consisted of: 50 °C (1 min), 5 °C/min to 120 °C, 10 °C/min to 250 °C, 250 °C (2 min).

2.3 Results and discussion

Figure 2-6 presents the TG and DTG curves acquired from both the original and demineralized xylans. Upon increasing the pyrolysis temperature, both materials exhibit mass loss that starts around 220 °C and is almost complete by 350 °C, but the effects of the pyrolysis temperature on the mass loss behavior are different. The DTG curves show the difference more clearly; only one peak is generated (at approximately 280 °C) by the demineralized xylan, while the original material produces two peaks, at 250 and 315 °C. The latter observation indicates that the original xylan contained two components with different thermal reactivities. The char yield at 400 °C was greater in the case of the original xylan. These characteristic features are consistent with results previously reported in the literature (Giudicianni et al., 2018; Patwardhan, Brown, et al., 2011; Sanchez-Silva et al., 2012; Shen, Gu, & Bridgwater, 2010b; Zhou et al., 2015).

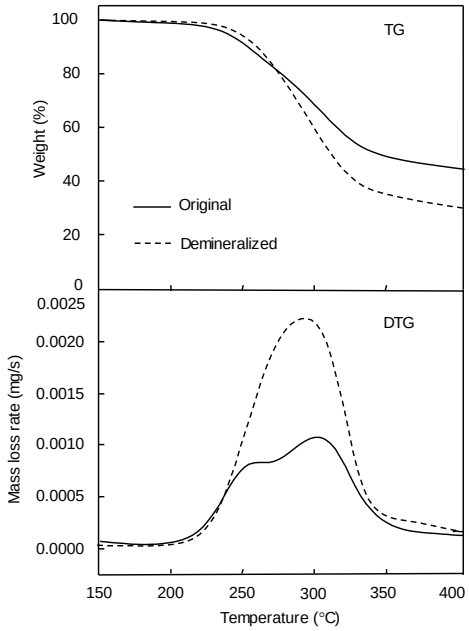

Fig. 2-6 The TG and DTG curves acquired from the original and demineralized xylans

The two different modes evident in the original xylan pyrolysis were assessed by conducting trials using heating conditions similar to those applied during TGA (heating at 10 °C/min to set temperatures between 220 and 340 °C and no temperature hold period). The resulting chars were subjected to methanolysis to determine the components that

decomposed during the pyrolysis. Fig. 2-7 summarizes the changes in the char recovery upon increasing the pyrolysis temperature for both the original and demineralized xylan pyrolysis. As was also observed in the TGA data, both materials decomposed over the temperature range of 220–340 °C.

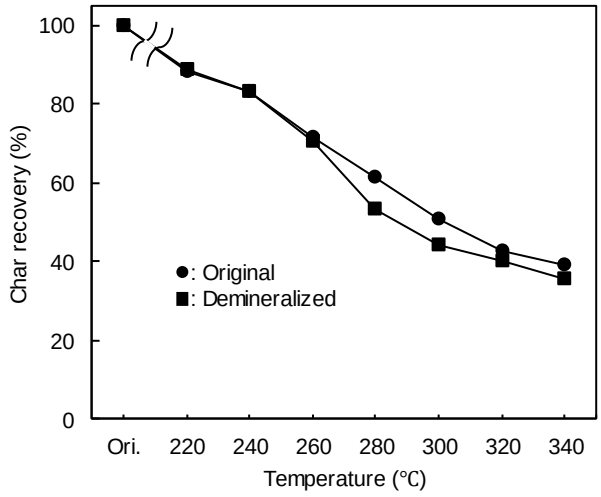

Fig. 2-7 The char recoveries from pyrolysis of the original and demineralized xylans as functions of temperature

Change in the recoveries of xylose and 4-*O*-MeGlcA during the pyrolysis are shown in Fig. 2-8, which provides important information regarding the reactivities of xylan during heating to temperatures between 220 and 340 °C. The 4-*O*-MeGlcA (primarily in the form of Na uronate) in the original xylan was evidently more thermally reactive than the free carboxylic acid and degraded over the lower temperature range of 220–280°C. It should be noted that half the xylose units in the xylan main chains also decomposed over this temperature range, although the rest decomposed within the higher temperature range of 280–320 °C. These results indicate that the 4-*O*-MeGlcA (primarily Na uronate) and some xylose units degraded at the temperature corresponding to the lower DTG peak (at 250 °C), while the rest of the xylose units decomposed at higher temperatures, producing the higher DTG peak (at 315 °C).

In contrast, during the pyrolysis of the demineralized xylan, both the xylose and 4-*O*-MeGlcA units decomposed simultaneously over the temperature range of 240–320 °C, which is intermediate between the two degradation modes of the original xylan.

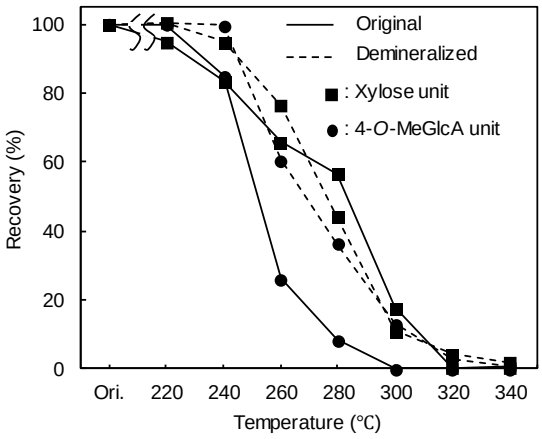

Fig. 2-8 The recoveries of xylose and 4-O-MeGlcA units from pyrolysis of the original and demineralized xylans as functions of temperature

Consequently, it is evident that the pyrolysis of the original xylan occurs heterogeneously, while the demineralized xylan pyrolysis is rather homogeneous. As illustrated in Fig. 2-9, 4-*O*-MeGlcA (primarily Na uronate) and neighboring xylose units decompose at lower temperatures in the original xylan, but this effect does not radiate to other more remote xylose units, likely due to the limited mobility of Na and Na-containing materials in the sample. Conversely, the acid catalysis effect of the free carboxyl groups in the demineralized xylan would affect all the xylan molecules.

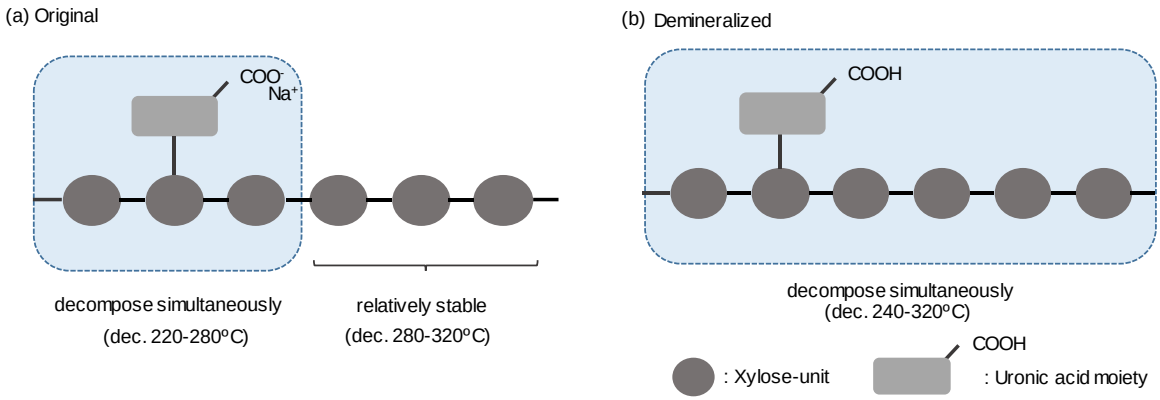

Fig. 2-9 Diagrams summarizing the thermal degradation behaviors of 4-O-MeGlcA and xylose units during pyrolysis of the (a) original and (b) demineralized xylans

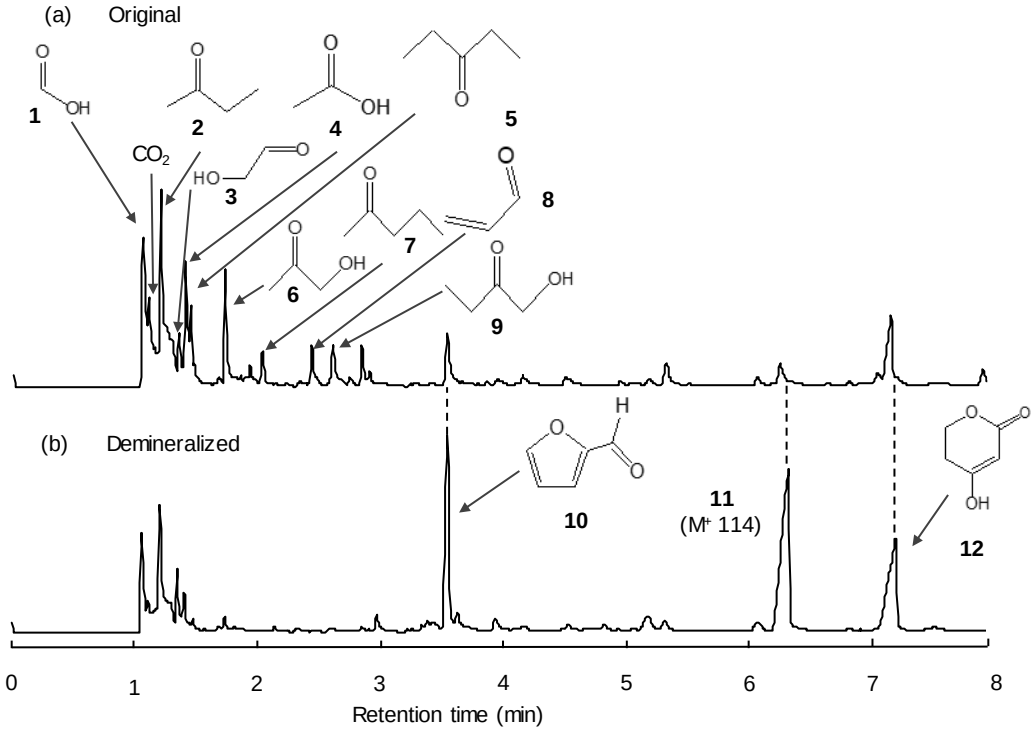

Fig. 2-10 The pyrograms obtained from the Py-GC-MS analysis of the (a) original and (b) demineralized xylans at 590 °C

The pyrograms obtained from Py-GC-MS analysis of the original and demineralized xylans at 590 °C are shown in Figs. 2-10 (a) and (b), respectively. Identification of the chemical structure associated with each peak was based primarily on comparing the retention times and mass spectra with those reported in the literature

(Patwardhan, Brown, et al., 2011; Ponder & Richards, 1991; Pouwels, Tom, Eijkel, & Boon, 1987; Shen, Gu, & Bridgwater, 2010a; Wang et al., 2013), except for compounds **2**, **5**, **7** and **9**.The chemical structures of these compounds were determined from the fragmentation patterns in Fig. 2-11. These compounds, which were obtained primarily from the pyrolysis of the original xylan, included ethyl and propyl chains, indicating that deoxygenation reactions proceeded during pyrolysis. The other products identified were formic acid (**1**), glycolaldehyde (**3**), acetic acid (**4**), hydroxyacetone (**6**) and acrolein (**8**). Hence, the original xylan generated low molecular weight (MW) ketones, aldehydes and acids as fragmentation products.

Contrary to this, the demineralized xylan showed a tendency to form furfural (**10**), 4-hydroxy-5,6-dihydro-2H-pyran-2-one (**12**, MW 114) and the unknown product **11** (M^+ 114), in agreement with previous literature reports (Ohnishi et al., 1977; Patwardhan, Brown, et al., 2011). The formation of these compounds is reasonably explained by the action of the free uronic acid in the demineralized xylan as an acid catalyst promoting depolymerization of the xylan main chains and dehydration reactions. Depolymerization followed by dehydration would be expected to give the product at MW 114 (132-18 (H_2O)) as well as furfural (MW 96, 132-18 (H_2O) x 2). Unknown product **11** is also believed to be a dehydration product, although the chemical structure is presently unknown.

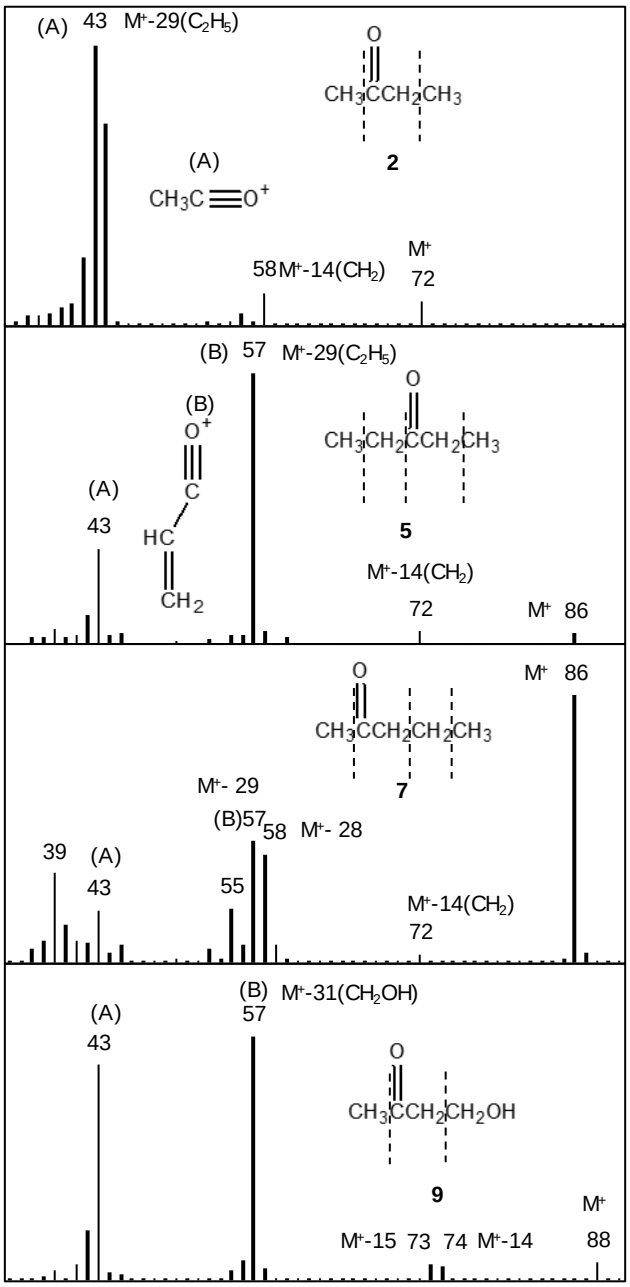

Fig. 2-11 Mass spectra of compounds 2, 5, 7 and 9 as generated during pyrolysis

Figure 2-12 provides the pyrograms obtained from the Py-GC-MS analysis of the original and demineralized xylans on different pyrofoils at 255, 280, 315, 386 and 423 °C. Peaks assigned to furfural (**10**) and compounds **11** and **12** are observed in the chromatograms obtained at 280 °C and above. These results indicate that the pyrolysis

reactions were similar to those occurring in the temperature range of 220–350 °C over which thermal degradation and mass loss were apparent in the TG data.

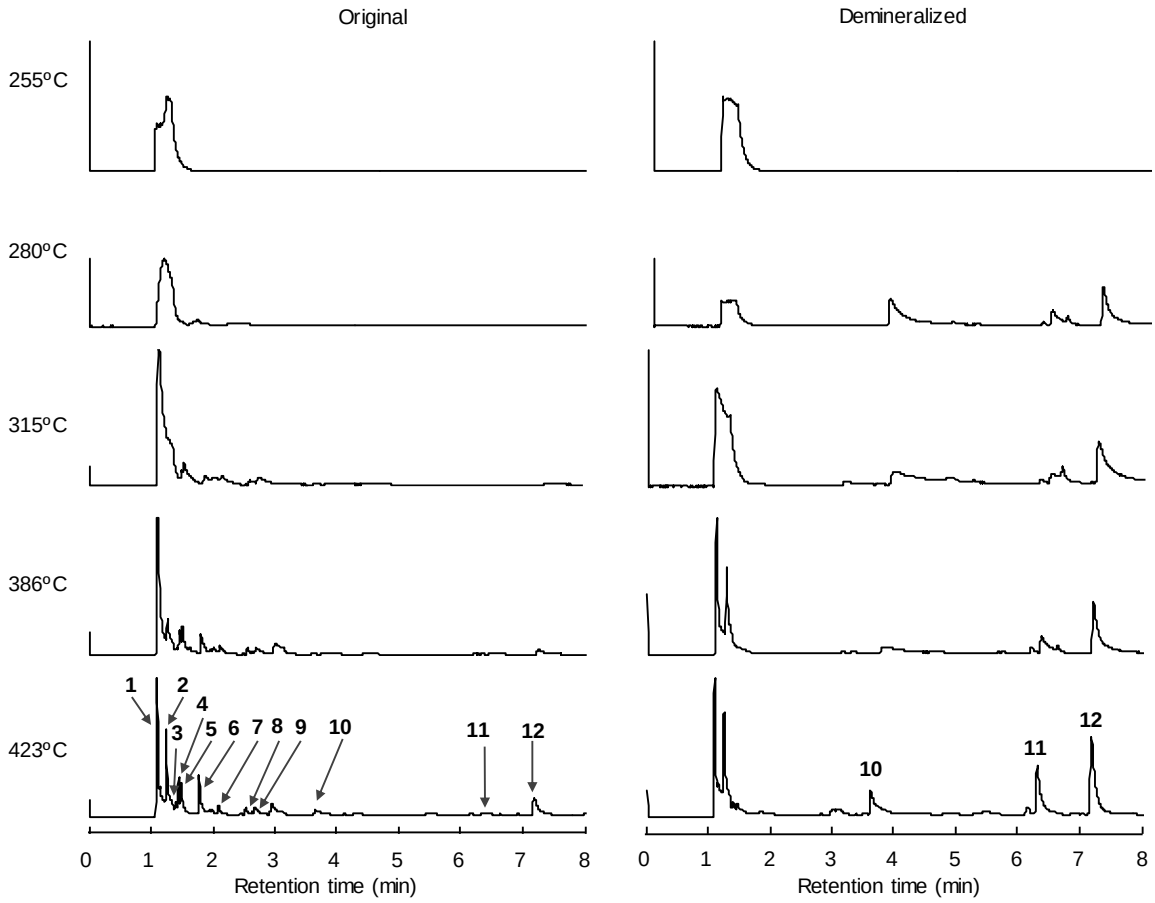

Fig. 2-12 The pyrograms obtained from the Py-GC-MS analysis of the original and demineralized xylans at different temperatures

The pyrograms generated by the original xylan are different depending on the pyrolysis temperature. Those obtained at 255 and 280 °C do not exhibit any signals at retention times greater than 1.5 min, although the 4-*O*-MeGlcA (primarily Na uronate) and half the xylose units in the xylan main chains were always decomposed. The signals originating from compounds **1-9** become significant at 315 °C and above, at which point the remainder of the xylose units degrade. These observations provide some insights into the pyrolytic reactions of the original xylan. The degradation of the 4-*O*-MeGlcA groups and some xylose units in the temperature range of 220–280 °C does not produce any significant quantities of low MW products. Thus, the low MW fragmentation and

deoxygenation products **1-9** are formed at the higher temperatures corresponding to the higher temperature DTG peak.

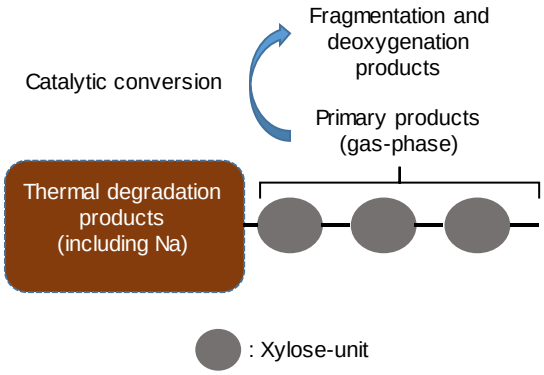

Fig. 2-13 Proposed fragmentation and deoxygenation mechanisms for the pyrolysis of the original xylan above 315 ºC

These characteristics of the original xylan pyrolysis can be explained by the proposed mechanism shown in Fig. 2-13, although further systematic studies are necessary to confirm this hypothesis. In this mechanism, thermal degradation products including Na, formed at lower pyrolysis temperatures, act as catalysts for the secondary degradation of the gas phase products resulting from the pyrolysis of the rest of the xylose units at higher temperatures (>280 °C). When the pyrolysis temperature is increased from 315 to 590 °C, secondary reactions producing fragmentation and deoxygenation products 1-9 become more prominent.

2.4 Conclusions

The role of uronic acid moieties during xylan pyrolysis was investigated, focusing on metal uronate and free uronic acid in original and demineralized commercial beech wood xylans. The following conclusions can be made.

1. The original xylan, containing metal uronate groups (primarily sodium salts), degrades over two different temperature ranges, producing two distinct DTG peaks.

Conversely, the demineralized xylan with free uronic acid degrades in an intermediate temperature range and shows one peak.

2. Char analysis following xylan pyrolysis based on methanolysis is a helpful means of understanding the structural decomposition at each pyrolysis temperature.

3. In the case of the original xylan, pyrolysis causes the metal (sodium) uronate and half the xylose units in the xylan main chains to degrade at relatively low temperatures, corresponding to the lower temperature DTG peak. The remainder of the xylose units degrade at the higher temperature, producing the higher peak. Thus, the effect of metal uronates is heterogeneous and occurs only in the vicinity of these groups.

4. During pyrolysis of the demineralized xylan, the acid catalysis of free uronic acid moieties affects all the xylan groups, and the pyrolysis occurs homogeneously.

5. Pyrolysis reactions are affected by the presence of both the metal (sodium) uronate and free uronic acid groups. Free uronic acid acts as an acid catalyst to enhance depolymerization and dehydration reactions and thus promotes the formation of furfural and 4-hydroxy-5,6-dihydro-2H-pyran-2-one, while the metal uronate enhances fragmentation and deoxygenation reactions.

6. The information obtained from this work provides useful insights into the wood pyrolysis mechanism.

Chapter 3

Thermal reactivity of hemicellulose and cellulose in cedar and beech wood cell walls

3.1 Introduction

The pyrolytic reactivity of wood polysaccharides has been studied using isolated cellulose and hemicelluloses (Shafizadeh, McGinnis, and Philpot 1972; Shen, Gu, and Bridgwater 2010; Wang et al. 2013; Yang et al. 2006, 2007). Cellulose, a crystalline polysaccharide, exhibits a higher thermal stability than amorphous hemicelluloses and exhibits the maximum thermal degradation rate at ~350 °C, that yields volatile products and char (Yang et al. 2006, 2007; Zhou et al. 2015). Xylan and glucomannan are the major hemicellulose for hardwood and softwood, respectively, whose structure is illustrated in Fig. 3-1. The pyrolytic reactivity of hemicellulose has received a wealth of interdependent research by using isolated wood xylan (Sanchez-Silva et al. 2012; Shafizadeh, McGinnis, and Philpot 1972; Shen, Gu, and Bridgwater 2010; Wang et al. 2013; Yang et al. 2006) and konjac glucomannan (Ohnishi et al., 1977; Patwardhan, Brown, et al., 2011; Räisänen, Pitkänen, Halttunen, & Hurtta, 2003; Shen, Gu, & Bridgwater, 2010a; X. Zhou, Li, Mabon, & Broadbelt, 2018), and in addition, numerous studies have concluded that the thermal stability of xylan is lower than glucomannan (Shafizadeh, McGinnis, and Philpot 1972; Wang et al. 2013; Werner, Pommer, and Broström 2014). Relating to the xylan instability, Wang *et al.* (Wang, Asmadi, and Kawamoto 2018) reported that the 4-*O*-methyl-D-glucuronic acid (4-*O*-MeGlcA) moiety and the Na salts in demineralized and original commercial beech xylan acted as acid and base catalysts, respectively, which promotes the thermal degradation of the xylose units in xylan. The observed changes to the catalytic performance were also supported from the different compositions of the

pyrolysis products; depolymerization/dehydration products such as furfural and 4-hydroxy-5,6-dihydro-2H-pyran-2-one were observed by acid catalysis, while fragmentation products were yielded by base catalysis.

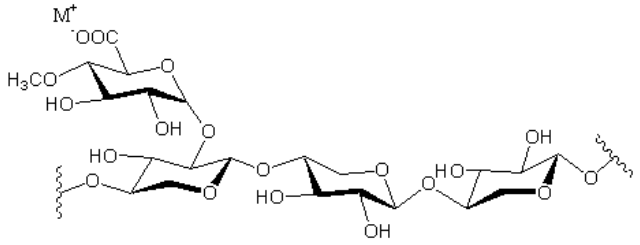

Xylan

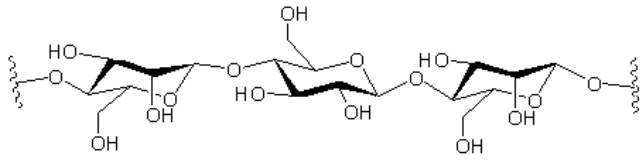

Glucomannan

Fig. 3-1 Chemical structure of xylan and glucomannan

Conversely, the reactivity of hemicellulose and cellulose in wood cell walls has not been discussed in the literature. Only thermogravimetric (TG) and differential TG (DTG) profiles of wood samples have been discussed with the thermal reactivity of isolated hemicellulose and cellulose (Shen and Gu 2009; Shen, Gu, and Bridgwater 2010; Yang et al. 2006, 2007; Zhou et al. 2015). The DTG curve of hardwood typically exhibits a shoulder in the lower temperature region along with a peak, which has been reported to originate from xylan and cellulose, respectively (Kim et al. 2006; Poletto 2016; Poletto et al. 2012). This assignment appears to be reasonable because the shoulder is not observed for the typical DTG curve of softwood that contains only a smaller amount of xylan. Nevertheless, there are no reports to evidence this explanation. For these reasons, the work herein evaluates the pyrolytic reactivity of hemicelluloses and cellulose in wood

by using Japanese cedar (*Cryptomeria japonica*, a softwood) and Japanese beech (*Fagus crenata*, a hardwood).

To evaluate the pyrolytic reactivity of wood polysaccharides in wood cell walls, hemicelluloses and cellulose remaining in heat-treated woods must be quantified during pyrolysis. Standard analysis methods for wood polysaccharides include hydrolysis (Harris et al., 1985) and methanolysis (Asmadi et al., 2017; Bertaud et al., 2002; Bleton et al., 1996; Li et al., 2007), which can be applied for this purpose. Herein, Japanese cedar and Japanese beech woods were pyrolyzed by heating to set temperatures from 220 to 380 °C (20 °C intervals and no holding period), and the thermal degradations of xylan, glucomannan and cellulose were evaluated from the remaining hydrolysable sugar content. Comparisons with isolated xylan and glucomannan provide insight into how the pyrolytic reactivity is influenced in wood cell wall. Finally, the obtained results allowed for the assignment of the TG/DTG curves.

3.2 Materials and methods

3.2.1 Materials

Beech wood xylan and konjac glucomannan were purchased from Megazyme (Wicklow, Ireland) and Carbosynth (Berkshire, United Kingdom), respectively, and used without any further purification. Extractive-free wood flour (80 mesh passed) was prepared from the sapwood of Japanese cedar and Japanese beech by extracting with acetone using a Soxhlet extractor.

3.2.2 TG analysis

TG analysis was conducted using a TGA-50 instrument (Shimadzu, Kyoto, Japan). Oven-dried Japanese cedar or Japanese beech wood (1 mg) was placed into a platinum pan and heated from room temperature to 800 °C, at a heating rate of 10 °C/min under a N_2 flow of 10 mL/min (purity: 99.9998%, JAPAN FINE PRODUCTS, Mie, Japan). N_2 was first passed through a deoxygenation column (GL Sciences, Japan) to remove any oxygen contamination.

3.2.3 Pyrolysis experiment

Figure 3-2 illustrates the experimental setup used in this study. A quartz glass tube (internal diameter 15 mm, length 400 mm, wall thickness 1.5 mm) was placed in an electric furnace (Asahi-Rika Seisakusho, Chiba, Japan). For each experiment, the sample (20 mg) was placed into a ceramic boat (As One, Osaka, Japan), and the ceramic boat placed within the glass tube. Thereafter, the air inside the glass tube was displaced by a N_2 flow (100 mL/min) for 5 min using a SEC-400MK3 mass flow controller (Horiba, Kyoto, Japan), and the sample subjected to heat treatment at a set temperature (220–380 °C, at 20 °C intervals), at a heating rate of 10 °C/min, which was the same heating rate used for TG analysis. The sample temperature was directly measured during the pyrolysis experiment by contacting the tip of a fine thermocouple (0.25 mm in diameter, type K, Shinnetsu Co., Ltd., Ibaraki, Japan) to the sample whilst recording with a thermologger (AM-8000, Anritsu, Kanagawa, Japan). When the temperature reached the designated temperature, the cover of the electric furnace was opened and the glass tube was immediately cooled to room temperature under a flow of air.

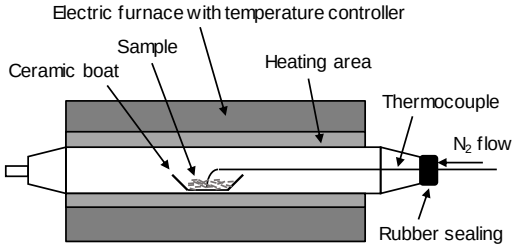

Fig. 3-2 Experimental setup for the pyrolysis experiment

3.2.4 Hydrolysable sugar analysis

Acid hydrolysis and methanolysis were conducted to determine the hydrolysable sugars from cellulose and hemicellulose/pectin in the heat-treated woods, respectively.

Hydrolysis was used to completely convert crystalline cellulose and was performed by treating the sample in a ceramic boat with 0.3 mL of an aqueous 72% H_2SO_4 solution at 30 °C in a glass tube for 1 h in a water bath. Thereafter, 8.4 mL of water was

added to the mixture for dilution and the solution was heated in an autoclave at 120 °C for 1 h to complete the hydrolysis reactions. After quenching the system, the sample was filtered with filter paper (Kiriyama Glass Works, Tokyo, Japan). An aliquot of the filtrate was taken and diluted 15 times with water and neutralized with Dionex OnGuard II A cartridge (Thermo Fisher Scientific, MA, USA). The glucose yield was determined by high-performance anion-exchange chromatography using a Dionex ICS-3000 instrument under the following conditions: column: CarboPac PA1 (4 mm x 250 mm); gas: N_2; flow-rate: 1 mL/min; pressure: 1 atm; eluent: mixture of 0.2M NaOH and distilled water; gradient-program: 15/85 (0-20min); detector: electron capture; detector temperature: 35 °C.

Milder methanolysis (Asmadi et al., 2017; Bertaud et al., 2002; Bleton et al., 1996; Li et al., 2007) was selected to determine the hydrolysable sugars from hemicellulose, pectin, and uronic acid groups. The ceramic boat containing heat-treated wood was placed into 4 mL of a 2 M solution of HCl in methanol in a glass tube comprising a screw cap and a Teflon-lined septum and heated at 60 °C for 16 h to complete the methanolysis reactions. After neutralization with 100 µL of pyridine, a portion of the mixture was mixed with a glucitol/methanol solution as an internal standard and dried under vacuum. Then, pyridine, hexamethyldisilazane and trimethylchlorosilane were added and the mixture was heated at 60 °C for 30 min under stirring. The resulting trimethylsilyl derivatives were analyzed by GC-MS using a Shimadzu-2010 Plus gas chromatograph (Shimadzu Corporation) coupled to a Shimadzu QP 2010 Ultra mass spectrometer (Shimadzu Corporation). The instrumental conditions comprised: column: Agilent CPSil 8CB (length: 30 m, diameter: 0.25 mm); injector temperature: 260 °C;; column temperature: 100 °C (2 min), 4 °C/min to 220 °C, 220 °C (2 min), 15 °C/min to 300 °C, 300 °C (2 min); carrier gas: helium; flow rate: 1.0 mL/min. The MS scan parameters included a scan range of 35–600 m/z and a scan-interval of 0.3 s. The signals originating from methyl glycosides were assigned based on the associated mass spectra and retention times, as compared with literature data (HA and Thomas 1988; Sundberg et al. 1996).

3.3 Results and discussion

3.3.1 Hemicellulose and other minor saccharide reactivity in wood cell walls

Figure 3-3 compares the pictures of heat-treated Japanese beech and Japanese cedar woods subjected to temperatures of 220–380 °C (10 °C/min). Discoloration of the beech wood was initiated at 240 °C, with the color changing to brown and darkening further as the temperature increased. Conversely, discoloration of the cedar wood occurred at a higher temperature range of 320–340 °C. Thus, in terms of discoloration, beech wood is more reactive than cedar wood. These results may originate from the different pyrolytic reactivity of the wood components, which will be discussed in the following paragraphs.

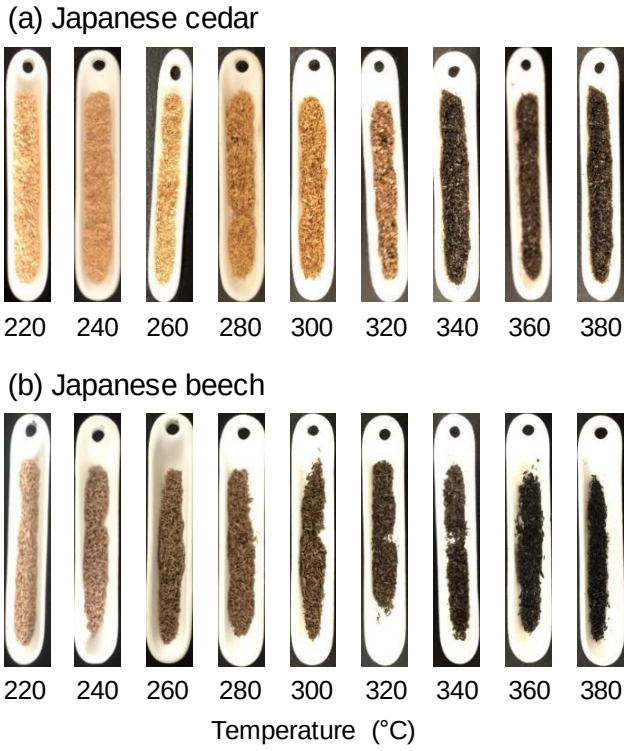

Fig. 3-3 Pictures of the appearance of: (a) Japanese cedar and (b) Japanese beech woods after being subjected to pyrolysis at various temperatures (10 °C/min, no holding period), under a nitrogen flow (100 mL/min)

Changes in the hydrolysable sugar content in the heat-treated woods are shown in Fig. 3-4, focusing on six sugar components: arabinose, glucose, galactose, mannose, xylose and 4-*O*-MeGlcA. The hydrolysable sugar content is shown as the percentage of sugar recovered against the yield from non-treated wood (normalized to 100%). Sugars other than glucose were determined as the corresponding methyl glycosides obtained by acidic methanolysis because of the instability of hemicellulose- and pectin-derived sugars when subjected to more severe hydrolysis conditions that hydrolyze stable crystalline cellulose.

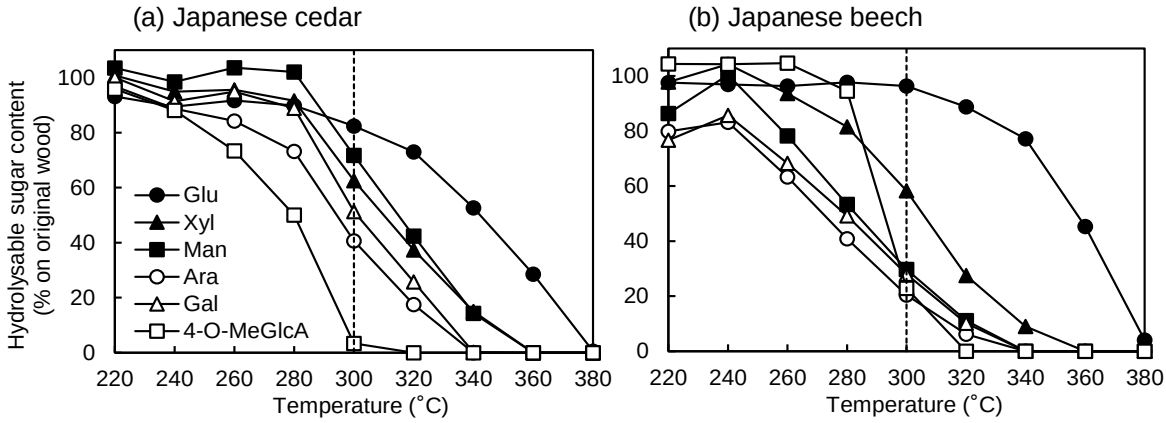

Fig. 3-4 Recovery rates of hydrolysable sugars from: (a) Japanese cedar and (b) Japanese beech woods after heating to various temperatures (10 °C/min, no holding period), under a nitrogen flow (100 mL/min)

● glucose (Glu), ▲ xylose (Xyl), ■ mannose (Man), ○ arabinose (Ara), △ galactose (Gal), □ 4-*O*-methyl-D-glucuronic acid (4-*O*-MeGlcA).

Table 3-1 (Rabemanolontsoa & Saka, 2013) shows sugar compositions determined from non-treated cedar and beech woods. The origins of these sugars should be discussed, based on literature (Haraguchi, 1985; Li et al., 2007; Meier & Vangedal, 1961; Mian & Timell, 1960; Reis & Vian, 2004; Scheller & Ulvskov, 2010; Thomas, 2015; X. Zhou et al., 2017), prior to comparing the pyrolysis results. A significant amount of glucose originates from cellulose, however, glucose is also the constituent of glucomannan. Different xylose and mannose contents in cedar and beech woods are explained by the well-known compositional difference of hemicellulose in hardwood and

softwood: xylan and trace amounts of glucomannan in hardwood, while softwood typically comprises glucomannan in major and xylan in minor amounts. Thus, changes in the yields of mannose and xylose directly indicate the degradation of glucomannan and xylan, respectively, during wood pyrolysis. The decrease in the recovery of glucose is related to cellulose degradation in beech, however, the contribution of glucomannan degradation must be considered for cedar.

Table 3-1 Monosaccharide compositions of beech and cedar woods (g kg−1 of the original oven-dried basis) (Rabemanolontsoa & Saka, 2013)

Sample	Glu	Man	Xyl	UA	Ara	Gal
Japanese cedar	447	57	64	9	6	12
Japanese beech	417	14	213	20	9	36

Glu: glucose, Man: mannose, Xyl: xylose, UA: uronic acid, Ara: arabinose, Gal: galactose

Xylan in both cedar and beech woods contains 4-*O*-MeGlcA as an acidic sugar component that is expected to act as an acid and base (as metal uronate) catalyst (Wang, Asmadi, & Kawamoto, 2018), indicating that this unit may accelerate the degradation of wood cell wall components. The effectiveness of this acceleration effect in cell walls is particularly discussed in the present paper. Typically, the 4-*O*-MeGlcA content is greater in hardwood than softwood, as recognized for beech (20 g/kg) and cedar (9 g/kg), Table 3-1.

The origins of arabinose and galactose are more complex. Arabinose is a component of softwood xylan but not of hardwood xylan. However, galactose is attached to the glucomannan chain of both types of wood species. For these minor sugars, the pectin content in the primary cell wall, which contains arabinose and galactose as the primary sugars (Caffall & Mohnen, 2009; Mohnen, 2008; Ridley et al., 2001; Thakur, Singh, & Handa, 1997; Voragen, Coenen, Verhoef, & Schols, 2009), cannot be ignored.

Accordingly, understanding the pyrolytic degradation of arabinose and galactose units is difficult with respect to the wood components.

In Fig. 3-4, degradation of glucose units is observed in the highest temperature region for both woods, which is consistent with the degradation of highly stable cellulose. Conversely, the temperature range where xylose and mannose units degrade is different; xylose and mannose units degrade at similar temperatures for cedar, however, in the pyrolysis of beech wood, the mannose units degrade at significantly lower temperatures than xylose. The xylose units in both woods are observed to degrade at similar temperatures, where mannose units in cedar also degrade. Consequently, hemicelluloses in the cell walls of both wood species are suggested to have similar reactivity, except for glucomannan in beech wood that is more reactive than other hemicelluloses.

The pyrolytic reactivity of the sugar units in hemicellulose in cedar and beech woods, as shown in Fig. 3-4, are compared with those of isolated xylan and glucomannan in Fig. 3-5, to elucidate the influence of the cell wall matrix. The results of the isolated hemicelluloses are shown in dashed lines. Commercial beech wood xylan, where the majority of the uronic acid moieties exist as Na salts, was used along with the demineralized (free carboxyl) sample as the isolated xylans, and their pyrolytic reactivities were evaluated by a similar procedure used in the present study (Wang et al., 2018). Based on the analysis data of ten softwood and hardwood species in our previous paper (Asmadi et al., 2017), most of the free carboxylic 4-*O*-MeGlcA groups in xylan would form the salts with alkali and alkaline earth metal cations, although some are involved in the formation of ester linkages with lignin as discussed later.

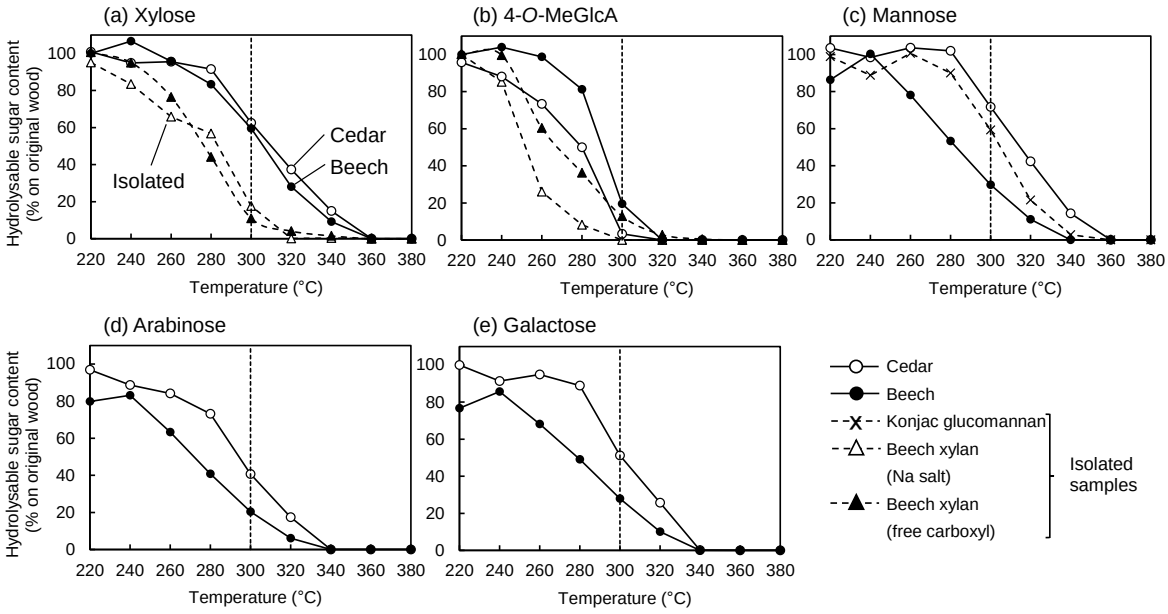

Fig. 3-5 Influence of pyrolysis temperature on recovery rates for: (a) xylose, (b) 4-*O*-MeGlcA, (c) mannose, (d) arabinose and (e) galactose in Japanese beech (●) and Japanese cedar (○) woods, compared with isolated xylan (△: Na^+ salt, ▲: free carboxyl) and isolated glucomannan (x)

Pyrolysis conditions: heating rate (10 °C/min) / nitrogen flow (100 mL/min) / no holding period.

Glucomannan was isolated from Japanese cedar wood according to a previously reported procedure that includes the extraction of the residues obtained by the pre-extraction of xylan from holocellulose (delignified wood) using an aqueous solution of sodium hydroxide (24%) and boric acid (5%). However, that procedure concluded that the boric acid contaminant could not be removed from the isolated glucomannan even when using resins. For these reasons, konjac glucomannan was used as the isolated glucomannan herein.

The degradation temperature of the xylose units in both woods shifted to higher temperatures when compared with the isolated xylans, suggesting that xylan in the cell walls of both woods is significantly stabilized. Furthermore, the reactivity is observed to be similar to the glucomannan in cedar wood, as described above. The 4-*O*-MeGlcA units are also stabilized in the woods, however, the observed stability is different for cedar and beech. These results indicate that the 4-*O*-MeGlcA units attached to the xylan chain are restricted in the wood cell walls, where 4-*O*-MeGlcA fails to properly function as an acid

and base catalyst for xylan degradation. These findings will provide new insight to research groups in the area of wood pyrolysis because xylan is currently believed to be more reactive than glucomannan in wood pyrolysis.

The reactivity of the mannose units exhibit the opposite trend for cedar and beech woods; mannose units in cedar wood degraded at slightly higher temperatures than konjac glucomannan, while the mannose units in beech wood degraded at significantly lower temperatures, although the glucomannan content is relatively low in beech. These results suggest that the environment where glucomannan exists is different in the cell wall matrix of cedar and beech woods. A possible explanation for the enhanced reactivity of beech wood glucomannan is that the 4-*O*-MeGlcA groups act as acid/base catalysts in the vicinity of glucomannan in the cell wall of beech wood, as discussed later.

Arabinose and galactose units in beech wood degrade at lower temperatures than those in cedar wood. The greater reactivity of the galactose units in beech can be explained by the reactivity of glucomannan, which was greater in beech than cedar, because galactose is the minor component of glucomannan in both woods. Nevertheless, the contribution of pectin must be considered for the reactivity of these minor sugar units. Discoloration of beech wood that initiated at a lower temperature of 240 °C, when compared with the cedar wood (Fig. 3-3), may be related to the greater reactivity of arabinose and galactose units along with glucomannan.

3.3.2 Cellulose reactivity and assignment of TG/DTG curves

Figure 3-6 illustrates the TG/DTG profiles measured for beech and cedar woods at the same heating rate (10 °C/min), used for the above pyrolysis experiments, along with the degradation behavior of cellulose and hemicelluloses, expressed as wt.% based on the content in the wood, which were roughly estimated from the yields of hydrolysable sugars. The xylan and glucomannan contents in the pyrolyzed woods were calculated by multiplying the respective content in the original wood by the recovery rate of methyl xyloside and methyl mannoside obtained by methanolysis, respectively. The cellulose content was determined from the glucose yield obtained by hydrolysis by subtracting the yield from glucomannan, assuming that the reactivity of the glucose and mannose units

in glucomannan is similar. Although the TG/DTG curves appear at slightly higher temperatures than the degradation of wood polysaccharides, the data set comparison is useful for TG/DTG curve assignment.

A shoulder is clearly observed in the beech DTG curve along with a peak, while the DTG curve of cedar exhibits only one broad peak. Such a difference has previously been believed to originate from the greater reactivity of xylan that is more abundant in hardwood (Zhou et al., 2017). The present investigation, however, clarifies that the glucomannan in beech is significantly more reactive than xylan, which suggests that the shoulder in the beech DTG curve is not related to hemicellulose reactivity.

Contrary to this, the degradation behavior of cellulose is different for cedar and beech woods. Cellulose in beech is stable up to ~320 °C, where xylan and glucomannan almost degrade. Thus, thermal degradation of cellulose occurs independently of hemicellulose degradation in the beech wood cell wall. Conversely, cellulose in cedar wood typically degrades together with xylan and glucomannan degradation. Consequently, as indicated in Fig. 3-6, the overlapping temperature ranges for the degradation of cedar cellulose and hemicelluloses leads to one broad DTG peak.

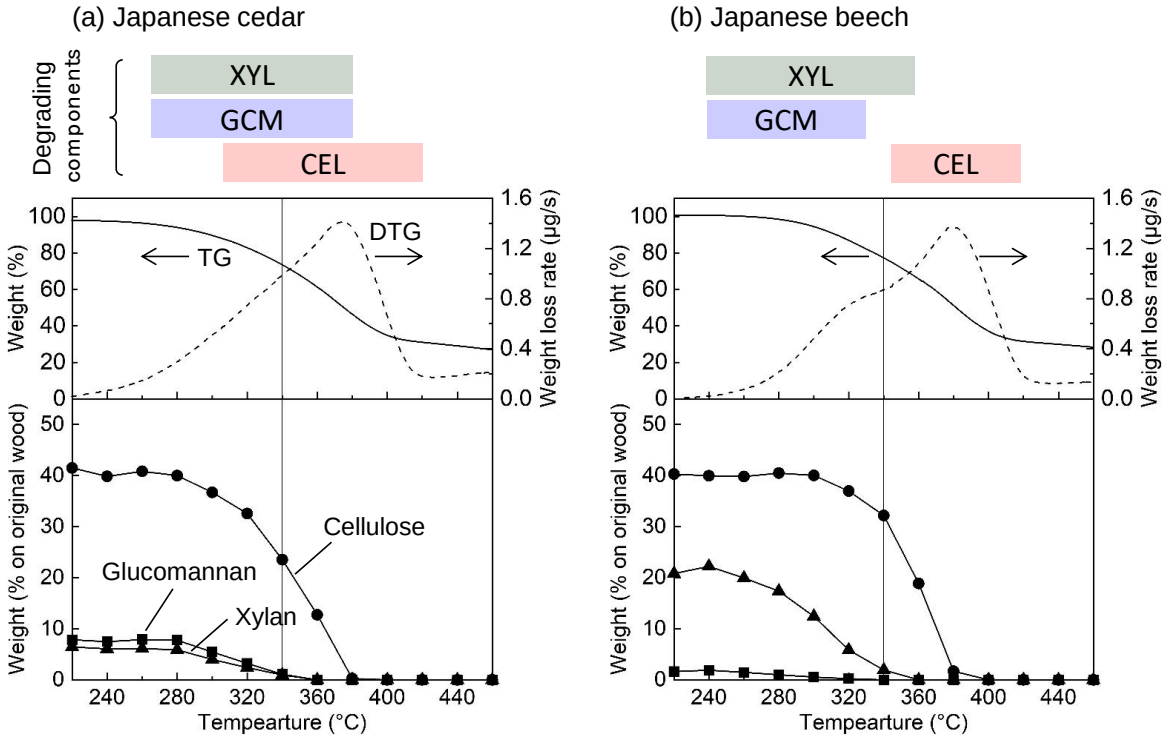

Fig. 3-6 Thermogravimetric (TG)/Derivative TG profiles showing the recovery of cellulose, xylan and glucomannan from: (a) Japanese cedar and (b) Japanese beech woods (only cellulose-originated glucose was counted to determine the glucose yield)

3.3.3 Influence of the cell wall ultra-structure

Esterification with lignin may partially explain the ineffective catalytic activity of 4-*O*-MeGlcA in the wood cell wall. Three types of lignin-carbohydrate complex (LCC) linkages, C□-ester with 4-*O*-MeGlcA, benzyl ether, and phenyl glycoside, Fig. 3-7, are reported in softwood and hardwood cell walls (Balakshin et al., 2011; Du et al., 2014; Takahashi & Koshijima, 1988a; Tarasov et al., 2018; Yuan et al., 2011). This ester formation renders a portion of the 4-*O*-MeGlcA moieties inactive as acid/base catalysts for hemicelluloses and cellulose. Although the esterification rate is not clear presently, free 4-*O*-MeGlcA moieties are suggested to exist in the wood cell wall based on the cation-exchange ability (Asmadi et al., 2017; DeGroot, 1985; Sjöström, Janson, Haglund, & Enström, 1965) and distribution of alkali and alkaline earth metal cations within the cell walls (Saka & Mimori, 1994). Accordingly, some of the 4-*O*-MeGlcA moieties in the cell wall are ineffective, even without the formation of the ester linkages with lignin.

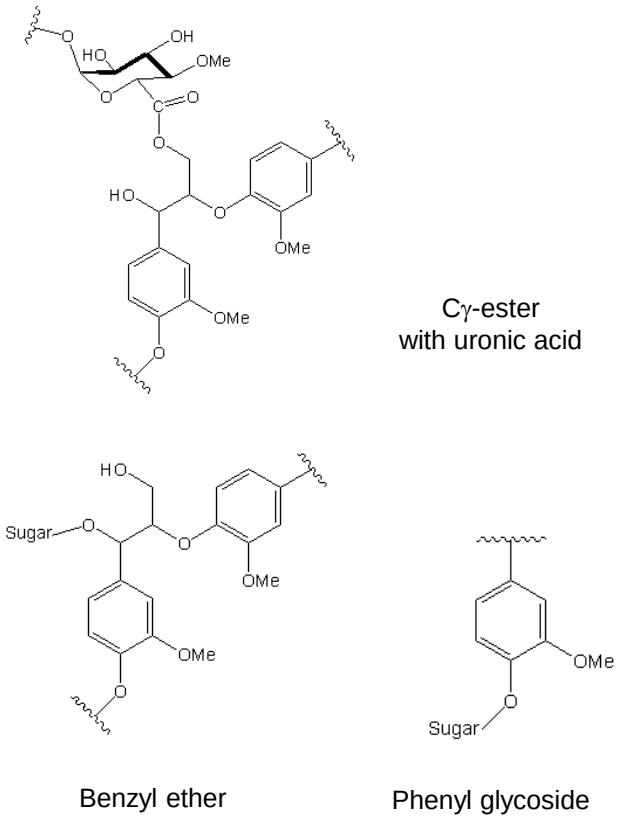

Fig. 3-7 Three types of lignin-carbohydrate complex linkages

Acetyl groups are attached to xylan in beech and glucomannan in cedar, although the isolated hemicelluloses in Fig. 3-5 do not contain any acetyl groups. Such acetyl groups may affect the xylan and glucomannan reactivity in wood cell walls. However, this would not be important because xylans in both woods exhibited similar reactivities.

Xylan and glucomannan are normally involved in the formation of LCC linkages with lignin (Tarasov et al., 2018), indicating that hemicellulose and lignin exist in proximity by the formation of chemical bonds. These structures in the matrix of the wood cell wall may restrict the mobility of the 4-*O*-MeGlcA moieties, although this hypothesis needs to be confirmed by further investigations on the wood cell wall matrix and pyrolytic reactivity. The greater reactivity of glucomannan in beech wood can be explained by this hypothesis; glucomannan exists in the vicinity of 4-*O*-MeGlcA in the beech wood cell wall. Whereas, an attack of the xylose main chain in xylan by 4-*O*-MeGlcA is not possible.

These results will be of significant interest to wood anatomists, as well as researchers in the field of pyrolysis.

The pyrolytic reactivity of cellulose is intrinsically determined by the crystalline nature. The molecules that comprise the nano-crystallites (tens of nm in cross-section) are stable, and hence, the thermal degradation is initiated from the surface molecules (H. Kawamoto & Saka, 2006; D. Y. Kim, Nishiyama, Wada, Kuga, & Okano, 2001; Zickler, Wagermaier, Funari, Burghammer, & Paris, 2007). Prior to the decomposition, there is an "induction period" that is observed to activate cellulose, which led to the concept of "active cellulose" formation (Bradbury, Sakai, & Shafizadeh, 1979; Clawson & Clawson, 1999). The role of the reducing end during the activation of cellulose for thermal discoloration (Matsuoka, Kawamoto, & Saka, 2014) and weight-loss behavior (Matsuoka, Kawamoto, & Saka, 2011) is also suggested. Thus, the cellulose crystallite surface and hemicellulose-lignin matrix interface plays an important role when determining the cellulose reactivity, as illustrated in Fig. 3-8, which is suggested to be different for cedar and beech woods. Degradation of hemicellulose can activate the surface molecules of cedar cellulose, however, this is not observed for beech.

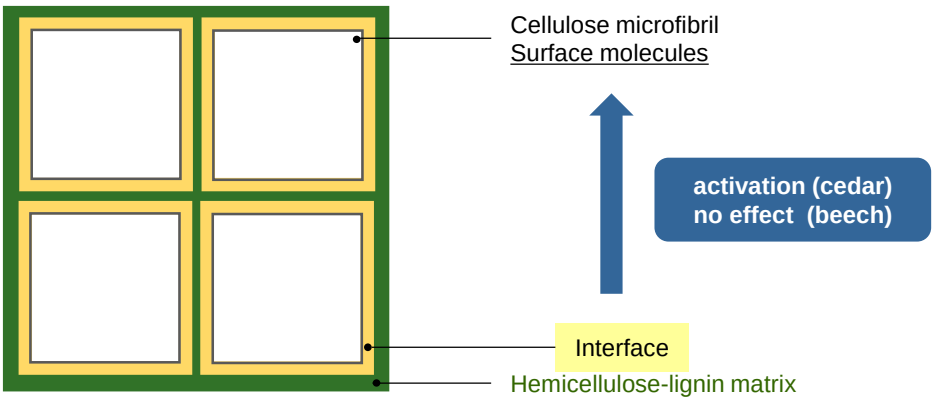

Fig. 3-8 Role of the hemicellulose-lignin matrix and cellulose microfibril surface interface for cellulose reactivity during pyrolysis, which is expected to be different for Japanese cedar and Japanese beech woods

The assembly of cellulose and hemicelluloses in the wood cell walls has received significant attention in the field of wood anatomy, and different arrangements are

proposed for softwood and hardwood cell walls, as illustrated in Fig. 3-9. Strong binding of glucomannan to cellulose in softwood cell walls has been reported (Åkerholm & Salmén, 2001; Kumagai & Endo, 2018; Salmén & Burgert, 2009; Terashima et al., 2009). Based on the results of dynamic mechanical analysis with FT-IR spectrometry, Åkerholm and Salmén (Åkerholm & Salmén, 2001) reported the close connection between cellulose and glucomannan in Norway spruce (*Picea Abies*) wood fibers, although xylan showed no mechanical interaction with cellulose. Kumagai and Endo (Kumagai & Endo, 2018) utilized a quartz crystal microbalance for studying the action of cellulase during enzymatic hydrolysis of lignocellulose nanofibers prepared from Japanese cedar (a softwood) and eucalyptus (a hardwood). The report concluded that cellulose is covered by glucomannan in Japanese cedar, because the removal of glucomannan by the mannase treatment was necessary for cellulase to bind to cellulose. Xylan and lignin are considered to exist between glucomannan-coated cellulose in softwood (Fig. 3-9(a)) (Salmén & Burgert, 2009).

Conversely, in the case of hardwood cell walls, Dammström (Dammström et al., 2009) reported the dynamic FT-IR analysis data of aspen (*Populous tremula*), suggesting that xylan is strongly associated with cellulose, instead of glucomannan in the case of softwood. Association of xylan on cellulose is also used to explain the helicoidal array of cellulose microfibrils; negatively-charged 4-*O*-MeGlcA moieties in xylan attached to the surface of cellulose microfibrils help to maintain the space between the microfibrils yielding a cholesteric mesophase (Reis & Vian, 2004; Reis, Vian, & Roland, 1994; Vian, Roland, Reis, & Mosiniak, 2014). However, there has been controversy because xylan in solution forms a three-fold helical screw conformation, hindering xylan combining with cellulose having a two-fold conformation (Busse-Wicher et al., 2014; Nieduszynski & Marchessault, 1971). Simmons *et al.* (Simmons et al., 2016) reported clear evidence for the binding of xylan to cellulose by solid-state NMR; xylan exhibiting a three-fold helical screw in solution flattens into a two-fold helicoidal screw to intimately bind to cellulose. These observations are also supported by theoretical calculations (Busse-Wicher et al., 2014, 2016; Mikkelsen, Flanagan, Wilson, Bacic, & Gidley, 2015; Pereira, Silveira, Dupree, & Skaf, 2017). These lines of information indicate that xylan binds to cellulose microfibrils instead of glucomannan in hardwood cell walls, as shown in Fig. 3-9(b).

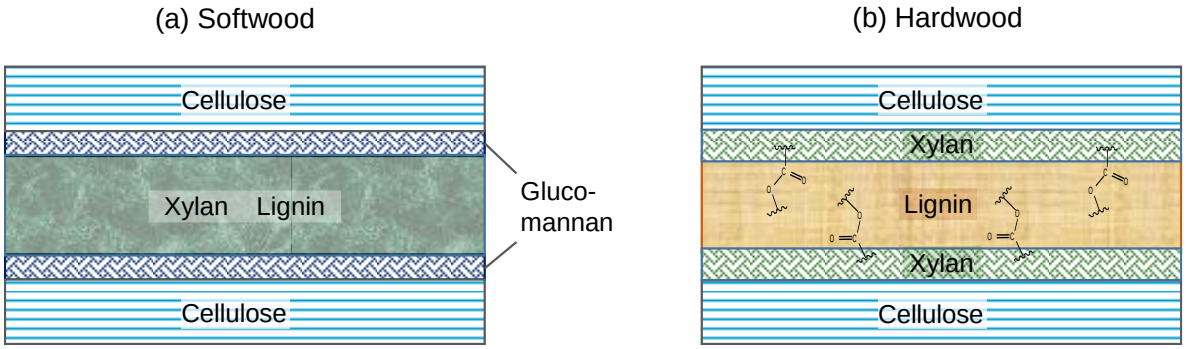

Fig. 3-9 Schematic view of the proposed cell wall arrangements of cellulose, hemicellulose and lignin for softwood and hardwood

The cellulose reactivity of cedar and beech woods may be influenced differently by the variation in the assembly, although elucidation of the detailed mechanisms hitherto is not fully understood. Hence, further information with respect to the wood anatomy is necessary.

3.4 Conclusions

The thermal reactivity of xylan, glucomannan and cellulose in Japanese beech and Japanese cedar woods was investigated. The TG/DTG profiles were assigned from the results obtained herein. The results were also compared with those of isolated xylan and glucomannan, to understand the influence of the cell wall. Xylan is observed to be significantly stabilized in the cell walls of both woods, and the reactivity is similar to that of glucomannan in cedar. Glucomannan becomes unstable in beech. The 4-*O*-MeGlcA moieties and the corresponding salts do not act as acid/base catalysts in the cell walls, except for glucomannan in beech. This observation is partially explained by the ester formation with lignin. The observed differences in the cedar and beech TG/DTG curves do not arise from the differences in hemicellulose reactivity, but from the differences in cellulose reactivity; cellulose decomposes together with hemicellulose in cedar, however, the decomposition occurs independently in beech. The nature of the hemicellulose and

cellulose microfibril assemblies for cedar and beech cell walls are considered as a reason for the different cellulose reactivity in cedar and beech woods.

Chapter 4

Location of uronic acid group in Japanese cedar and Japanese beech wood cell walls as evaluated by the influences of minerals on thermal reactivity

4.1 Introduction

Wood has a heterogeneous cell wall structure consisting of nano-sized cellulose microfibrils surrounded by the hemicellulose–lignin matrix. The types and contents of hemicellulose are different depending on the plant species. In hardwood, xylan is dominant (10–30 wt%) and the content of glucomannan is quite small (3–5 wt%), while softwood contains more glucomannan (14–25 wt%) and less xylan (5–15 wt%) (Haraguchi, 1985). The assembly of hemicelluloses in the matrix has been studied and is suggested to be different in the cell walls of softwoods and hardwoods. Glucomannan has been reported to bind to the surface of cellulose microfibrils in softwood (Åkerholm & Salmén, 2001; Kumagai & Endo, 2018; Maeda, Awano, Takabe, & Fujita, 2000; Terashima et al., 2009), while xylan associates with cellulose in hardwood (Awano, Takabe, & Fujita, 2001; Dammström et al., 2009; Simmons et al., 2016; Vian et al., 2014). Recently, however, xylan is also reported to bind to cellulose in spruce, which is a softwood (Terrett et al., 2019). Thus, the location of hemicellulose in the cell wall has not been completely clarified. Such ultrastructure of cell walls may affect the thermal degradation reactivity of the component polysaccharides.

Thermogravimetric (TG) analysis is frequently used to identify softwood and hardwood species (Shen, Gu, & Bridgwater, 2010b, 2010a; Yang et al., 2007, 2006). Crystalline cellulose is more thermally stable than isolated hemicellulose, which has amorphous properties, so these components are thought to decompose over different

temperature ranges. Pyrolysis of hardwoods occurs in two ranges, depending on the pyrolysis temperature, and gives a characteristic derivative thermogravimetric (DTG) curve with a clear shoulder in the lower temperature range. This shoulder is generally attributed to the degradation of xylan, because isolated xylan is more reactive than glucomannan or cellulose. On the contrary, no clear shoulders are observed on the DTG curves of softwoods. This is thought to be caused by the high content of glucomannan in softwood, which is less reactive than xylan (Shafizadeh et al., 1972; Wang, Ru, Lin, & Luo, 2013b; Wang et al., 2015; Werner et al., 2014).

Our previous study using Japanese cedar (*Cryptomeria japonica*, a softwood) and Japanese beech (*Fagus crenata*, a hardwood) (Wang, Minami, & Kawamoto, 2020) questioned the above interpretation of the DTG curves. Xylan was remarkably stable against pyrolysis in both wood cell walls as compared to isolated xylan and exhibited similar reactivity to glucomannan in cedar. In contrast, glucomannan in beech wood was quite reactive and decomposed at a lower temperature than xylan, which is the opposite of that observed in isolated samples. Therefore, the pyrolysis behavior of hemicellulose in wood cannot be explained by the thermal reactivity of isolated hemicelluloses. The difference in DTG curves between cedar and beech wood was explained by the different thermal decomposition behaviors of cellulose, which was synchronized with hemicellulose degradation in cedar, but was independent in beech.

The 4-*O*-methyl-D-glucuronic acid (4-*O*-MeGlcA) bound to the xylose chain of xylan and its salt act as acid and base catalysts, respectively, during pyrolysis, which can promote the thermal degradation of nearby components. This effect has been confirmed by comparing the thermal reactivities between isolated xylans containing the Na salt of 4-*O*-MeGlcA and demineralized sample with the free carboxylic acid (Wang, Asmadi, and Kawamoto 2018). Given that the catalytic effects of the free acid and the metal salt are different, we considered that the location of 4-*O*-MeGlcA can be established by identifying the components for which the reactivity changes with demineralization. Most of the 4-*O*-MeGlcA in wood are thought to be present as metal salts or esters with lignin (Asmadi et al., 2017; Balakshin et al., 2011; Du et al., 2014; Tarasov et al., 2018). Asmadi et al. (Asmadi et al., 2017) reported a good linear relationship between the amounts of metal cations and uronic acids by using 5 softwood and 5 hardwood species and they

concluded that most of the metal cations bind to uronic acid to form salts. Metal cations can be removed from wood by washing with a weakly acidic solution (Fig. 4-1).

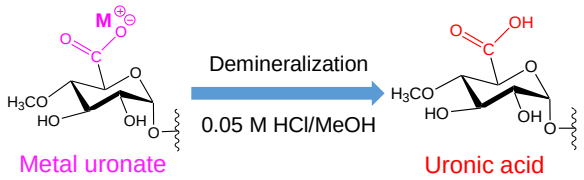

Fig. 4-1 Metal uronate changes to uronic acid by treatment with dilute acidic solution

In the present study, the pyrolytic reactivity of xylan, glucomannan, and cellulose in cedar and beech wood and their demineralized samples were evaluated from the recovery of hydrolyzable sugar after heating to 220–380 °C at a heating rate of 10 °C/min under N_2 flow without a holding period. The TG and DTG curves were measured at the same heating rate of 10 °C/min under N_2 flow and compared with the reactivity results to explain the weight-loss behavior in terms of the degradation of hemicellulose and cellulose. The location of 4-*O*-MeGlcA in beech and cedar wood is discussed based on the present results.

Table 4-1 Metal cation composition of original Japanese cedar and Japanese beech wood

	Content/ ppm				
	Na^+	K^+	Mg^{2+}	Ca^{2+}	Others
Cedar	47	400	100	600	6
Beech	85	830	300	770	18

Others: Cu, Fe, Data from Asmadi et al.

4.2 Experimental

4.2.1 Materials

Wood flour (passing 80 mesh) prepared from the sapwood of Japanese cedar and Japanese beech wood was extracted with acetone using a Soxhlet extractor, and then dried in an oven at 105 °C for 24 h. Following the process of wood demineralization (Asmadi et al., 2017; Hosoya, Kawamoto, & Saka, 2007), wood flour (1 g) was suspended in a solution of 0.05 M HCl in methanol (30 mL) and stirred for 24 h at room temperature. After filtration, the wood flour was washed with distilled water several times until the supernatant became neutral and the residue was dried in an oven at 105 °C for 24 h. The process was repeated twice to ensure the complete removal of metal cations. Complete removal of minerals by this treatment was confirmed with the no residue remaining after incineration of the demineralized sample in air at 600 °C for 2 h. The 0.05 M HCl/MeOH may penetrate into cell walls and remove metal cations from uronate salts. Commercially available beech wood xylan (Megazyme, Wicklow, Ireland) and konjac glucomannan (Carbosynth, Berkshire, United Kingdom) were used as isolated hemicelluloses (Wang et al., 2020).

The characterizations of original and demineralized wood samples are described in previous reports (Asmadi et al., 2010, 2017). The metal cation composition of the original wood is summarized in Table 4-1 (Asmadi et al., 2010). K^+ and Ca^{2+} were the major components, and lesser amounts of Mg^{2+} and Na^+ were also present, along with low amounts of Fe and Cu cations. Although the contents of metal cations in the demineralized wood samples were not determined, previous report of our laboratory shows the reduction rates by using the similar demineralization procedure: content (ppm) 1100 to 15 (K), 100 to 42 (Na), 780 to 64 (Ca), 280 to 3.8 (Mg) for Japanese cedar wood (Takashi Hosoya et al., 2007).

4.2.2 TG analysis

TG analysis was conducted using a TGA-50 instrument (Shimadzu, Kyoto, Japan). Wood flour (1 mg) was placed into a platinum pan and heated from room temperature to 800 °C at a heating rate of 10 °C/min under a N_2 flow of 10 mL/min (purity: 99.9998%, Japan Fine Products, Mie, Japan). N_2 was first passed through a deoxygenation column (GL Sciences, Tokyo, Japan) to remove any oxygen contamination.

4.2.3 Pyrolysis

The experimental setup used in this research is illustrated in Fig. 4-2, and the experimental procedure is described in detail in a previous report (Wang et al., 2020). A quartz glass tube (internal diameter 15 mm, length 400 mm, wall thickness 1.5 mm) was placed in an electric furnace (Asahi-Rika Seisakusho, Chiba, Japan). For each experiment, the sample (20 mg) was placed in a ceramic boat (As One, Osaka, Japan), which was then placed in the center of the glass tube. Thereafter, the air inside the glass tube was displaced by a N_2 flow (100 mL/min) for 5 min using a mass flow controller (SEC-400MK3; Horiba, Kyoto, Japan). The sample was subjected to heat treatment at a set temperature (220–380 °C, at 20 °C intervals), at a heating rate of 10 °C/min, which was the same heating rate used for TG analysis. The sample temperature was directly measured during the pyrolysis experiment by contacting the tip of a fine thermocouple (0.25 mm in diameter, type K, Shinnetsu, Ibaraki, Japan) to the sample and the data were recorded with a thermologger (AM-8000, Anritsu, Kanagawa, Japan). When the temperature reached the designated temperature, the cover of the electric furnace was opened, and the glass tube was immediately cooled to room temperature under a flow of air.

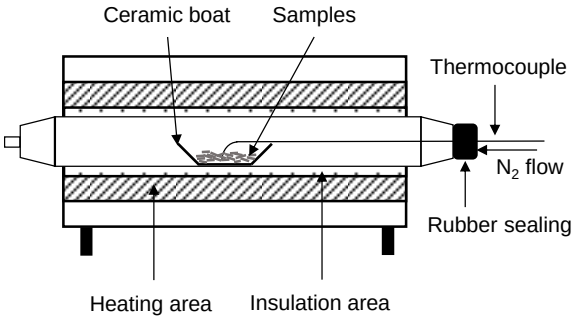

Fig. 4-2 Experimental setup

Pyrolysis was repeated several times for each condition to confirm the reproducibility. The data are shown as average values. The amounts of unreacted hemicellulose and cellulose remaining in heat-treated wood samples were evaluated by the yields of hydrolyzable sugars.

4.2.4 Determination of hydrolyzable sugars

Hydrolyzable sugars were determined according to the procedure described in a previous report (Wang et al., 2020). Acid hydrolysis was used to convert cellulose in the heat-treated wood into glucose (Harris et al., 1985). Hydrolysis was performed in 0.3 mL of 72% H_2SO_4 solution at 30 °C for 1 h. The mixture was diluted with 8.4 mL of water and heated to 120 °C (in an autoclave) for 1 h. After neutralization by elution on a Dionex OnGuard II A cartridge (Thermo Fisher Scientific, Waltham, MA, USA), the glucose yield was determined by high-performance anion-exchange chromatography using a Prominence chromatograph (Shimadzu, Kyoto, Japan) equipped with an electrochemical detector (Decade Elite, Antec Scientific, Zoeterwoude, Netherlands). The separation conditions were: column, CarboPac PA1 (4 x 250 mm); eluent, 85% distilled water/15% 0.2M NaOH; column oven temperature, 35 °C.

Mild methanolysis was conducted to determine the yields of the hydrolyzable sugars from hemicellulose, pectin, and uronic acid as methyl glycosides (Asmadi et al., 2017; Bertaud et al., 2002; Bleton et al., 1996; Li et al., 2007). Methanolysis was performed in 2 M HCl in methanol (KOKUSAN CHEMICAL, Tokyo, Japan) at 60 °C for 16 h. After neutralization with pyridine, the methanolysis products were trimethylsilylated with pyridine, hexamethyldisilazane, and trimethylchlorosilane at 60 °C for 30 min. The products were analyzed by gas chromatography–mass spectrometry (QP-2010 Ultra; Shimadzu, Kyoto, Japan). The instrumental conditions were: column, CPSil 8CB (30 m × 0.25 mm i.d.; Agilent, Santa Clara, CA, USA); injector temperature, 260 °C; split ratio, 1:50; column temperature, 100 °C (2 min), 4 °C/min to 220 °C, 220 °C (2 min), 15 °C/min to 300 °C, 300 °C (2 min); carrier gas, helium. The signals originating from hemicellulose and 4-*O*-MeGlcA were assigned based on the associated mass spectra and retention times, as compared with literature data (Bertaud et al., 2002; Bleton et al., 1996; Mejanelle, Bleton, Tchapla, & Goursaud, 2002; Sundberg et al., 1996).

4.3 Results and discussion

4.3.1 TG / DTG profile

Figure 4-3 illustrates the TG/DTG profiles measured for the original and demineralized cedar and beech wood samples. The different DTG curves in shape of the original cedar and beech wood samples are maintained after the demineralization treatment; a shoulder is clearly visible in the beech DTG curves, but not in the cedar DTG curves. This difference were explained in our previous study (Wang et al., 2020) in terms of the different thermal degradation behaviors of hemicellulose and cellulose in wood. Hemicellulose and cellulose degrade independently in beech wood, but degrade together in cedar wood. Thus, such characteristic behaviors were not changed by demineralization. However, for both wood types, the TG/DTG curves shifted to the higher temperature side by demineralization, indicating that some components of wood are stabilized by changing the 4-*O*-MeGlcA moiety from metal uronate to free acid. The temperature range in which the weight loss of cedar wood occurred was narrowed by demineralization, which was different from the behavior of beech wood.

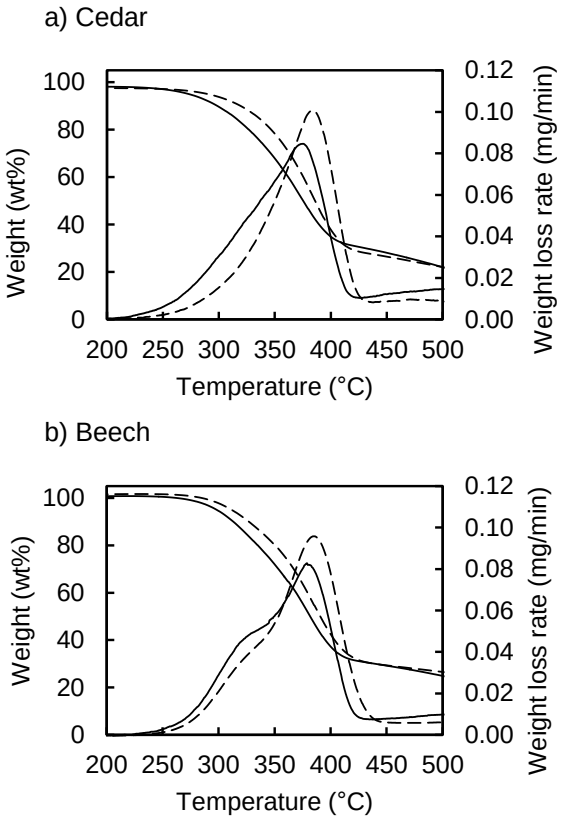

Fig. 4-3 TG/DTG curves obtained for original (—) and demineralized (---) Japanese cedar and Japanese beech wood

4.3.2 Reactivity of hemicellulose and cellulose in wood

To understand the decomposition of hemicellulose and cellulose during pyrolysis, the hydrolyzable sugar was recovered from wood samples that were pyrolyzed at each temperature between 220 °C and 380 °C. By using the same heating rate of 10 °C/min to TG analysis, the results of TG analysis can be discussed in terms of the degradation of hemicellulose and cellulose. The recovery of mannose indicates the stability of glucomannan, because all determined mannose is derived from the glucomannan remaining in the pyrolyzed wood. Xylose recovery shows the stability of xylan for the same reason. However, glucomannan also contains glucose as a constituent sugar, so some adjustment is required to assess the reactivity of cellulose. The amount of cellulose-derived glucose was determined by subtracting the amount of glucomannan-derived glucose, assuming that the sugar composition of glucomannan is mannose: glucose = 3:

1 (Timell, 1967; Tyminski & Timell, 1960) and both units have the same thermal degradation reactivity.

The remaining amounts of xylan, glucomannan, and cellulose in pyrolyzed wood, which was determined from the recovery of hydrolyzable sugar and the composition of the original and demineralized wood, are plotted against the pyrolysis temperature in Fig. 4-4 and compared with the DTG curves. Weight loss caused by the thermal degradation of lignin was also involved in these DTG curves, but the contribution was small because of the properties of lignin, which tends to be converted to char (Asmadi et al., 2011; Haruo Kawamoto 2017; Wang et al. 2009).

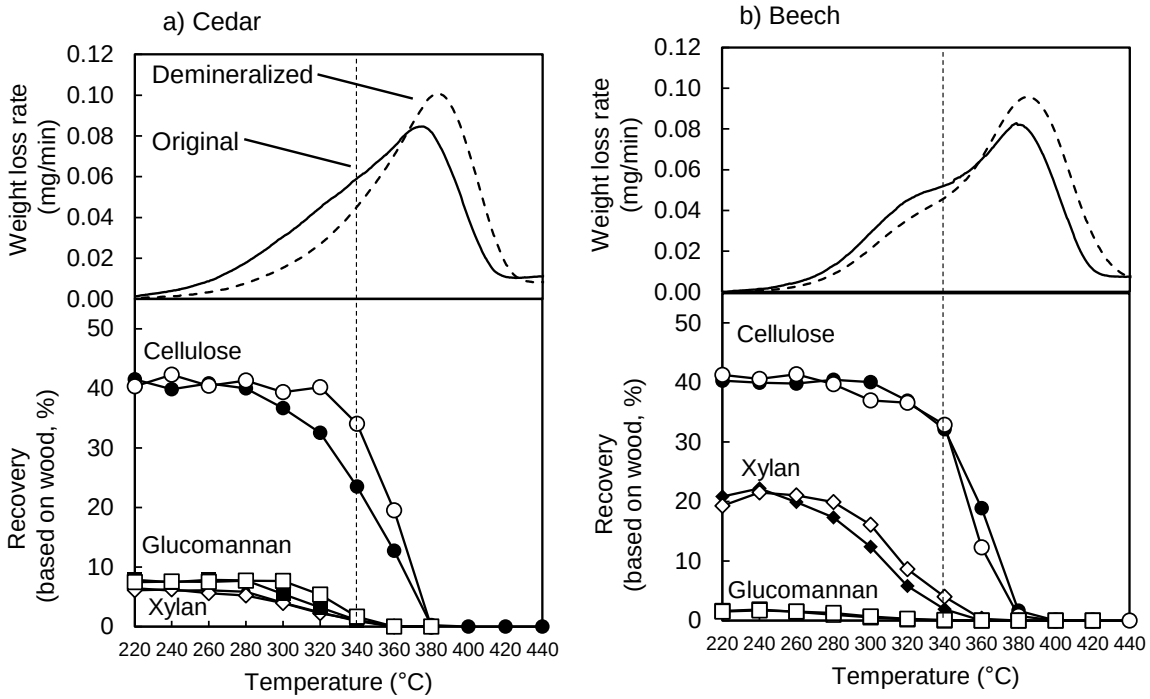

Fig. 4-4 Comparison of the DTG curves with the recovery ratios of cellulose (●: original, ○: demineralized), xylan (◆: original, ◇: demineralized) and glucomannan (■: original, □: demineralized), which were evaluated from the hydrolyzable sugars in pyrolysis of original and demineralized Japanese cedar and Japanese beech wood

Although the effect of demineralization on the pyrolytic reactivity of cellulose in beech wood was very limited, the cellulose in cedar wood was stabilized by

demineralization. For cedar hemicellulose, glucomannan was stabilized, but the xylan reactivity was not affected. These results are surprising because the 4-*O*-MeGlcA moiety is bound to xylan. Based on these results, we concluded that the 4-*O*-MeGlcA is close to glucomannan and cellulose in cedar instead of the xylose units of xylan. Consequently, the shift of the TG/DTG curves of cedar wood by demineralization is explained by the change in reactivity of cellulose and glucomannan. The narrowing of the temperature range in which cellulose and glucomannan in cedar wood decompose is consistent with the above-mentioned trend in the TG/DTG curves of cedar wood.

The influence of demineralization of beech wood were very different from that of cedar wood. By demineralization, the degradation temperature of xylan in beech wood was shifted to lower temperature, but the influence on the reactivity of cellulose was small. Therefore, changes in the TG/DTG curve of beech wood are mostly explained by changes in the reactivity of xylan in the temperature range of 260–340 °C. This is reasonable because the 4-*O*-MeGlcA is bound to xylan. Because of its low content, the contribution of glucomannan to the TG/DTG curve is very small in beech wood.

In Fig. 4-5, the recovery of xylose, mannose, and 4-*O*-MeGlcA, normalized as 100% for untreated samples, is compared with that of isolated glucomannan (Wang er al., 2020) and xylan (Wang et al., 2018), which were reported in previous work. These comparisons provide an understanding of the thermal reactivity of xylan, glucomannan, and 4-*O*-MeGlcA moieties in xylan in wood compared with isolated hemicellulose. The isolated xylan contained a sodium salt of 4-*O*-MeGlcA, which was converted to a free acid by demineralization (Wang et al., 2018). Demineralized konjac glucomannan was not shown, since it does not contain any acidic groups.

The isolated xylan was more reactive than glucomannan because of the influences of 4-*O*-MeGlcA (acidic) and its sodium salt (basic). As already mentioned, xylan (xylose unit and 4-*O*-MeGlcA) was remarkably stable in both wood types and exhibited similar reactivity to glucomannan in cedar. This trend was not changed by demineralization in both woods, indicating that minerals contained in wood do not play a critical role in the stabilizing effects of xylan in the cell walls.

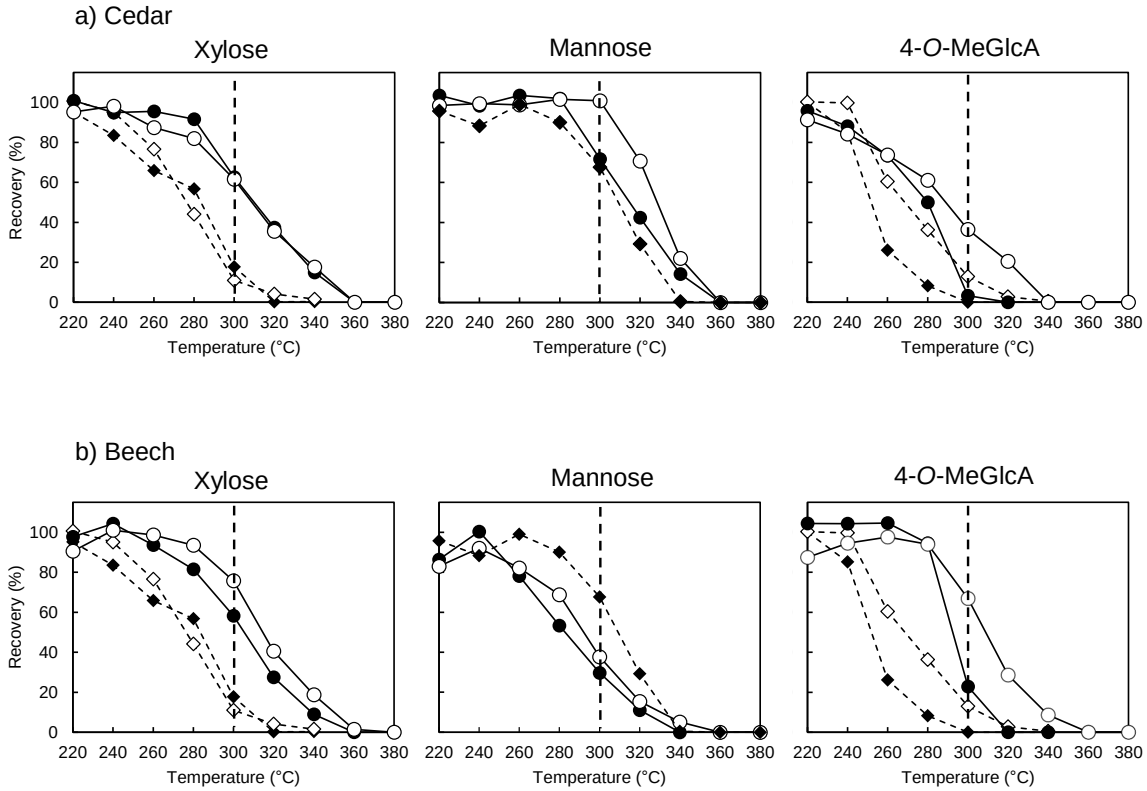

Fig. 4-5 Changes in recovery ratios of xylose, mannose and 4-*O*-MeGlcA determined from the methanolysis of original (●) and demineralized (○) cedar and beech wood after pyrolysis (solid lines), as compared with those from isolated xylan and glucomannan (dashed lines) after pyrolysis (◆: original, ◇: demineralized)

The beech xylan was slightly stabilized by demineralization, although the reactivity of cedar xylan did not change. These results indicate that the 4-*O*-MeGlcA moiety bound to xylan affects the thermal degradation of xylose units in beech, but not in cedar. Although this result is difficult to explain based on our current knowledge, it is possible that the 4-*O*-MeGlcA of cedar xylan may not have access to the xylose units (for some unknown reason). Nevertheless, these effects of 4-*O*-MeGlcA are far less than the differences observed in the pyrolysis of wood and isolated xylan.

The glucomannan reactivity was very different for cedar and beech, because the glucomannan in beech wood was more reactive than isolated glucomannan, as described in our previous report (Wang et al., 2020). The reactivity in beech was slightly reduced by demineralization, but was still much greater than that in isolated glucomannan. Therefore, it is suggested that the 4-*O*-MeGlcA is close to glucomannan and affects the

thermal reactivity, which may improve the reactivity of glucomannan in beech wood, unlike in cedar.

As described earlier, the cedar glucomannan was stabilized by demineralization, especially in the temperature range of 300–320 °C. This temperature range is close to the range in which the reactivity of 4-*O*-MeGlcA decreased by demineralization. Although some detail is lacking at this point, it appears that the stabilization of glucomannan may be related to the altered reactivity of the 4-*O*-MeGlcA. It is suggested that the location of glucomannan in both wood types is close to the 4-*O*-MeGlcA, but the reactivity is very different in cedar and beech. Accordingly, other factors must be considered to explain these different reactivities.

The reactivity of the 4-*O*-MeGlcA was different for cedar and beech wood. It was quite stable over the relatively low temperature range of 220–280 °C in beech, but degraded in cedar. Explanation of these differences is difficult at present, but the environment around the 4-*O*-MeGlcA in wood is likely to differ between cedar and beech. As described above for cedar wood, by demineralization, the 4-*O*-MeGlcA in both wood types was stabilized in the temperature range of 300–320 °C.

4.3.3 Location of uronic acid in cellulose and hemicellulose aggregates in cell wall

The wood cell wall polysaccharides influenced by demineralization are summarized in Table 4-2. The 4-*O*-MeGlcA bound to xylan may be near the affected component. The most interesting finding is the effect on cedar wood, indicating that the 4-*O*-MeGlcA is closer to cellulose and glucomannan. In softwood cell walls, glucomannan is thought to bind strongly to the surface of cellulose microfibrils (Terashima et al., 2009). If this is true, it cannot explain the effects of demineralization observed in this study. Instead of the previous model, a new model shown in Fig. 4-6 (a) is proposed to explain the present results. In this model, 4-*O*-MeGlcA bound to xylan is placed between cellulose and glucomannan, although the amount of 4-*O*-MeGlcA is unknown.

Table 4-2 Summary of the influences of demineralization on thermal reactivities of cellulose, hemicelluloses and uronic acid in pyrolysis of Japanese cedar and Japanese beech wood

	Cellulose	Xylan	Glucoma -nnan	Uronic acid
Cedar	++	nd	++	++
Beech	nd	+	+	++

nd: not detected

+ and ++ : degree of stabilization by demineralization

The association of xylan with cellulose has been shown to explain the formation of helicoid-type arrays of cellulose microfibrils in the cell wall (Simmons et al., 2016). Cellulose microfibrils surrounded by xylan can be moved to place helicoid arrays by repulsion between negatively charged 4-*O*-MeGlcA. Very recently, Terrett et al. studied the polymer interactions in never-dried cell walls of spruce, a softwood, using ^{13}C multidimensional solid-state nuclear magnetic resonance spectroscopy. They proposed a new molecular architecture of softwood, in which both glucomannan and xylan bind to the surface of cellulose microfibrils (Terrett et al., 2019). This is consistent with the model in Fig. 4-6 (a), and these lines of literature information support the current research proposal. As mentioned earlier, however, there are still many unknowns about the thermal reactivity of hemicellulose and cellulose in cedar wood. Lignin may be involved in these unique thermal properties, which we will discuss elsewhere.

Regarding the assembly of beech wood cell walls, the observed influences of demineralization on the reactivity of xylan and glucomannan indicate the close proximity of these components, as illustrated in Fig. 4-6 (b). A notable property in beech wood was the significantly improved reactivity of glucomannan, while xylan containing the 4-*O*-MeGlcA was stabilized. To explain these characteristics, the 4-*O*-MeGlcA needs to be placed in a specific position in the aggregate. Lignin and lignin–carbohydrate complex linkages such as Cγ-ester with 4-*O*-MeGlcA, benzyl ether, and phenyl glycoside are considered to tighten the aggregate structure. This will also be discussed elsewhere.

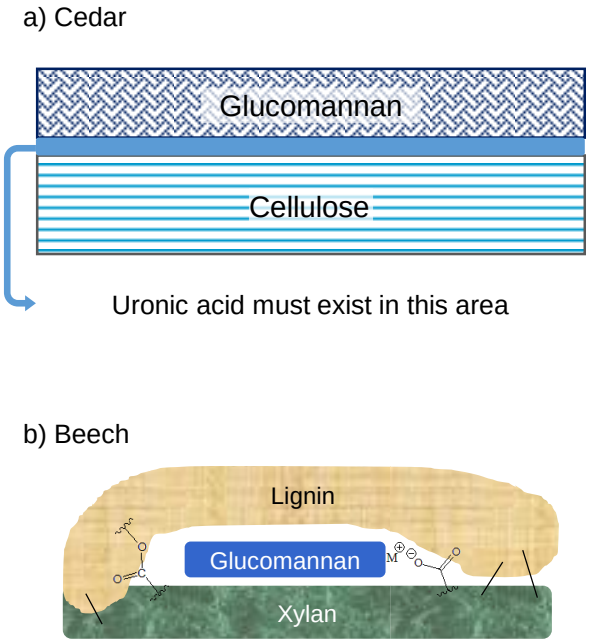

Fig. 4-6 Location of uronic acid groups in cell walls as proposed for cedar (a) and beech (b) wood based on the present results

4.4 Conclusions

The influences of minerals in cedar and beech wood were investigated to understand the location of the 4-*O*-MeGlcA in wood cell walls and the influences on the pyrolytic reactivity of hemicellulose and cellulose in wood. The following conclusions are obtained:

1. The TG/DTG curves shifted to higher temperature with demineralization treatment. This was caused by changes in the reactivity of cellulose and glucomannan in the case of cedar, but was related to changes in the reactivity of xylan and glucomannan in the case of beech.

2. When compared with the reactivity of isolated hemicellulose, xylan was significantly stabilized in both wood types, but glucomannan was more reactive in beech wood. These trends did not change with demineralization treatment.

3. The effects of demineralization indicated the location of the 4-*O*-MeGlcA, which was close to glucomannan and cellulose in cedar, but was close to glucomannan and xylan in beech.

4. The cell wall structures of cedar and beech wood were discussed with reference to the arrangement of hemicellulose and cellulose. However, it is considered that the arrangement in cedar wood is complex and many unknowns remain concerning the thermal reactivity of hemicellulose and cellulose.

Chapter 5

Effect of delignification on thermal degradation reactivities of hemicellulose and cellulose in wood cell walls

5.1 Introduction

The thermal degradation reactivities of component polymers in wood provide a fundamental basis for understanding the pyrolysis of wood and other lignocellulosic biomasses as well as the changes in the physical properties of wood due to heat treatment. Isolated polymers have been used to study thermal degradation reactivity and pathways. Moreover, our previous study (Wang et al., 2020) using Japanese cedar (*Cryptomeria japonica*, a softwood) and Japanese beech (*Fagus crenata*, a hardwood) showed that the thermal degradation reactivities of cellulose and hemicellulose differed substantially between the wood cell walls and isolated samples. Isolated xylan was more reactive than isolated glucomannan owing to the catalytic action of 4-*O*-methyl-D-glucuronic acid (4-*O*-MeGlcA) groups bound to the xylose chain (Wang et al., 2018), but the xylan reactivity was substantially reduced in the cell walls of both woods. The glucomannan reactivity in beech was improved compared with that of the isolated xylan, but this was not observed in the case of cedar.

In addition to the different hemicellulose reactivities, the thermal degradation behaviors of cellulose and hemicellulose were different in cedar and beech woods (Wang et al., 2020). Cellulose and hemicellulose degraded synchronously in cedar wood, while the same components decomposed independently in different temperature ranges in beech wood. These observations reasonably explain the differential thermogravimetric (DTG)

curves for cedar and beech woods. The DTG curve of cedar wood had one wide peak, while one shoulder was clearly visible on the lower-temperature side of the peak in beech wood. This is a common difference between the softwood and hardwood DTG curves (Shen et al., 2010a; Wang et al., 2018; Yang et al. 2007).

To understand the role of 4-*O*-MeGlcA as a catalyst, the location of 4-*O*-MeGlcA in the cell walls was evaluated for cedar and beech, based on the effect of demineralization on thermal degradation reactivity (Wang et al., 2021). Because demineralization converts metal salts (base) into free acids, the components affected by demineralization should be near 4-*O*-MeGlcA. The results showed that 4-*O*-MeGlcA is located near xylan and glucomannan in beech but is located near cellulose and glucomannan in cedar. The latter arrangement cannot be explained by the ultrastructure that has been proposed for softwood cell walls, where glucomannan is tightly bound to the surface of cellulose microfibrils (Åkerholm & Salmén, 2001; Kumagai & Endo, 2018; Terashima et al., 2009). Such an arrangement would affect pyrolysis characteristics, which differ for cedar and beech woods.

Thus, hemicellulose and cellulose are located at specific positions in the cell wall, which determines their reactivities. The next question to be addressed is the influence of lignification on the thermal degradation reactivities of hemicellulose and cellulose in the cell walls. Although the state of existence of lignin in cell walls (e.g., a network or particulate structure) is still controversial (Norgren & Edlund, 2014; Radotić, Mićić, & Jeremić, 2005), lignin makes the cell wall a hard material. Lignin–carbohydrate complex (LCC) linkages such as Cγ-ester with the 4-*O*-MeGlcA group, benzyl ether, and phenyl glycoside types (Balakshin, Capanema, & Berlin, 2014; Balakshin et al., 2011; Du et al., 2014; Takahashi & Koshijima, 1988a; Tarasov et al., 2018; Yuan et al., 2011) fix the location of hemicellulose within the cell wall. Furthermore, several researchers (Jin, Katsumata, Lam, & Iiyama, 2006; Nair & Yan, 2015; Zhang et al., 2015) have proposed covalent linkages between lignin and cellulose.

In this study, the influence of lignification on the thermal degradation reactivities of hemicellulose and cellulose was investigated using holocellulose samples prepared by removing lignin from cedar and beech woods. The pyrolytic reactivities of hemicellulose

and cellulose were evaluated according to the recovery of hydrolyzable sugars from the heat-treated holocellulose. As pyrolysis experiments were performed at the same heating rate as that used in the thermogravimetric (TG) analysis, TG/DTG curves were measured for holocellulose samples are used to discuss with the decomposition of hemicellulose and cellulose at each temperature.

5.2 Experimental

5.2.1 Materials

Holocellulose samples were prepared from Japanese cedar and Japanese beech according to the following procedure (Wise, Murphy, & D'Addieco, 1946). A wood sample (25 g, passed through an 80 mesh) was mixed with 1.5 L of 0.2 M acetic acid. Sodium chlorite (10 g) followed by glacial acetic acid (2 mL) was added under stirring, and the mixture was stirred for 1 h at 70 °C–80 °C. The same amounts of sodium chlorite and glacial acetic acid were added every 1 h (four times for softwood, five times for hardwood) to complete the reaction. After centrifugation, the suspended solids were collected and washed with distilled water until the solution became clear, and sodium chlorite was removed. The resulting solid product was washed with acetone to remove water and dried in an oven.

5.2.2 TG analysis

TG analysis (TGA-50, Shimadzu, Kyoto, Japan) was performed on holocellulose samples from Japanese cedar and beech. Each sample (1 mg) was placed in a platinum pan and heated from room temperature to 800 °C at a heating rate of 10 °C/min under a N_2 flow of 10 mL/min (purity: 99.9998%, JAPAN FINE PRODUCTS, Mie, Japan). Before being supplied to the TG equipment, the N_2 gas was passed through a deoxygenation column (Model 1000 O_2 filter, GL Sciences, Tokyo, Japan) to remove oxygen.

5.2.3 Pyrolysis

Figure 5-1 illustrates the experimental setup used in this study. An electric furnace (ARF-20KC, Asahi-Rika, Chiba, Japan) was used to heat the samples. For each experiment, a sample (20 mg) in a ceramic boat (As One, Osaka, Japan) was placed in a quartz glass tube (inner diameter: 15 mm; length: 400 mm; wall thickness: 1.5 mm). N_2 then passed through the glass tube at a flow rate of 100 mL/min for 5 min to replace the air in the glass tube. The N_2 flow rate was maintained by a mass flow controller (SEC-400MK3, Horiba, Kyoto, Japan). The sample was heated to a designated temperature (220 °C–380 °C at 20 °C intervals) at a heating rate of 10 °C/min, the same heating rate used for the TG analysis. The sample temperature was measured directly during the pyrolysis experiment by touching the tip of a fine thermocouple (0.25 mm in diameter) to the sample. When the sample temperature reached the designated temperature, the cover of the electric furnace was opened and the glass tube was immediately cooled to room temperature under an airflow.

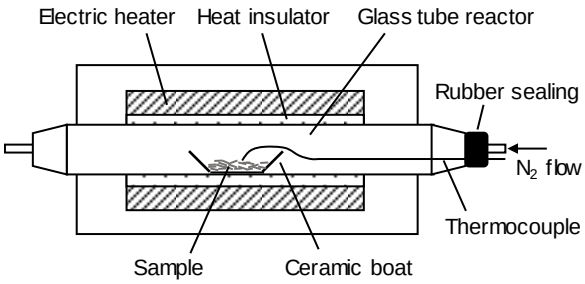

Fig. 5-1 Experimental setup

5.2.4 Hydrolyzable sugar analysis

Acid hydrolysis and methanolysis were separately conducted to convert cellulose and hemicellulose/pectin in the heat-treated samples into sugars and methyl glycosides, respectively. Hydrolysis was performed by treating each sample together with the ceramic boat with 0.3 mL of an aqueous 72% H_2SO_4 solution at 30 °C in a sealed glass vial for 1 h in a water bath and shaking several times. Then, 8.4 mL of water was added and the mixture was heated in an autoclave at 120 °C for 1 h to complete the hydrolysis reaction. The mixture was filtered, and an aliquot of the filtrate was diluted 15 times with water; this was then neutralized with a Dionex OnGuard II A cartridge (Thermo Fisher Scientific,

MA, USA). The glucose yield was determined via high-performance anion-exchange chromatography using a Prominence system (Shimadzu, Kyoto, Japan) equipped with an electrochemical detector (DECADE Elite, Antec Scientific, Zoeterwoude, Netherlands). A CarboPac PA1 column (4 mm × 250 mm) was used with an eluent of 85% distilled water/15% 0.2 M NaOH, flow rate of 1 mL/min, and column oven temperature of 35 °C.

Mild methanolysis (Asmadi et al., 2017; Bertaud et al., 2002; Bleton et al., 1996; Li et al., 2007) was conducted to determine the hydrolyzable sugars according to the methyl glycosides from the hemicellulose, pectin, and uronic acid groups. The ceramic boat and heat-treated sample were added to 4 mL of 2 M HCl in methanol solution (KOKUSAN CHEMICAL, Tokyo, Japan) in a sealed glass tube and heated at 60 °C for 16 h to complete the methanolysis reaction. After neutralization with pyridine, a portion of the mixture was mixed with a glucitol/methanol solution as an internal standard and dried under vacuum. Then, the resulting methyl glycoside mixture was trimethylsilylated with pyridine, hexamethyldisilazane, and trimethylchlorosilane. The mixture was analyzed via gas chromatography–mass spectroscopy (GC–MS) using a QP2010 Ultra (Shimadzu, Kyoto, Japan). An Agilent CPSil 8CB column (length: 30 m; diameter: 0.25 mm) was used with an injector temperature of 260 °C, split ratio of 1:50, helium as the carrier gas, and a flow rate of 1.0 mL/min. The column temperature was kept at 100 °C for 2 min, increased at 4 °C/min to 220 °C, kept at 220 °C for 2 min, increased at 15 °C/min to 300 °C, and kept at 300 °C for 2 min. The signals originating from xylose, mannose, arabinose, galactose, and 4-*O*-MeGlcA were assigned based on the associated mass spectra and retention times in the literature (HA and Thomas 1988; Sundberg et al. 1996).

5.3 Results and discussion

5.3.1 TG/DTG profile in terms of component degradation

The TG/DTG curves measured for the holocellulose samples prepared from cedar and beech woods are illustrated in Fig. 5-2. Delignification lowered the temperature range in which weight loss occurred for both woods. In particular, the DTG peak temperatures

were substantially lowered from 379 °C to 341 °C for cedar and from 381 °C to 353 °C for beech. This indicates that the cellulose in wood becomes very reactive when lignin is removed because crystalline cellulose is more thermally stable than amorphous hemicellulose. The shapes of the DTG curves for cedar and beech woods are different because of the different degradation behaviors of cellulose and hemicellulose (Wang et al., 2020); these components degrade together in cedar but independently in beech. Removing lignin changed the shape of the DTG curve for cedar to that for beech: a shoulder can clearly be observed below the peak temperature.

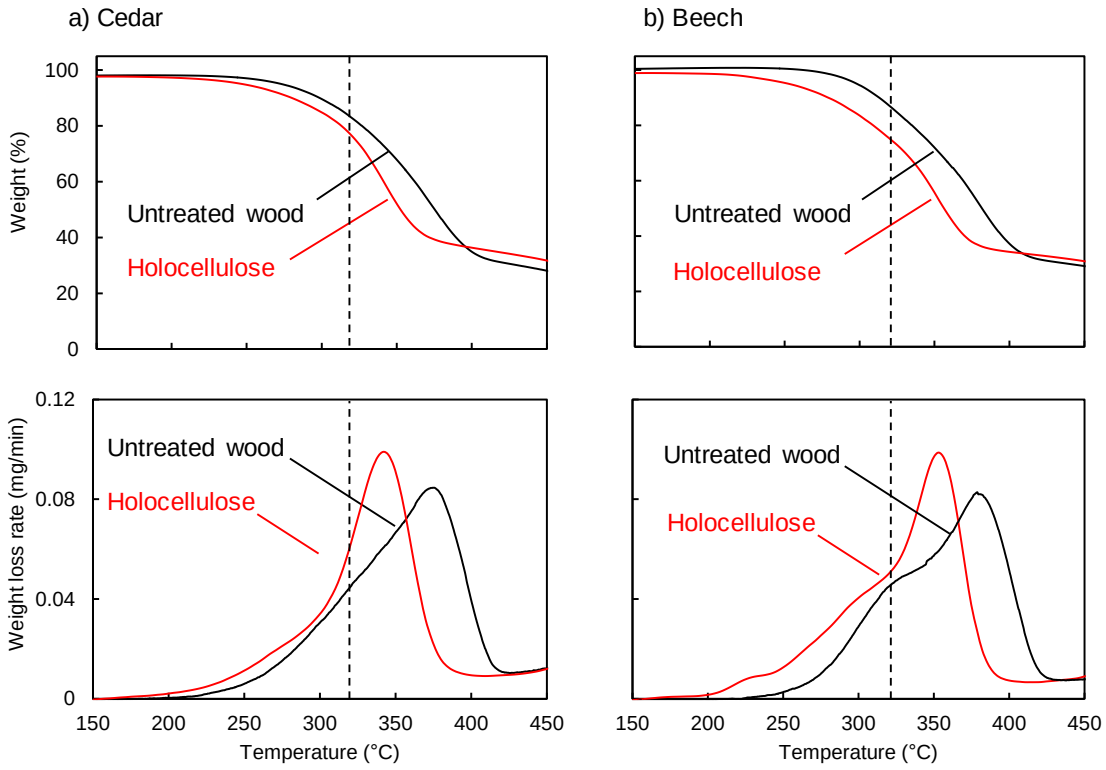

Fig. 5-2 TG/DTG curves of untreated Japanese cedar and Japanese beech wood compared with wood after delignification

To explain the TG/DTG profiles, the thermal degradation reactivities of hemicellulose and cellulose in holocellulose were determined according to the recovery rates of hydrolyzable sugars from heat-treated samples and compared with those of wood samples in previous reports (Wang et al., 2018, 2020). The reactivities of xylan and

glucomannan were directly determined from the recovery rates of xylose and mannose, respectively, because these are the characteristic constituent sugars of these hemicelluloses. However, glucose is produced from cellulose and glucomannan, so the cellulose reactivity was determined according to the cellulose-derived glucose. This was estimated by subtracting the amount of glucose formed from glucomannan under the assumption that the mannose: glucose molar ratio in glucomannan is 3: 1 (Timell, 1967; Tyminski & Timell, 1960) and that both units have the same thermal degradation reactivity.

The amounts of cellulose, xylan, and glucomannan remaining in the pyrolyzed holocellulose were estimated based on the recovery data of the hydrolyzable sugars and their contents in each wood type; the corresponding results are plotted against the pyrolysis temperature in Fig. 5-3. By comparison with the DTG curves, the weight loss behavior during the heating process can be explained in terms of the degradation of cellulose and hemicellulose; this is because the same heating rate as that in the TG analysis was used with no heating time at a constant temperature. The influence of delignification can be discussed by comparing the corresponding figures reported for the pyrolysis of cedar and beech woods.

As indicated by the TG analysis, cellulose reactivity increased when lignin was removed. Although wood cellulose degraded continuously and gradually as the pyrolysis temperature was increased, the cellulose degradation in holocellulose was divided into two modes depending on the pyrolysis temperature. Degradation started at 260 °C–280 °C, and the reactivity increased sharply above 320 °C. In the low-temperature degradation mode (260 °C–280 °C), hemicellulose degraded together with cellulose. Consequently, the polysaccharide components that degraded at the DTG shoulder and peak temperatures could not be clearly separated into hemicellulose and cellulose. Most hemicellulose and 20%–25% of cellulose decomposed below the DTG shoulder temperature (around 320 °C) for both wood types, but the remaining cellulose degraded around the peak temperatures (above 320 °C) after the hemicellulose degraded.

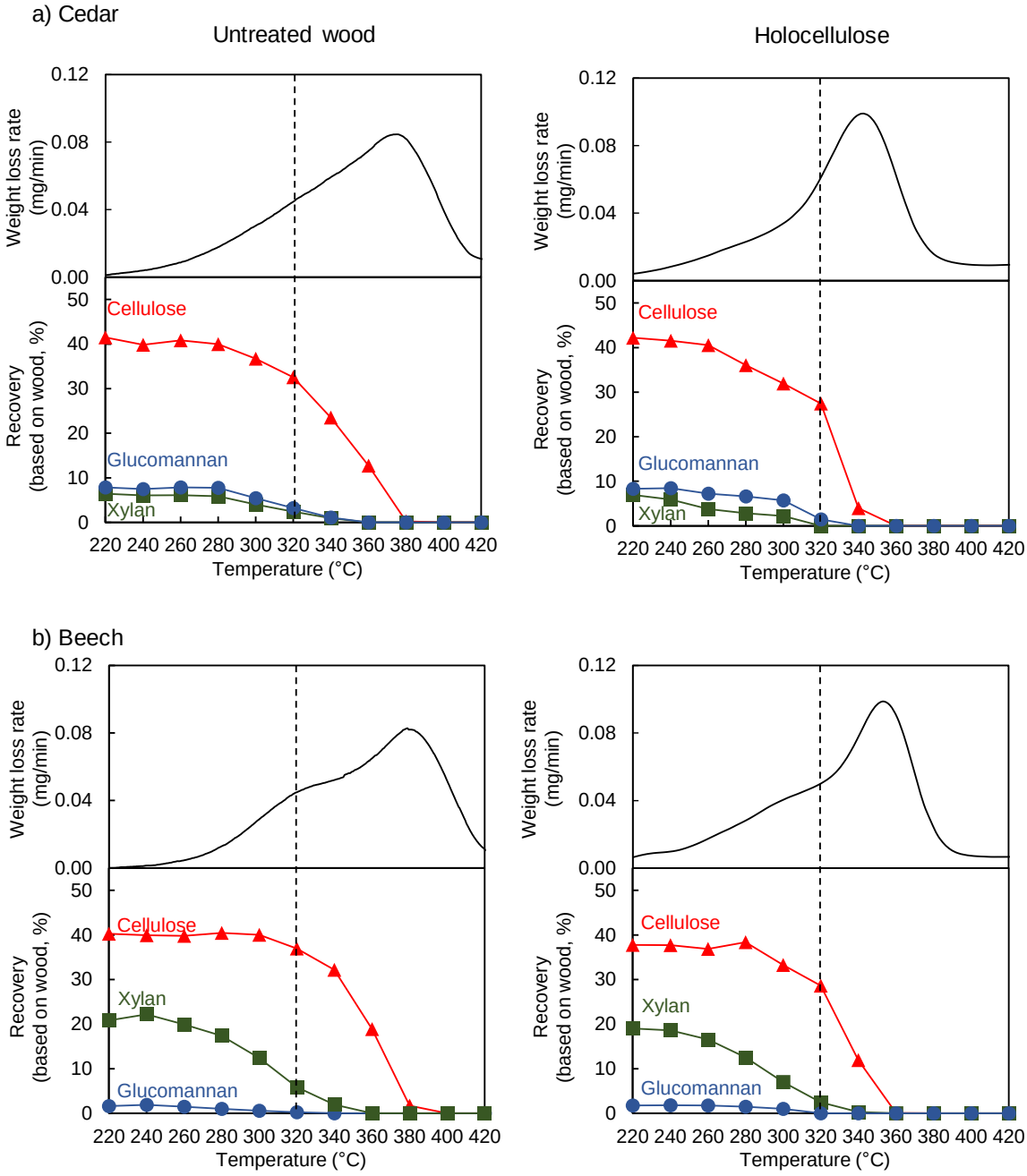

Fig. 5-3 DTG curves with recovery of cellulose (▲), glucomannan (●) and xylan (■) based on the wood content from untreated wood compared with wood after delignification of Japanese cedar and Japanese beech wood

Results of untreated wood were (Wang et al., 2020)

5.3.2 Reactivities of isolated and wood polysaccharides

Figure 5-4 shows the recovery rates of hydrolyzable sugars plotted against the pyrolysis temperature, with holocellulose normalized as 100%. The results for isolated hemicellulose (Wang et al., 2020) and Whatman cellulose are also included for comparison. These plots can be used to discuss the cellulose and hemicellulose reactivities in holocellulose as compared with those of the original wood and isolated samples.

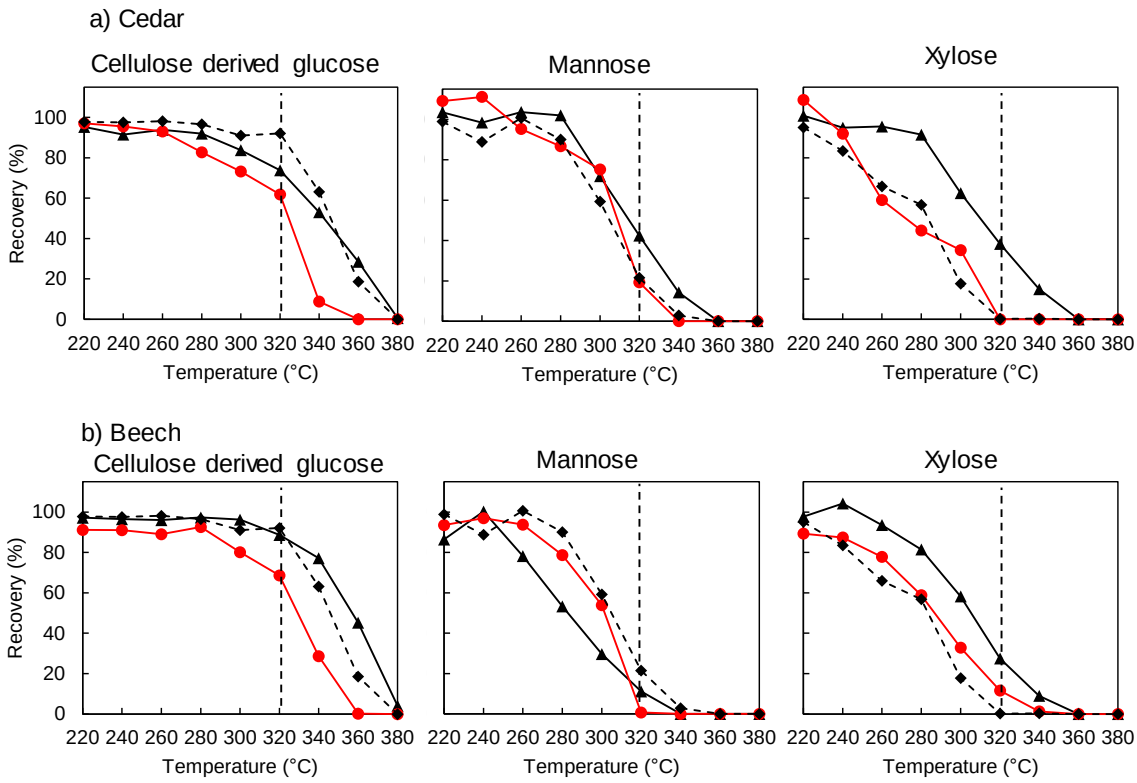

Fig. 5-4 Thermal reactivities of cellulose derived glucose, mannose and xylose from untreated wood (▲), and holocelllulose (●) of Japanese cedar and Japanese beech wood compared with isolated cellulose, xylan and glucomannan (◆)

Whatman cellulose is an example of pure cellulose; it withstood heating up to 320 °C and then degraded rapidly at higher temperatures. The low-temperature cellulose degradation mode as observed for holocellulose at 260 °C–320 °C was not detected. Accordingly, holocellulose is characterized by this low-temperature cellulose degradation, which may be caused by matrix degradation as discussed later. This phenomenon appears

when lignin is removed from wood. It should be noted that the degradation behaviors of cellulose were different in cedar and beech woods but similar in their holocellulose samples.

As described in the previous paper (Wang et al., 2020), the hemicellulose reactivity in wood was different from those of isolated hemicelluloses, and the reactivity varied depending on the type of hemicellulose and wood. Xylan in wood was less reactive than isolated xylan, but glucomannan in beech was more reactive than isolated glucomannan. Removing lignin changed their reactivities to be similar to those of isolated xylan and glucomannan. A similar trend was observed for 4-*O*-MeGlcA, as shown in Fig. 5-5. Thus, lignin plays an important role in determining the thermal reactivities of hemicellulose and cellulose in wood; this role is probably due to the restraints of the specific locations of xylan, glucomannan, and 4-*O*-MeGlcA in the cell walls as discussed later. Removing lignin increases the mobility of these components in holocellulose.

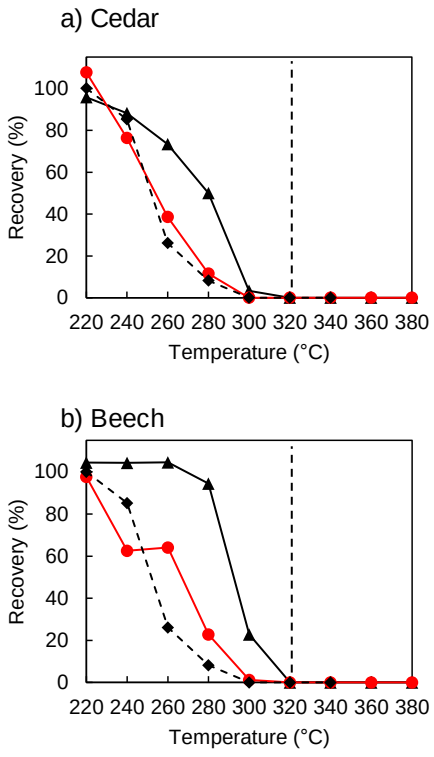

Fig. 5-5 Thermal reactivities of 4-O-MeGlcA from untreated wood (▲) and holocelllulose (●) of Japanese cedar and Japanese beech wood compared with isolated xylan (◆)

The data in Figs. 5-4 and 5-5 are rearranged in Fig. 5-6 to understand the differences depending on the wood type. Although the temperature ranges at which cellulose and hemicellulose decomposed were similar, the shapes of the graphs differ for cedar and beech holocellulose. With cedar holocellulose, the recovery–temperature relationships of mannose and xylose show similar trends. Two reflection points can be observed at 260 °C and 300 °C; this indicates that the reactivity changed at these temperatures. This tendency is not observed for beech holocellulose. Thus, these results indicate that xylan and glucomannan degraded synchronously in cedar holocellulose, and the degradation can be divided into three types depending on the reactivity: <260 °C, 260 °C–300 °C, and >300 °C. The recovery–temperature relationship of cellulose-derived glucose indicates that the degradations of cellulose and hemicellulose occurred synchronously in cedar. The cellulose degradation started around 260 °C, at which point approximately half of the xylan and some glucomannan decomposed. After the rapid degradation of the remaining hemicellulose around 300 °C–320 °C, cellulose quickly degraded at 320 °C–340 °C. Therefore, the characteristic thermal degradation behaviors observed for cedar were maintained when lignin was removed. Unlike for beech holocellulose, the cellulose degradation is intimately related to the hemicellulose degradation in cedar holocellulose.

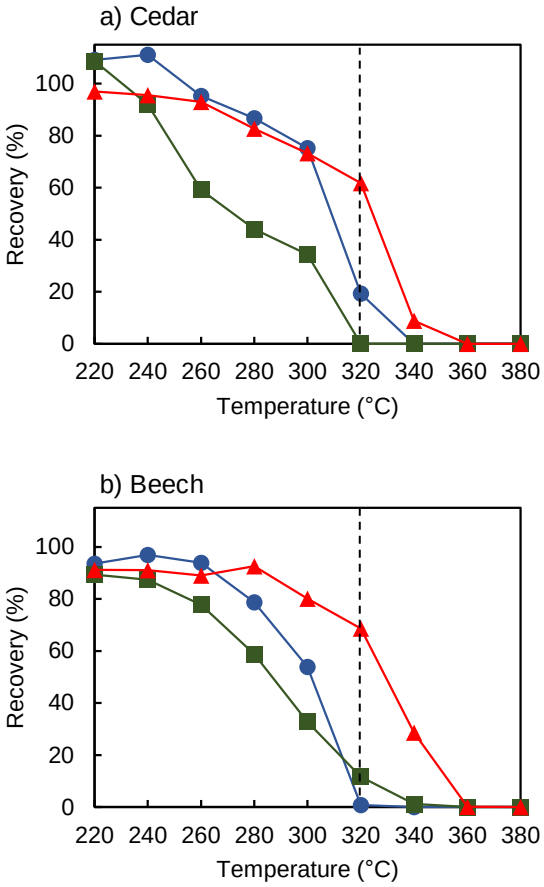

Fig. 5-6 Thermal recovery rate of polysaccharides (glucose: ▲, mannose: ●, xylose: ■) from Japanese cedar and Japanese beech wood after delignification

5.3.3 Role of lignification

On the basis of the present results, the role of lignification in wood pyrolysis is discussed using a schematic of a single cellulose microfibril surrounded by a matrix (Fig. 5-7), although further studies are necessary to confirm the following proposal. Xylan, glucomannan, and 4-*O*-MeGlcA are anchored in specific locations within the matrix. Meanwhile, 4-*O*-MeGlcA and its salts act as acid and base catalysts, respectively (Wang et al., 2018), which increases the thermal degradation reactivity of adjacent components. However, previous experimental results (Wang et al., 2018, 2020) indicated that the catalytic activity is not effective in wood. For example, 4-*O*-MeGlcA is bound to xylan, but the xylan was very stable in both wood samples. Rather, 4-*O*-MeGlcA influences the glucomannan degradation in beech wood. All these features disappeared in holocellulose.

These results can be reasonably explained by considering the role of lignin (lignification), which physically strengthens the ultrastructure formed between hemicellulose and the cellulose interface in the matrix. The formation of LCC linkages (Balakshin et al., 2011; Du et al., 2014; Tarasov et al., 2018) may also be involved in this process.

The thermal degradation of cellulose is known to occur nonuniformly at the crystallite level (Kawamoto and Saka 2006; Kim et al. 2001; Zickler et al. 2007); surface molecules preferentially tend to decompose as internal molecules are more stable owing to stabilization by filling the crystallites. Accordingly, the reactivity of surface molecules plays an important role in the thermal degradation of cellulose (Kawamoto, 2016; Matsuoka et al., 2014; Nomura, Kawamoto, & Saka, 2017), and the matrix and its degradation are expected to affect the reactivity of cellulose microfibrils by affecting the surface cellulose molecules at the interface. This induced cellulose degradation may explain the low-temperature degradation mode of cellulose, which was observed in both types of holocellulose in the temperature range of 260 °C–320 °C (Fig. 5-4).

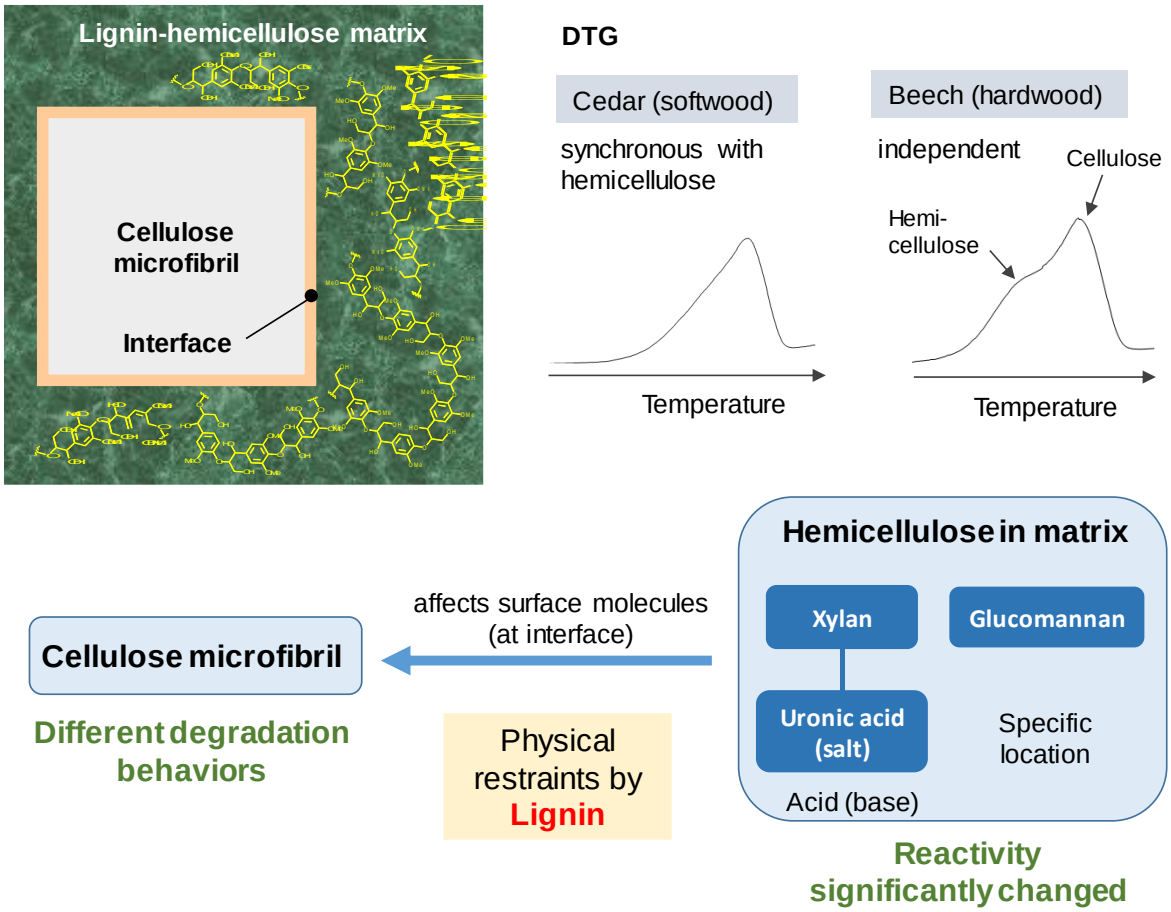

Fig. 5-7 Possible explanation of the effect of lignification on the thermal behavior of cellulose and hemicellulose from softwood and hardwood

In order to understand the effect of low-temperature cellulose degradation (260 °C–320 °C) on the high-temperature cellulose degradation (>320 °C), TG analysis was conducted for holocellulose samples at different heating rates of 1, 5, and 10 °C/min (Fig. 5-8). By decreasing the heating rate, TG and DTG curves shifted to lower temperature side. Although researchers try to explain these shifts with the time lag in temperature measurement (Kan, Strezov, & Evans, 2016), heating rates and sample weight (1 mg) used in the present TG analysis are very small to account for such a large shift (DTG peak temperature: 342 °C → 326 °C → 297 °C (10 °C/min → 5 °C/min → 1 °C/min) for cedar holocellulose, 357 °C → 338 °C → 307 °C (10 °C/min →5 °C/min →1 °C/min) for beech holocellulose).

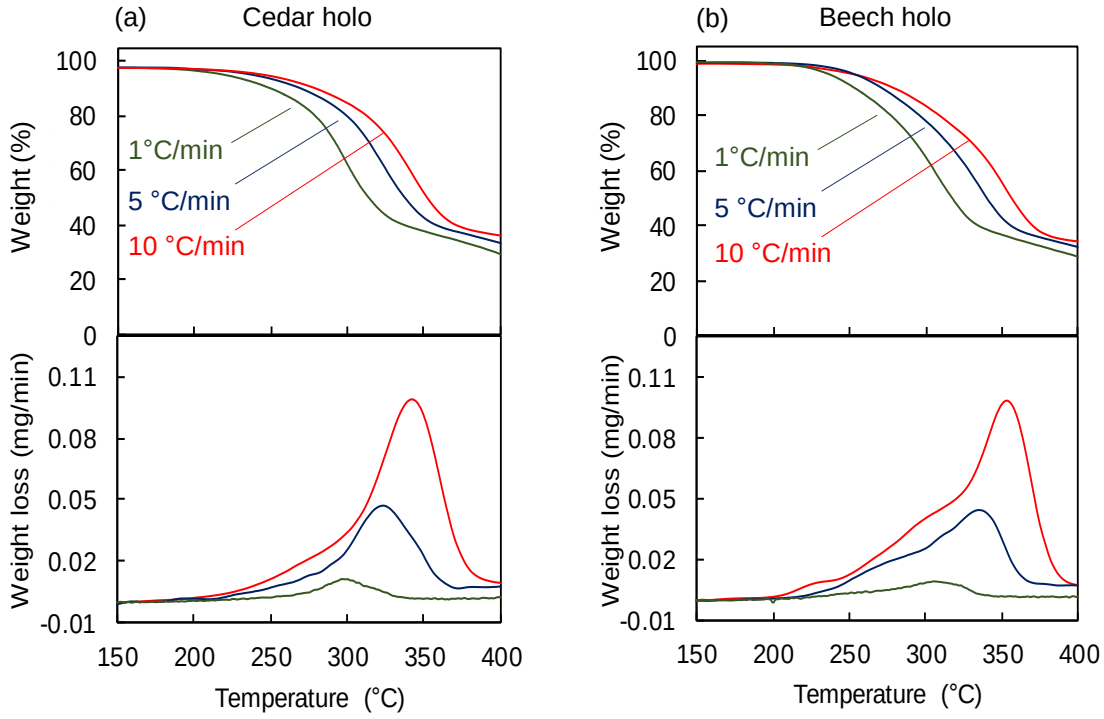

Fig. 5-8 TG/DTG curves measured for (a) cedar and (b) beech holocellulose samples at different heating rates of 1, 5, and 10 °C/min

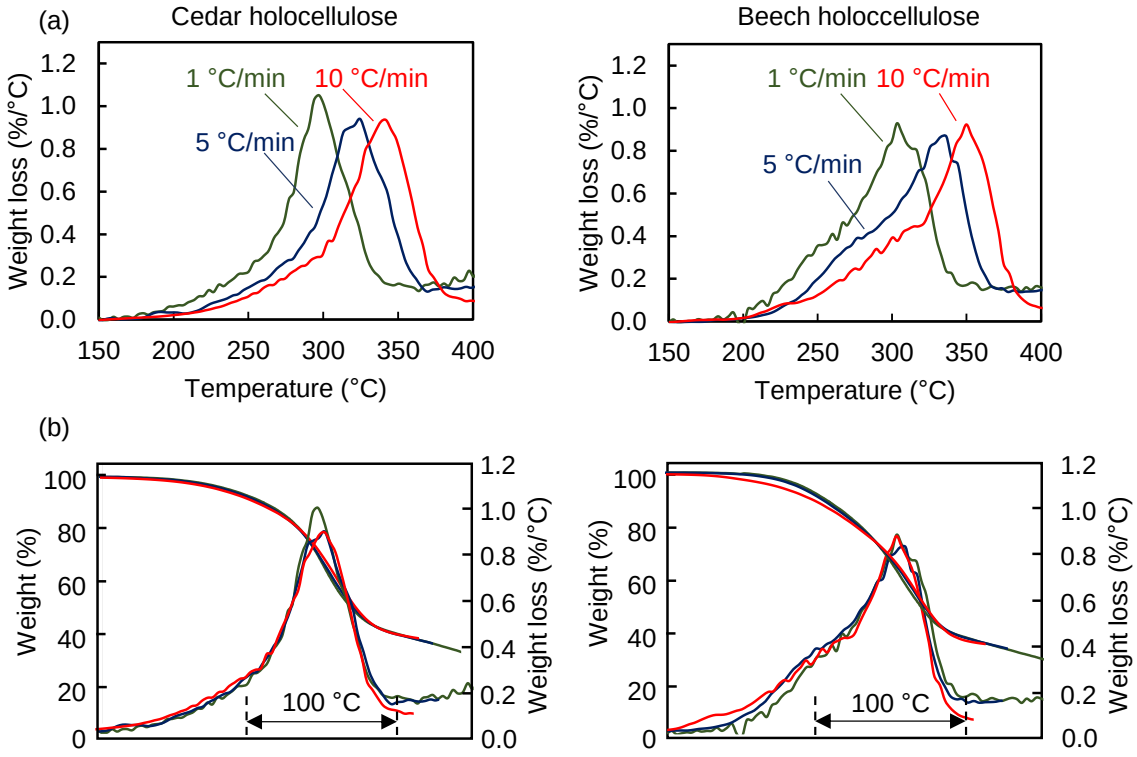

Fig. 5-9 TG/DTG curves of cedar and beech holocellulose samples redrawn with the unit of weight-loss rate changed from mg/min to mg/°C (a) and further moved with respect to the temperature axis so that the peaks of the DTG curves are aligned (b)

By redrawing the TG/DTG curves in Fig. 5-8 with the unit of weight-loss rate changed from mg/min to mg/°C, the appearance of TG/DTG curves becomes very similar (Fig. 5-9a). This is confirmed by Fig. 5-9b, where TG/DTG curves are moved with respect to the temperature axis so that the peaks of the DTG curves are aligned. Surprisingly, these graphs match well. These results lead to a hypothesis; low- and high-temperature modes of cellulose degradation are closely related. Although the temperature range where thermal degradation of cellulose occurs is different depending on the heating rate, once thermal degradation of cellulose begins in low-temperature mode, temperature range of the high-temperature mode of cellulose degradation is determined. Such hypothesis gives insights in understanding cellulose pyrolysis, although further studied are necessary to confirm it.

5.4 Conclusions

The thermal degradation reactivities of cellulose and hemicellulose in cedar and beech holocellulose were investigated via TG analysis and the recovery rates of hydrolyzable sugars. The following conclusions were obtained:

1. The TG/DTG profiles of cedar and beech wood samples were different but became similar for holocellulose when lignin was removed.
2. Removing lignin made the reactivity of hemicellulose similar to that of isolated hemicellulose while increasing the reactivity of cellulose. Additionally, the cellulose degradation can be divided into two modes: low temperature (260 °C–320 °C) and high temperature (>320 °C).
3. The TG/DTG profiles can be explained in terms of the degradation of hemicellulose and cellulose. For both types of holocellulose, 20%–25% of cellulose degraded at the DTG shoulder temperature (<320 °C) with the degradation of hemicellulose, while the remaining cellulose degraded around the DTG peak temperature (>320 °C).
4. Cellulose degraded in response to the hemicellulose degradation in cedar holocellulose, which is in contrast to the results for beech holocellulose. This indicates that cellulose is intimately associated with hemicellulose in cedar and holocellulose.
5. The hemicellulose in cedar holocellulose can be divided into three groups depending on the thermal degradation reactivity: >260 °C, 260 °C–300 °C, and >300 °C.
6. Lignin (delignification) is proposed to have a role in the thermal degradation of cedar and beech woods.
7. These findings provide insights into the research fields of wood pyrolysis and cell wall ultrastructures.

Chapter 6

Thermal degradation reactivity of hemicellulose and cellulose in ball-milled cedar and beech wood

6.1 Introduction

Pyrolysis-based technologies have received significant attention in recent years owing to their potential for converting wood biomass into biofuels and biochemicals (Bridgwater 2012; Wang et al. 2017). Cellulose, hemicellulose, and lignin are the major components of wood, and their thermal degradation reactivities provide the fundamental basis for pyrolysis-based technologies. Cellulose microfibrils are embedded in the hemicellulose-lignin matrix within the nanoscale cell wall structure, whose properties can also affect the thermal reactivity of the wood. However, this relationship has not been fully elucidated because the thermal reactivities of wood components have primarily been investigated using isolated components. Thermogravimetric (TG) analysis is frequently used for such studies, but to our knowledge, the results have not yet been discussed in terms of the degradation of wood components at each temperature.

Our group (Wang et al., 2020) previously evaluated the thermal degradation reactivities of hemicellulose and cellulose in wood by assessing the quantity of hydrolyzable sugars that remained after heat-treating Japanese cedar (*Cryptomeria japonica*, a softwood) and Japanese beech (*Fagus crenata*, a hardwood). The treatment involved conditions similar to those used for TG analysis, no heating time at constant temperatures. Employing this method, the results of TG analysis can be explained by the thermal degradation of wood polysaccharides at each temperature. Isolated xylan degraded at a lower temperature than isolated glucomannan because of the catalytic action of 4-*O*-methyl-D-glucuronic acid (4-*O*-MeGlcA) and its salt (base), which were bound to the xylose chains (Wang et al., 2018). However, the xylans in cedar and beech woods

were stable at lower temperatures and degraded in the temperature range similar to that of isolated glucomannan. In contrast, the glucomannan in beech wood was very reactive (Wang et al., 2020). Therefore, the hemicellulose reactivity in wood is quite different from that of isolated xylan or isolated glucomannan. The thermal reactivity of cellulose in cedar and beech were also different; cellulose degraded together with hemicellulose in cedar wood, but independently in beech wood (Wang et al., 2020).

The distinct thermal degradation reactivities of cedar and beech woods may be attributed to the specific placement of cell wall components. The location of 4-*O*-MeGlcA was evaluated via demineralization, which converts metal salts to free 4-*O*-MeGlcA. The results indicated that it is located near cellulose and glucomannan in cedar wood, but near xylan and glucomannan in beech wood (Wang et al., 2021).

Lignin is believed to play an important role in determining the thermal reactivity of hemicellulose in wood because the reactivities of xylan and glucomannan in wood became similar to those of isolated xylan and glucomannan by removing lignin (Wang et al., 2021b). The different thermal degradation behaviors of cedar and beech woods largely disappeared, and their differential thermogravimetric (DTG) curves adopted similar shapes, although the tendency for hemicellulose/cellulose co-degradation in cedar was maintained. Based on these results, lignification during the biosynthesis of cell walls is considered to (i) introduce enhanced physical restraint and (ii) fix the specific placement of hemicellulose in cell walls, particularly for 4-*O*-MeGlcA.

The thermal degradation of cellulose in cedar and beech woods was improved after delignification (relative to pure cellulose). The thermal degradation of cellulose in holocellulose occurred in two stages depending on the pyrolysis temperature (with some cellulose degrading below 320 °C and the rest degrading at higher temperatures) (Wang et al., 2021b). The improved reactivity may be related to the formation of pores in the matrix when the lignin was removed; however, the details of this activation mechanism are not entirely understood.

Ball milling can disrupt the matrix in wood cell walls, but this process does not remove any components from the wood. Therefore, assessing the effects of ball milling on the hemicellulose and cellulose reactivities in wood can improve our understanding of

the thermal degradation of these components in wood cell walls. Ball milling is a commonly-used method for pretreating wood and other lignocellulosic biomass to improve enzyme reactivity (Hideno, Kawashima, Anzoua, & Yamada, 2013; Piras, Fernández-Prieto, & De Borggraeve, 2019; Sipponen, Laakso, & Baumberger, 2014; Sun & Cheng, 2002) and to separate lignin (Crestini, Melone, Sette, & Saladino, 2011; Fujimoto, Matsumoto, Chang, & Meshitsuka, 2005; Ikeda, Holtman, Kadla, Chang, & Jameel, 2002; Obst & Kirk, 1988). This process is also known to reduce the crystallinity of cellulose (Hideno, 2016; Ling et al., 2019; Mattonai, Pawcenis, del Seppia, Łojewska, & Ribechini, 2018) and cleave the lignin β-ether linkage (Fujimoto, Matsumoto, Chang, & Meshitsuka, 2005; Ikeda, Holtman, Kadla, Chang, & Jameel, 2002) , i.e., the dominant type of linkage. Although several research groups have reported on the TG analysis of ball-milled wood, to our knowledge, this method's impact on the thermal reactivities of cellulose and hemicellulose in wood have not been investigated.

In the present study, cedar and beech wood samples were ball-milled for various amounts of time (ranging from 10 min to 48 h), and the thermal degradation reactivities of the resulting wood samples were investigated using TG analysis. The amount of hydrolyzable sugar remaining in pyrolyzed ball-milled wood was also evaluated after treating samples at a heating rate similar to TG analysis (with no time spent heating at a constant temperature). The effects of the ball milling process on the thermal degradation reactivities of hemicellulose and cellulose are discussed in terms of the cleavage of lignin β-ether linkages, the loss of cellulose crystallinity, and the cell wall ultrastructure.

6.2 Experimental

6.2.1 Preparation and characterization of ball-milled samples

Extractive-free Japanese cedar (*Cryptomeria japonica*) and Japanese beech (*Fagus crenata*) (80 mesh passed), and isolated cellulose (Whatman CF-11, Whatman plc, Maidstone, UK) powders were ball-milled using a vibratory ball mill (VS-1, Chuo Kakohki, Aichi, Japan). Approximately 150 g of each powder was placed in a stainless steel jar (inner diameter = 110 mm, height = 120 mm) with about 450 stainless steel balls (diameter = 12.7 mm), which occupied about 80% of the jar's inner volume. The jar was

sealed with a lid and vibrated for a predetermined, designated time (between 10 min and 48 h). During the ball milling process, the jar was cooled by an outer-layer water-cooled jacket. Ball-milling process was conducted in air, but no extensive oxidation was expected to occur, since literature (Forziati, Stone, Rowen, & Appel, 1950; Schwanninger, Rodrigues, Pereira, & Hinterstoisser, 2004) reports that any differences were not observed in the FT-IR spectra of ball-milled wood samples in nitrogen and in air.

It has been reported that the ball milling process decreases the cellulose crystallinity (Hideno, 2016; Ling et al., 2019; Mattonai et al., 2018) and the degree of polymerization of lignin due to cleavage of the ether linkages (Fujimoto, Matsumoto, Chang, & Meshitsuka, 2005; Ikeda, Holtman, Kadla, Chang, & Jameel, 2002). To study the effect of these changes on pyrolysis, the unmilled and ball-milled samples were analyzed by X-ray diffraction (XRD; RINT 2000V, Rigaku, Tokyo, Japan). The cellulose crystallinity index was determined from the obtained XRD pattern using Equation (1) (Segal, Creely, Martin, & Conrad, 1959),

$$Xc = \frac{I_{002} - I_{am}}{I_{002}} \times 100 \quad (1)$$

where I_{002} is the peak intensity of the 002 lattice diffraction of cellulose, and I_{am} is that of the nearby amorphous region.

Thioacidolysis is an acid-catalyzed solvolysis technique that employs ethanethiol, and the yield of thioacidolysis products (trithioethyl monolignols) represents an index of the number of β-ether linkages in lignin. Thioacidolysis was performed according to a published procedure (Rolando, Monties, & Lapierre, 1992), and the thioacidolysis products were quantified using gas chromatography-mass spectrometry (GC-MS; QP2010 Ultra, Shimadzu, Kyoto, Japan) after trimethylsilyl derivatization. The GC-MS used a CP-Sil 8CB column (Agilent Technologies, CA, USA; length = 30 m, diameter = 0.25 mm, thickness = 0.25 μm) where the injector temperature = 260 °C; split ratio = 1:50; column temperature = 130 °C (5 min), +5 °C/min until 260 °C, 260 °C (5 min); carrier gas = H_2. The quantitative determination of G and S monomers was performed based on the peak areas of total-ion chromatograms by comparing those of tetracosane (C_{24}) and hexacosane (C_{26}) used as internal standards (Rolando et al., 1992; Sipponen et al., 2014). A typical example of the total-ion chromatogram is illustrated in Fig. 6-1.

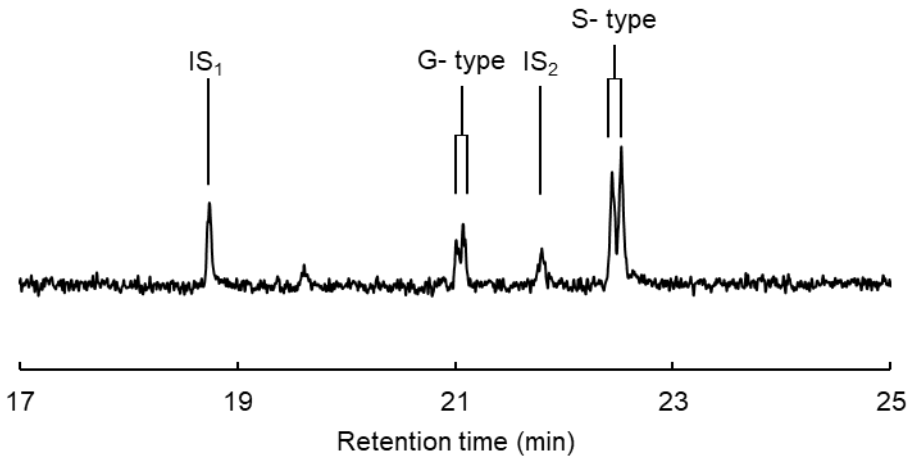

Fig. 6-1 A typical examples of chromatogram of thioacidolysis mixture obtained from 4-hour-ball-milled beech wood ball-milledIS_1: tetracosane (C_{24}) IS_2: hexacosane (C_{26})

6.2.2 TG analysis

TG analysis was conducted by a TGA-50 equipment (Shimadzu, Kyoto, Japan). Ball-milled wood samples from Japanese cedar and Japanese beech wood (1 mg) was heated from room temperature up to 800 °C in a platinum pan at a heating rate of 10°C/min under a N_2 flow 10 mL/min (purity: 99.9998%, JAPAN FINE PRODUCTS, Mieken, Japan). A deoxygenation column (GL Sciences, Japan) was used to remove any O_2 contamination in N_2.

6.2.3 Pyrolysis experiment

Figure 6-2 illustrates the pyrolysis experimental setup. An electric furnace (ARF-20KC, Asahi-Rika, Chiba, Japan) was used to heat the samples. In each pyrolysis experiment, the sample was placed in a ceramic boat (AS ONE, Osaka, Japan), which was inserted into a quartz glass tube (inner diameter = 15 mm, length = 400 mm, wall thickness = 1.5 mm). N_2 gas was supplied into the glass tube at a flow rate of 100 mL/min using a mass flow controller (SEC-400MK3, Horiba, Kyoto, Japan). The sample was heated from room temperature to a designated temperatures (i.e., 20 °C intervals between 220 and 380 °C) at the same heating rate as in the TG analysis (10 °C/min) to allow for

accurate comparisons. The sample temperature was measured by placing a fine thermocouple (0.25 mm in diameter; SHINNETSU, Ibaraki, Japan) in contact with the sample. When the sample temperature reached the designated temperature, the cover of the electric furnace was opened and the glass tube was immediately cooled to room temperature under a flow of air.

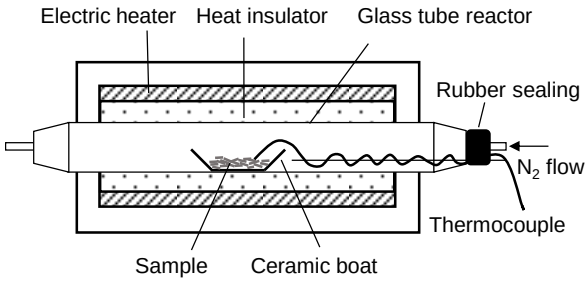

Fig. 6-2 Experimental setup

6.2.4 Hydrolysable sugar analysis

Acid hydrolysis and methanolysis of the pyrolyzed samples were performed separately to convert cellulose into glucose and hemicellulose/pectin into methyl glycosides, respectively. For the hydrolysis experiments, each sample was treated with 0.3 mL of aqueous 72% H_2SO_4 solution in a ceramic boat at 30 °C for 1 h in a sealed glass vial. Then, 8.4 mL of distilled water was added to the mixture and heated in an autoclave at 120 °C for 1 h to complete the hydrolysis reaction. After the hydrolysate solution was filtered, diluted, and neutralized, the glucose yield was determined via high-performance anion-exchange chromatography using a Prominence system (Shimadzu) equipped with an electrochemical detector (DECADE Elite, Antec Scientific, Zoeterwoude, Netherlands) under the following conditions: column = CarboPac PA1 (4 mm × 250 mm); eluent = 85% distilled water/15% 0.2 M NaOH; flow rate = 1 mL/min; column oven temperature = 35 °C.

The Milder methanolysis (Asmadi et al., 2017; Bertaud et al., 2002; Bleton et al., 1996; Li et al., 2007) was performed to determine the yields of hydrolyzable sugars, such as methyl glycosides, derived from hemicellulose, pectin, and uronic acid groups. Each pyrolyzed sample was placed in a sealed glass vial along with the ceramic boat, and 4 mL of 2 M HCl solution in methanol was added. The vial was then heated at 60 °C for 16 h

to complete the methanolysis reaction. After neutralization, the addition of internal standard (glucitol) and trimethylsilyl derivatization, the resulting products were analyzed by GC-MS under the aforementioned conditions, except the temperature program was changed to the following: 100 °C (2 min), 4 °C/min up to 220 °C, 220 °C (2 min), 15 °C/min up to 300 °C, 300 °C (2 min). The peaks originating from hemicellulose/pectin and 4-*O*-MeGlcA were assigned based on the mass spectra, and the retention times were compared with published data (HA and Thomas 1988; Sundberg et al. 1996). Typical examples of chromatograms from sugar analysis are illustrated in Fig. 6-3.

In the present study, the hydrolysable sugar analysis was conducted three times and the average value was used for discussion. In addition, the pyrolysis experiments were repeated more than twice to confirm the reproducibility of the results.

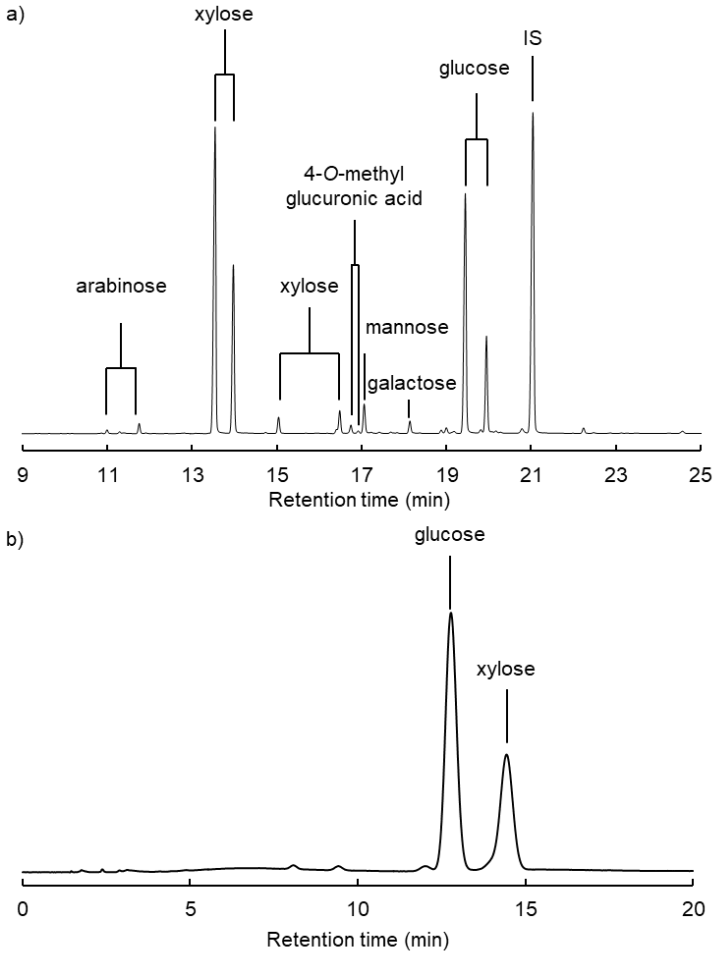

Fig. 6-3 Typical example of chromatograms of reaction mixtures obtained by methanolysis (a) and hydrolysis (b) of 4-hour-ball-milled beech wood. (IS: glucitol)

6.3 Results and discussion

6.3.1 Characterization and TG analysis of ball-milled wood

The intensity of the XRD signals originating from cellulose crystallites decreased with increasing milling time for both cedar and beech wood samples (Fig. 6-4); this phenomenon has also been reported previously (Jiang, Wang, Zhang, & Wolcott, 2017). The crystallinity index calculated from the X-ray diffractograms using the 002 lattice diffraction decreased from 68% to 5% after ball milling for 1-2 h (Fig. 6-5).

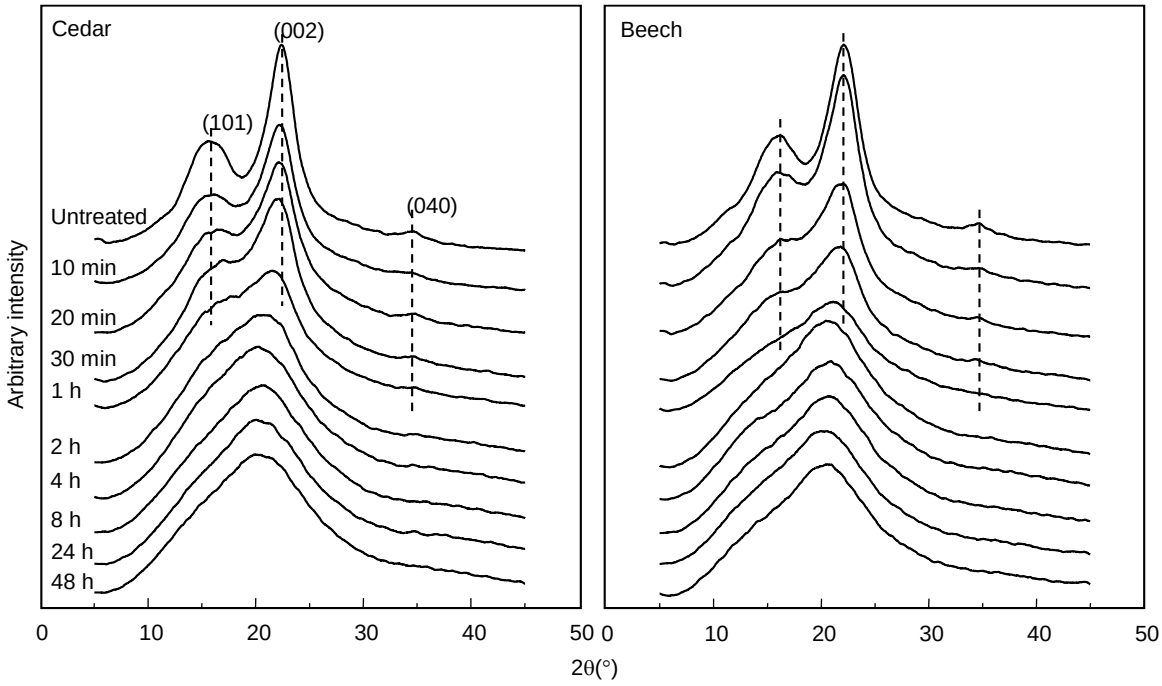

Fig. 6-4 Effect of ball-milling time on the cellulose crystallinity in Japanese (a) cedar and (b) beech wood

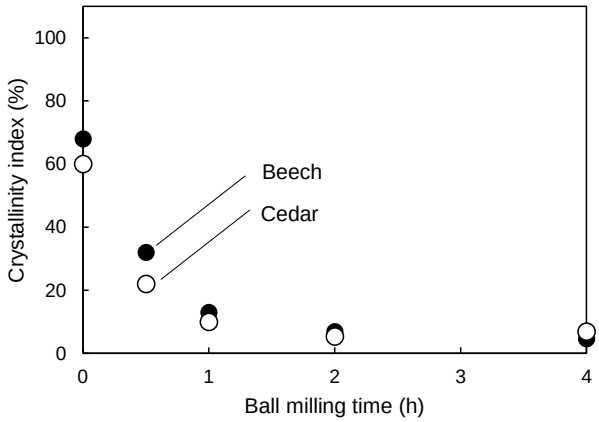

Fig. 6-5 Influence of ball-milling time on the crystallinity index evaluated by XRD analysis for cedar (●) and beech (○) wood

Although there is less information regarding the effect of ball milling on lignin than on cellulose, some literature reports (Hideno, 2016; Ling et al., 2019; Mattonai et al., 2018) determined that ball milling reduced the degree of polymerization of lignin and increased the phenolic structure by cleaving the ether linkages. Therefore, the β-ether structures remaining in the ball-milled wood samples were quantified using the thioacidolysis method to evaluate the effect of ball milling time on the cleavage of the β-ether bonds (the most abundant type of linkage in lignin). Thioacidolysis involves ethanethiol-assisted, acid-catalyzed solvolysis and leads to the formation of trithioethyl monomeric products through the cleavage of β-ether bonds. The derivatization followed by reductive cleavage (DFRC) method has also been used for quantitative analysis of the β-ether linkages, but Holtman et al. (Holtman, Chang, Jameel, & Kadla, 2003) reported that thioacidolysis was a better strategy for evaluating the β-ether linkages in ball-milled wood.

The relative yields of thioacidolysis products, namely guaiacyl (G)-type in cedar and G- and syringyl (S)-types in beech, are plotted as a function of the milling time in Fig. 6-6. These yields (normalized relative to 100% for unmilled wood) decreased as the milling time increased, and were about 20% after 4 h for both woods. This indicates that the β-ether linkages were cleaved during the ball milling process, and that the efficiency

was similar for cedar and beech woods, but slightly higher for cedar. No significant difference was observed between the S- and G-types in beech wood.

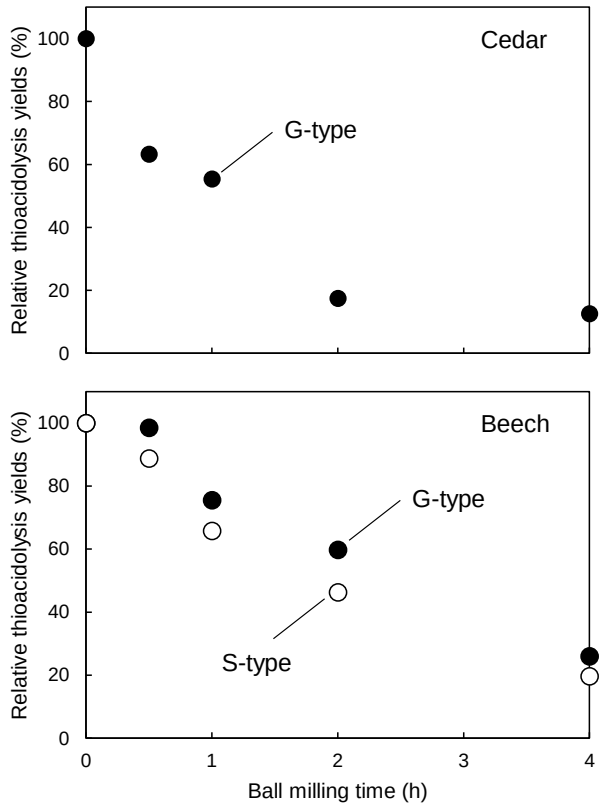

Fig. 6-6 Influence of ball-milling time on the yields of thioacidolysis products from (a) cedar and (b) beech wood

The TG and DTG profiles obtained for the ball-milled cedar and beech woods are presented in Figs. 6-7 and 6-8, respectively. The TG/DTG curves of the ball-milled woods for the 10 min and 4 h experiments are shown in Fig. 6-9 to represent typical examples and for comparison with the unmilled wood. As the ball milling time increased, the TG curve shifted toward lower temperatures and tended to level off after 4 hours of milling.

The characteristics of the DTG curves of cedar and beech were largely unchanged; the beech DTG curve has a distinct shoulder, but cedar has one wide peak.

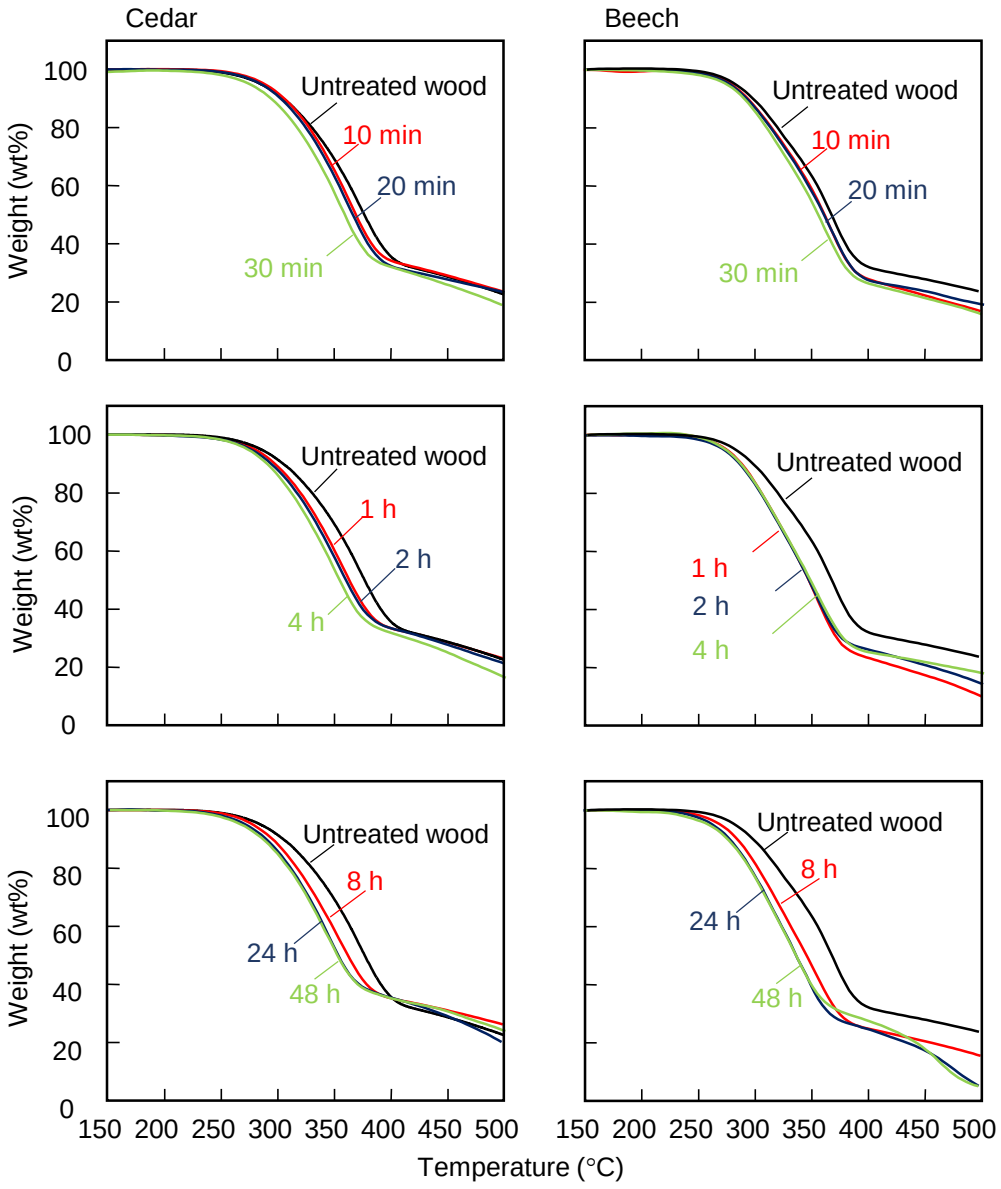

Fig. 6-7 Influence of milling time on the TG curves of ball-milled (a) cedar and (b) beech wood

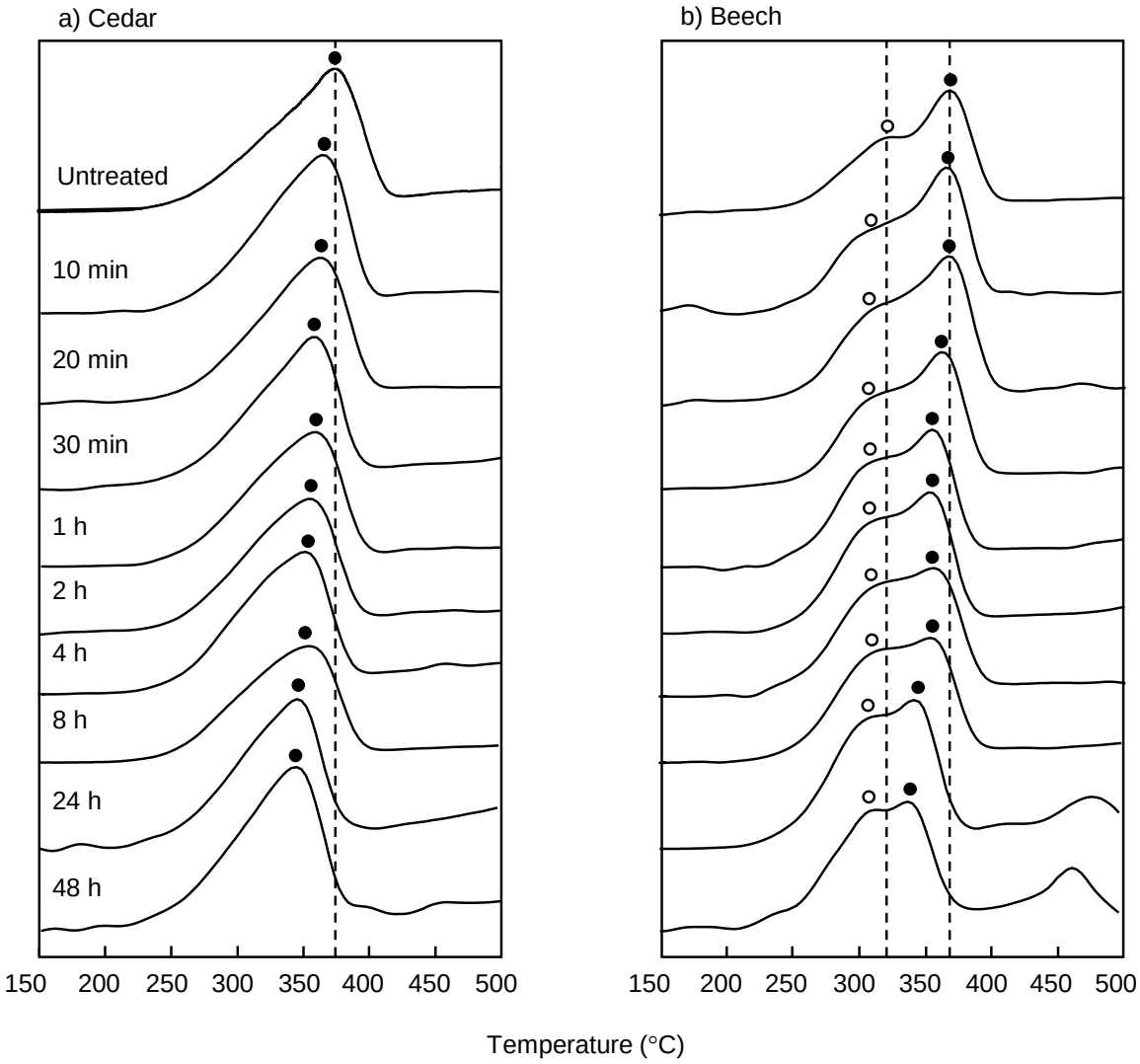

Fig. 6-8 Influence of milling time on the DTG curves of ball-milled (a) cedar and (b) beech wood

After a very short (10-min) milling time, the temperature ranges in which the TG curves changed were different for cedar versus beech samples; the change occurred near the DTG shoulder temperature for beech, but near the DTG peak temperature for cedar. Accordingly, the DTG peak tended to shift more for cedar, whereas the DTG shoulder shifted for beech. Specifically, the DTG peak temperature shifted from 374 to 365 °C (cedar), or 367 to 362 °C (beech), and the DTG shoulder temperature of beech shifted from 320 to 302 °C. These observations indicate that some heat-resistant cellulose in the cedar wood became reactive after short-term ball milling, while the hemicellulose was influenced to a greater extent in the beech wood.

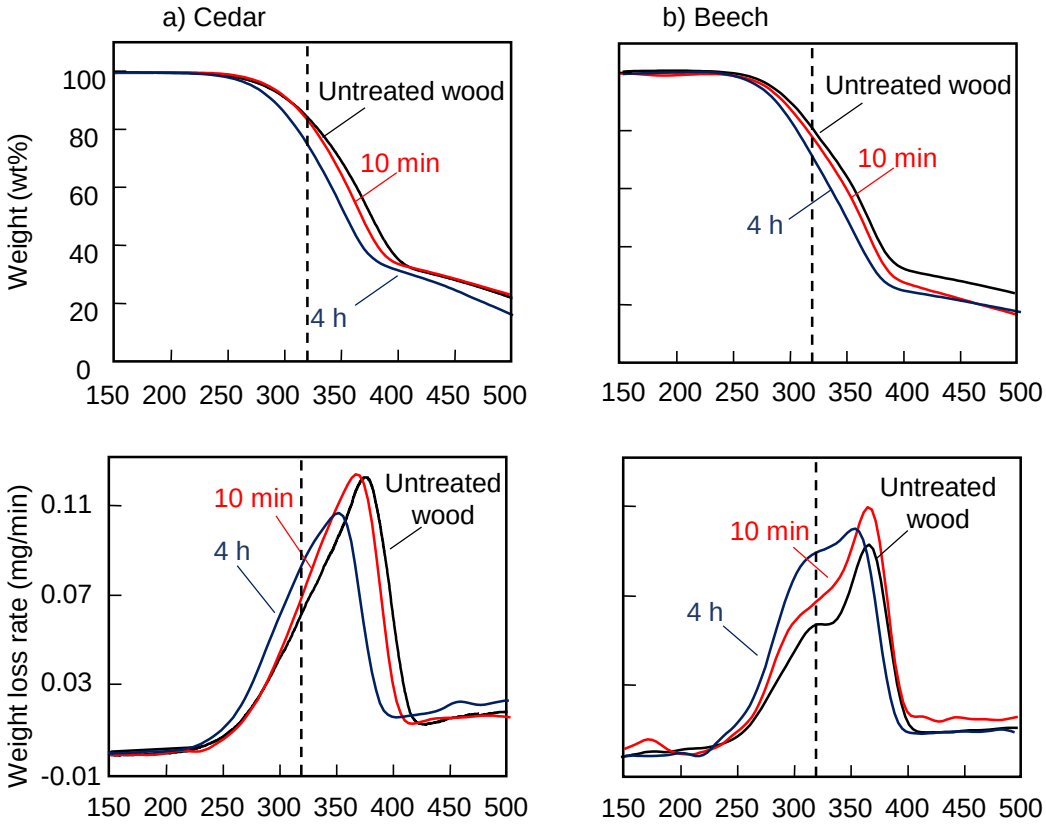

Fig. 6-9 TG/DTG curves of ball-milled (a) cedar and (b) beech wood for 10 min and 4 h

When the milling time was extended to 4 h, the TG curves of both woods shifted toward lower temperatures, within the wider temperature range of 250-400 °C. The DTG peak temperatures decreased more significantly and became similar (cedar = 354 °C and beech = 355 °C). This result indicated that their cellulose reactivities became similar after 4 hours of milling, although unmilled cedar cellulose was more stable. The ball-milled wood also exhibited improved weight-loss rates in the temperature range near the DTG shoulder in beech, thus changing the shape of DTG curve.

6.3.2 Polysaccharide reactivity

The amount of unreacted hemicellulose and cellulose remaining in 4-hour-ball-milled wood after pyrolysis was evaluated based on the hydrolyzable sugars, and the results are plotted against the pyrolysis temperature in Fig. 6-10. The recovery rates are shown as normalized values relative to the contents in unmilled wood (Rabemanolontsoa

& Saka, 2013). The quantities of xylan and glucomannan were determined based on the yields of methyl xyloside and methyl mannoside, respectively, obtained after methanolysis. The amount of cellulose-derived glucose in the hydrolysate was calculated by subtracting the yield of glucose derived from glucomannan, which was obtained from the methyl mannoside yield by assuming that (i) the mannose:glucose ratio in glucomannan was 3:1 (Timell, 1967; Tyminski & Timell, 1960) and (ii) their thermal reactivities were the same.

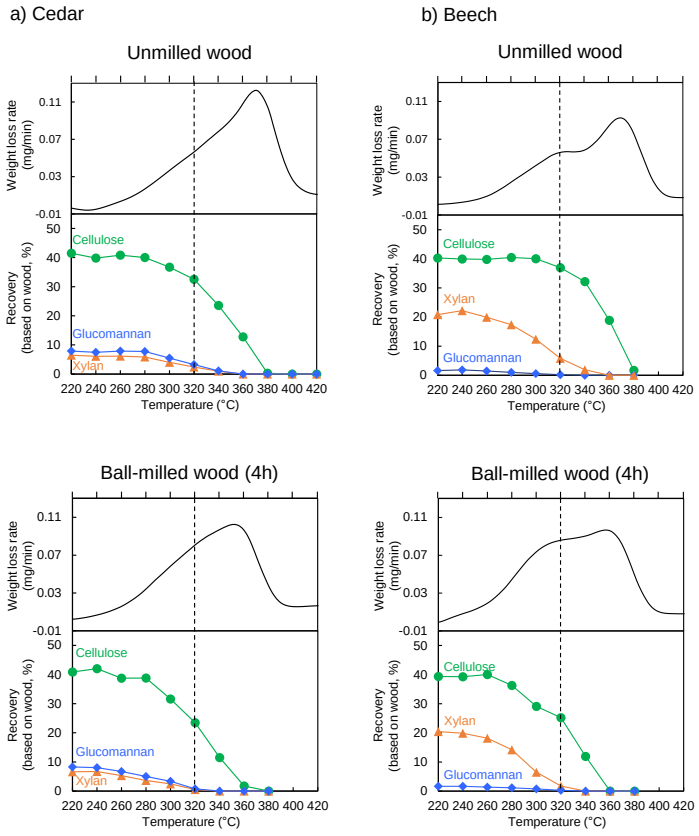

Fig. 6-10 Thermal degradation behaviors of cellulose (●), glucomannan (◆) and xylan (▲) in 4-hour-ball-milled cedar and beech wood (4h), compared with the DTG curves

Results of unmilled wood were obtained from Wang et al.

The recovery data are compared with the DTG profiles in Fig. 6-10. Because the heating conditions applied in the pyrolysis experiments were similar to those used for TG analysis, the results from these two types of experiments can be directly compared. Previously reported results for the unmilled woods (Wang, Minami, & Kawamoto, 2020) are also included for comparison.

In the 4-hour ball-milled samples, some of the cellulose degraded at temperatures lower than 320 °C (where most of the hemicellulose degraded), whereas the cellulose in unmilled cedar and beech woods was relatively more stable in this temperature range. Therefore, the cellulose in ball-milled wood tended to degrade in two different temperature ranges. A similar trend was reported for holocellulose, but the degradation in the lower temperature range w as greater for ball-milled wood. In this work, it was determined that 39% and 38% of the cellulose in ball-milled cedar and beech woods, respectively, degraded below 320 °C; the remaining cellulose degraded at higher temperatures around the DTG peaks. This result is consistent with the characteristics of the DTG curve of ball-milled beech wood, i.e., the shoulder intensity increased significantly. Although the DTG shoulder was not clearly observed for ball-milled cedar wood, the weight-loss rate at temperatures below 320 °C increased.

It is interesting to note that ball milling and delignification have similar effects on cellulose reactivity in wood, although the ball milling process does not remove any components from the wood. About 80% of the β-ether linkages were cleaved after ball milling for 4 h (Fig. 6-6), suggesting that the enhanced thermal reactivity of cellulose may be related to the cleavage of lignin ether linkages, rather than the formation of pores in the cell wall matrices due to lignin removal. Loosening the cell wall structure by cleaving lignin chains is considered a potential reason for this observation, and this relationship is discussed further below.

The recovery rates of hydrolyzable sugars derived from cellulose, xylan, and glucomannan in ball-milled wood (after 10 min and 4 h) were compared with those of pure cellulose (Whatman CF-11), isolated xylan, and isolated glucomannan, respectively, to better understand the polysaccharide reactivity in ball-milled wood (Fig. 6-11). The results of 4-hour-ball-milled pure cellulose are also included for comparison. The recovery data are summarized for each ball-milled wood in Fig. 6-12.

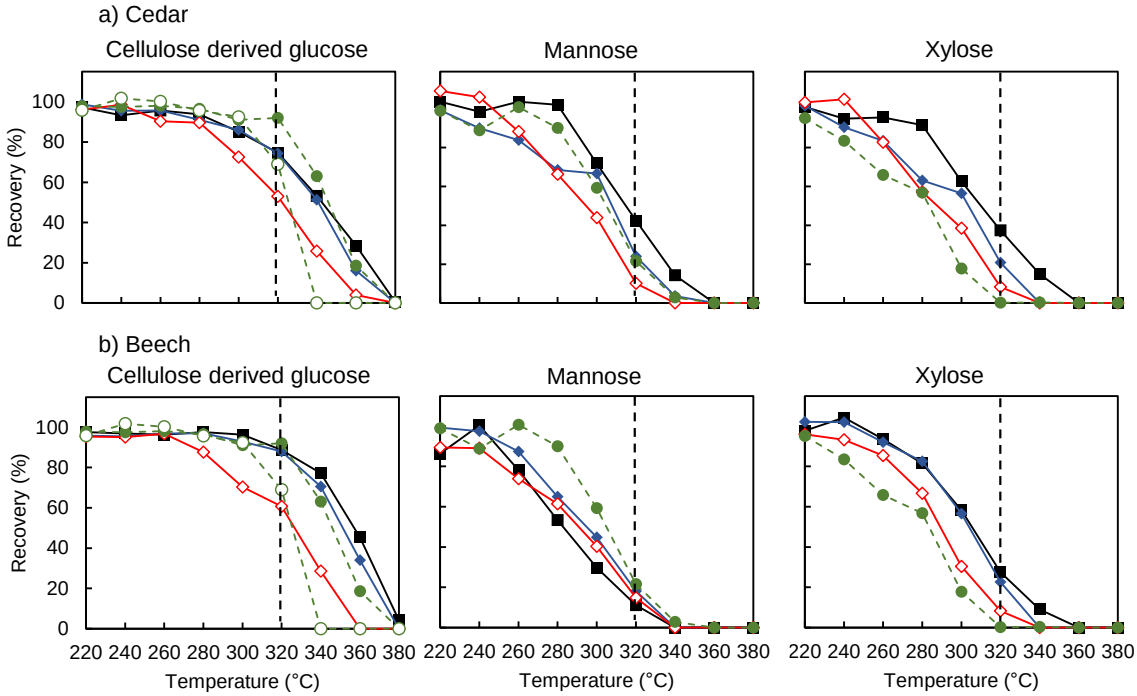

Fig. 6-11 Recovery rates of hydrolyzable sugars (cellulose-derived glucose, mannose and xylose) after pyrolysis of ball-milled (a) cedar and (b) beech wood for 10 min (◆) and 4h (◇), compared with unmilled wood (■), Whatman CF-11 cellulose (●: unmilled, ○:ball-milled (4h) and isolated hemicellulose (●)

In the case of cedar wood, even after a short milling time of 10 min, the recovery rates of hydrolyzable sugars from xylan and glucomannan decreased greatly, although their contributions to the weight loss were small (Fig. 6-9). Interestingly, clear discontinuities were observed at 300 °C for mannose and xylose in the cedar wood, indicating that xylan and glucomannan in ball-milled cedar wood are divided into two parts with different reactivities; 62% of xylan and 57% of glucomannan degraded at temperatures <300 °C, and the remaining portions degraded at higher temperatures. A similar trend was observed for the thermal degradation of cellulose in ball-milled cedar wood (4 h), as described earlier, although the discontinuous temperature observed for xylan and glucomannan (300 °C) was slightly lower than that of cellulose (320 °C). This trend is clearly visible in Fig. 6-12.

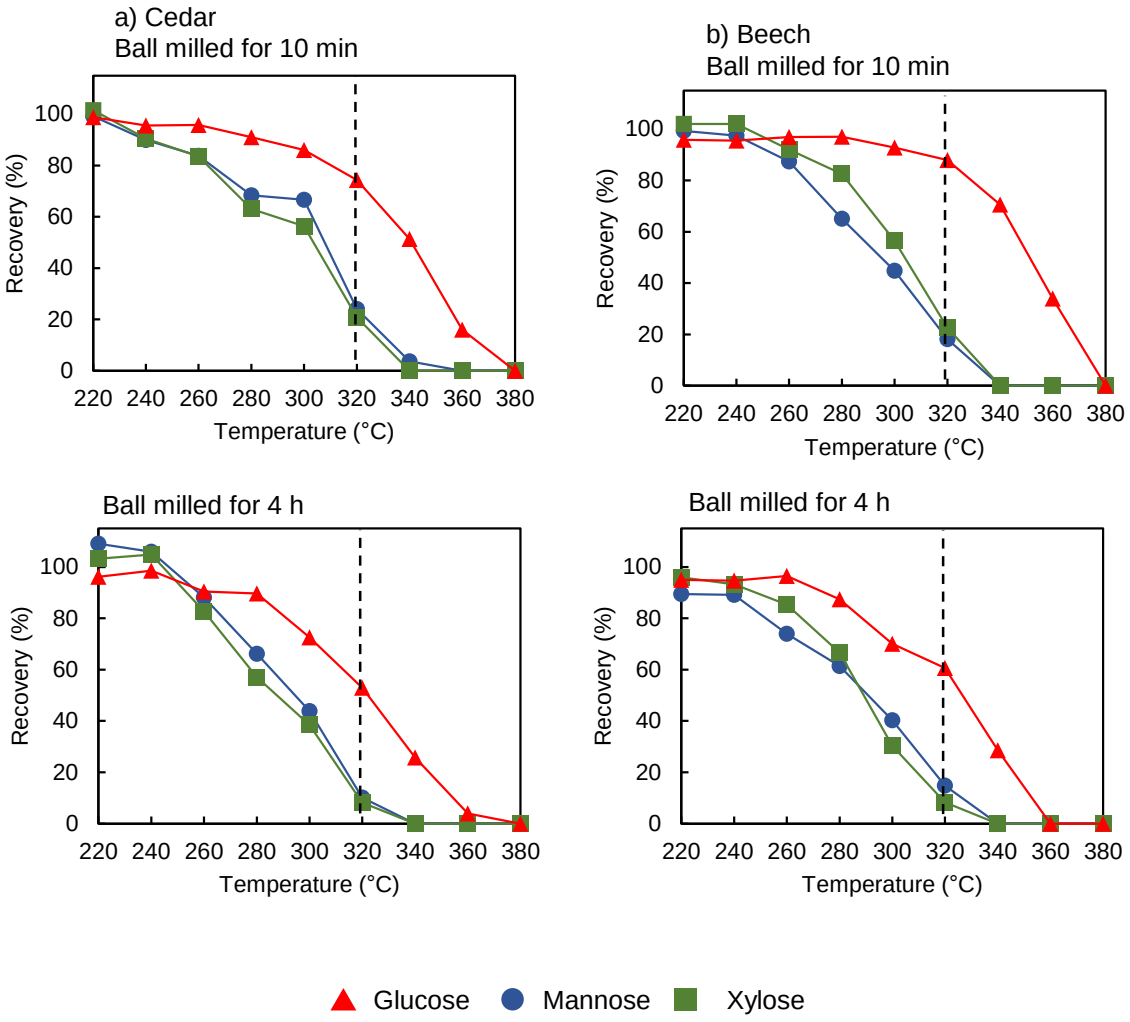

Fig. 6-12 Recovery rates of hydrolyzable sugars, cellulose-derived glucose (▲), mannose (●) and xylose (■), in pyrolysis of ball-milled cedar and beech wood for 10 min and 4 h

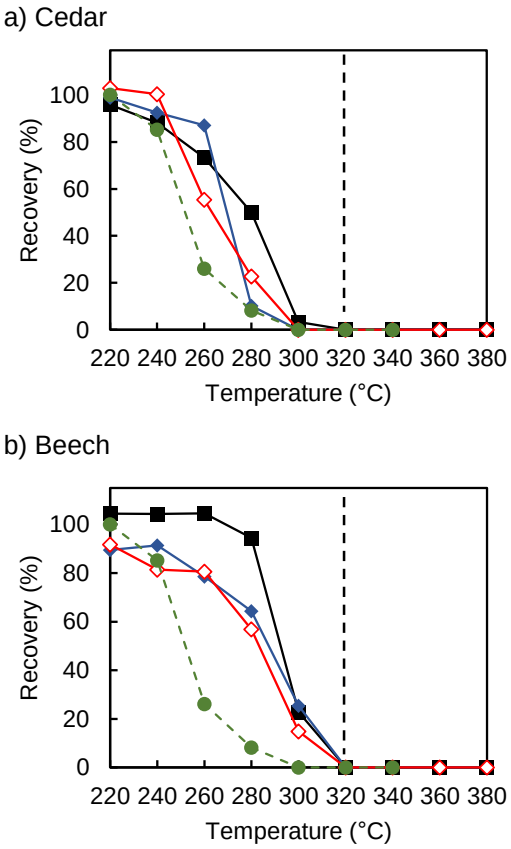

Fig. 6-13 Thermal reactivities 4-O-MeGlcA from untreated wood (■), ball-milled wood for 10 min (◆) and 4h (◇) of Japanese cedar and beech compared with isolated hemicellulose (●)

The aforementioned features were only observed for cedar samples, so they may be related to the thermal degradation characteristics specific to cedar wood, in which cellulose degrades together with hemicellulose. The close assembly of xylan, glucomannan, and cellulose microfibrils (surface molecules) was demonstrated based on the conversion of metal salts to free 4-*O*-MeGlcA (Wang, Minami, & Kawamoto, 2020). In general, the thermal degradation behaviors of cellulose and hemicellulose presented in the current study support such assembly.

The crystallinity of cellulose in cedar wood decreased from 68% to 51% following 10 minutes of milling, and some of the lignin β-ether linkages were cleaved (Figs. 6-5 and 6-6). Such modifications improved the mobility of the assembled xylan, glucomannan, and cellulose in cedar wood, resulting in enhanced thermal degradation and weight reduction at temperatures around the DTG peak where cellulose degraded

(~370 °C, Fig. 6-9). The recovery data presented in Fig. 6-11 confirm the improved cellulose reactivity in this temperature range.

The recovery data for the 10-min-ball-milled beech wood (Fig. 6-11) indicate that the reactivities of xylan and cellulose increased. This is consistent with the changes in the TG/DTG profiles shown in Fig. 6-9, in which the TG/DTG curves shifted in the wide temperature range between 250-400 °C. In contrast, the glucomannan reactivity decreased (Fig. 6-11). This is also reasonably explained by the improved mobility of the matrix. The high glucomannan reactivity observed in beech wood was explained based on the 4-*O*-MeGlcA located near glucomannan (Wang, Minami, & Kawamoto, 2020), although it is bound to the xylose chain in xylan. The improved mobility of the cell wall matrix may diminish this effect.

When the milling time was increased to 4 h, the reactivity of xylan in beech wood increased, and xylan and glucomannan in both woods degraded in a similar temperature range, which was much lower than that of isolated glucomannan (Figs. 6-11 and 6-12). This is interesting because isolated xylan bearing 4-O-MeGlcA moieties was more reactive than isolated glucomannan because of the catalytic effect of 4-*O*-MeGlcA (salts or free carboxyls) was more reactive than isolated glucomannan because of the base or acid catalysis of 4-*O*-MeGlcA (Wang, Minami, & Kawamoto, 2018). Therefore, ball milling should make the matrix components more homogeneous, thus allowing 4-*O*-MeGlcA to influence most of the hemicellulose components equally. This is an aspect of ball-milled wood that was not observed for holocellulose pyrolysis, where the thermal degradation reactivities of xylan and glucomannan were similar to those of isolated xylan and isolated glucomannan, respectively. This is likely because the delignification process did not allow the matrix components to mix efficiently.

The recovery rate of 4-*O*-MeGlcA is shown in Fig. 6-13. The thermal degradation reactivity of 4-*O*-MeGlcA in holocellulose was improved to a level similar to that of isolated xylan (Wang, Minami, Asmadi, & Kawamoto, 2021); however, the improvement was not very significant in ball-milled wood, particularly for beech. This may be related to the ester linkages formed with lignin, which may be resistant to the ball milling process, but further investigations are necessary to better explain this enhanced stability.

As discussed earlier, cellulose in wood degraded in two stages (some at temperatures below 320 °C and some at higher temperatures). In contrast, ball-milled Whatman cellulose degraded only in one mode corresponding to the high-temperature degradation of ball-milled wood. Therefore, the low-temperature degradation is characteristic of cellulose in wood. Because the matrix covers cellulose microfibrils in wood, these distinctions likely result from matrix effects. The-low-temperature-mode degradation would be explained by matrix –induced degradation as discussed later.

6.3.3 Role of ball milling on thermal reactivity of wood polysaccharides

The impact of ball milling on the polysaccharide reactivity of wood cell walls is discussed here by using a schematic image of the interface between cellulose microfibril and hemicellulose-lignin matrix depicted in Fig. 6-14. Cellulose microfibrils play an important role owing to their crystalline nature. Cellulose molecules inside the crystallites are more stable than the surface molecules because of the packing in the crystallites, so the reactivity of the surface molecules is a critical factor for initiating the thermal degradation of bulk cellulose. The difference between cellulose in wood and pure cellulose lies in this feature. Therefore, the reactivity of the matrix and its influence on the surface cellulose molecules must be considered to comprehensively understand the thermal degradation of cellulose in wood cell walls.

Our group's previous work (Wang et al., 2020) indicated that the xylan and glucomannan reactivities are significantly influenced by the matrix construction. The arrangement of these molecules (including 4-*O*-MeGlcA, which has a catalytic effect) is precisely determined in wood cell walls, and it is different in cedar (softwood) versus beech (hardwood) (Wang, Minami, & Kawamoto, 2021a). Because these characteristic reactivities disappeared following the removal of lignin, the physical restraining effect of lignification during cell wall biosynthesis is considered to be the main reason for these distinctions (Wang, Minami, Asmadi, et al., 2021b). Overall, the matrix is considered to be rigid and tightly associated with cellulose microfibrils in unmilled wood cell walls. Due to this tightly coagulated structure, hemicellulose and surface cellulose molecules in wood are stable for thermal degradation. The mobility must be sufficient to rearrange these polysaccharides into the transition state of thermal degradation reaction.

After the ball milling process, the crystallinity index of cellulose in wood decreased significantly, indicating that the matrix and the interface with the cellulose microfibrils was disturbed in such a way to improve the mobility. Cleavage of the lignin β-ether linkages diminishes the physical restraining effect and should help further improve the mobility of the matrix components. These modifications would improve the thermal degradation reactivity of xylan and glucomannan. In addition to the improved mobility, the ball milling process created a more homogeneous distribution of 4-*O*-MeGlcA, which improves the reactivity of glucomannan to similar levels of xylan degradation due to the catalytic effect of 4-*O*-MeGlcA. This feature is not the case for holocellulose, in which xylan and glucomannan have the same reactivity as isolated xylan and glucomannan. Therefore, xylan and glucomannan in both cedar and beech holocelluloses exist without affecting each other.

Unlike beech wood, short (10-min) ball milling significantly improved the reactivity of xylan and glucomannan, and the reactivity of cellulose was also improved. These results may correlate with the characteristic thermal degradation of cedar wood; cellulose, xylan and glucomannan degrade together like one ingredient (Wang et al., 2020). Xylan and glucomannan may strongly coagulate with the surface molecules of cellulose microfibrils. This is also supported by the fact that delignification and the subsequent removal of xylan are necessary to isolate glucomannan from softwood (Timell, 1961). Due to the rigid nature of crystalline cellulose microfibrils, ball milling disrupts the interface more efficiently.

Through loosening the matrix and the interface by ball milling, the surface cellulose molecules of cellulose microfibrils may become reactive and degrade in the low-temperature range in two modes of cellulose degradation that is characteristic of cellulose in holocellulose and ball-milled wood. The 4-*O*-MeGlcA groups and other matrix components and their thermal degradation products may induce the cellulose degradation in this temperature range through the action on the surface cellulose molecules. This proposed mechanism provides a reasonable explanation for why the thermal degradation of cellulose proceeds in two stages.

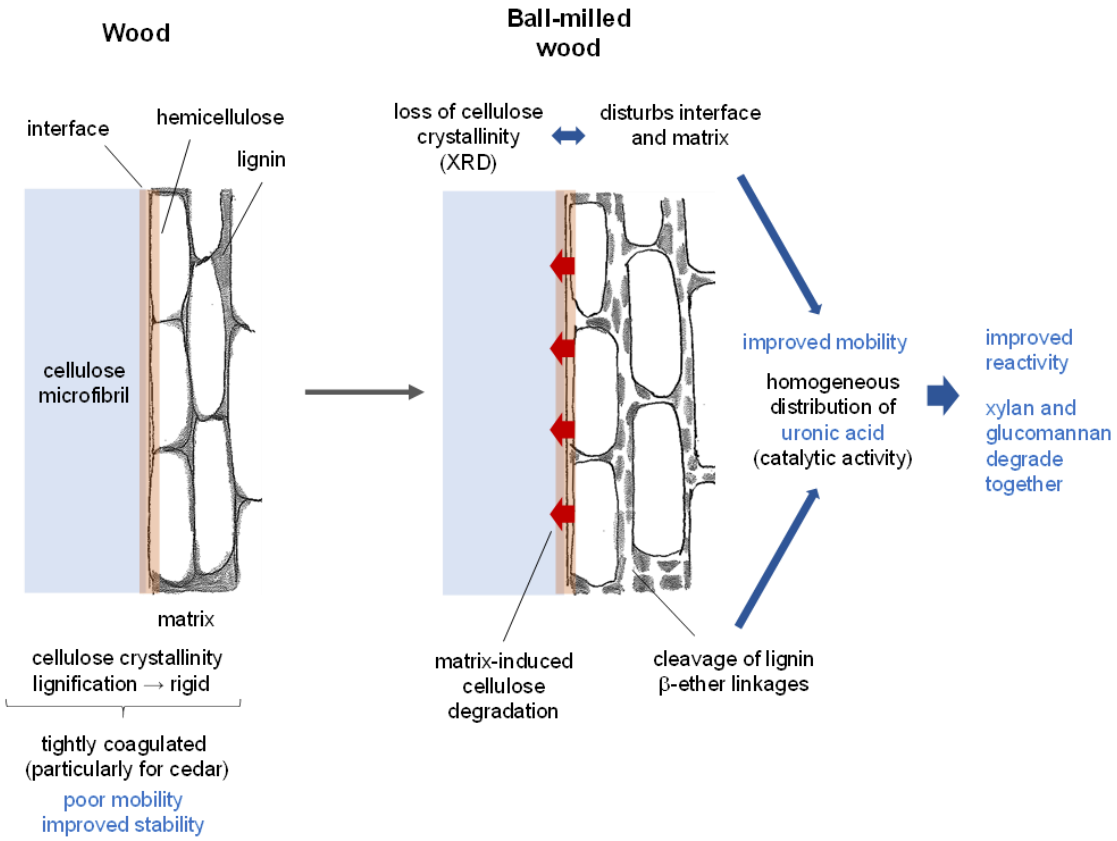

Fig. 6-14 Schematic images of the hemicellulose-lignin matrix and the interface with cellulose microfibril and their modifications expected to be caused by ball-milling process

6.4 Conclusions

The thermal reactivities of hemicellulose and cellulose in ball-milled cedar and beech woods were evaluated to understand the effect of ball milling on wood pyrolysis. The main findings are as follows:

1. Lignin β-ether linkages were cleaved during ball milling, along with the decrease in the cellulose crystallinity. These modifications would improve the mobility of matrix and the interface with cellulose microfibrils.

2. Short-term ball milling (10 min) significantly improved the thermal degradation reactivities of xylan and glucomannan in cedar wood, but did not for beech wood. These components degraded together in two temperature ranges (below 300 °C and above),

depending on the reactivity; this was not the case for beech wood. It was suggested that xylan, glucomannan and cellulose are more intimately coagulated in cedar (softwood) than beech (hardwood).

4. Long-term ball milling (4 h) increased the thermal degradation reactivities of xylan and glucomannan (except for the glucomannan in beech wood, whose reactivity decreased after ball milling), due to the improved mobility. All of these hemicelluloses degraded in a similar temperature range, likely because of the influence of catalytic 4-*O*-MeGlcA, which was more homogeneously distributed throughout the matrix after ball milling.

3. Long-term ball milling (4 h) increased the thermal degradation reactivity of cellulose, which degraded in two different temperature ranges (below 320 °C and above). Improved mobility of surface molecules of cellulose microfibrils and the degradation induced by the matrix and its thermal degradation were considered for the reasons.

5. The effects of ball milling on the thermal degradation reactivities of cellulose and hemicellulose were explainable in terms of the disturbance of the cell wall ultrastructure and cleavage of lignin ether linkages. Tightly coagulated matrix and interface structures due to lignification would make wood polysaccharides very stable against heat.

Chapter 7
CONCLUDING REMARKS

In this thesis, thermal degradation reactivity of hemicellulose and cellulose from isolated sample and several kinds of processed wood samples were investigated to understand the interaction between each comonents. The following conclusions are obtained and summarized in Table. 7-1.

Table 7-1 Summary for the thermal reactivity of cellulose, xylan and glucomannan of each kind of sample

+ : more reactive
- : more stable
S : similar

(C) : cedar
(B) : beech

	Cellulose		Glucomannan		Xylan	
	C	B	C	B	C	B
Wood	+ (co-degrade with hemicell)	S	-	++	--	--
Holocellulose	++ (two modes)	++	S	S	S	S
Ball-milled	++ (two modes)	++	++	++	S	S

In the case of the original xylan, differential thermogravimetric (DTG) shoulder at lower temperature and peak at higher temperature were assigned to the degradation of sodium uronate with some xylose units (at lower temperatures) and to the decomposition of the remaining xylose units (at higher temperatures). In contrast, the demineralized xylan generated only one DTG peak in the intermediate temperature range, corresponding to the simultaneous decomposition of both uronic acid and xylose units. Thus, the effect

of sodium uronate on the pyrolysis of the original xylan was only regional, whereas the free uronic acid affected the demineralized xylan in a more homogeneous manner and accelerate the decomposition of xylose units. Additional data from pyrolysis-gas chromatography-mass spectrometry revealed that the compositions of the pyrolysis products were also different for these two xylan samples.

In the pyrolysis of Japanese cedar and Japanese beech wood, the xylan in both woods was remarkably stable and degraded across a similar temperature range to the glucomannan degradation, which indicated that uronic acid did not act as base or acid catalyst might be due to the ester linkages with lignin. Thus, the majority of the hemicellulose fractions in cedar and beech unexpectedly exhibited similar reactivity, except for glucomannan in beech that degraded at lower temperatures. Differing TG/DTG profiles, measured for cedar and beech under similar heating conditions, were explained by the different cellulose reactivity, rather than the hemicellulose reactivity; cellulose decomposed with hemicellulose in cedar, while such decomposition was independent in beech. The observed reactivity is a new finding that is different from the currently understood ideas and may originate from the effects of the cell walls. The research herein provides important information on the kinetics and thermochemical conversion of lignocellulosic biomass.

The location of uronic acid in the cell wall is evaluated by identifying the components affected by demineralization in pyrolysis of cedar and beech wood. The thermal reactivities of xylan and glucomannan in beech were changed by demineralization, but in cedar, glucomannan and cellulose reactivities were changed. Therefore, the location of uronic acid in the cell wall was established and differed between cedar and beech; close to glucomannan and xylan in beech, but close to glucomannan and cellulose in cedar.

Results from pyrolysis of holocellulose showed that the reactivities of xylan and glucomannan in both woods became similar to those of the corresponding isolated samples when lignin was removed. By contrast, the cellulose in both woods became more reactive when lignin was removed, and the degradation could be separated into two modes depending on the reactivity (lower temperature, < 320 °C and higher temperature, >

320 °C). These results were analyzed in terms of the effect of lignin on the matrix of cell walls and the interaction between the matrix and surface molecules of cellulose microfibrils. Differential thermogravimetric curves of the holocellulose samples were obtained and explained in terms of the degradation of hemicellulose and cellulose.

In the condition of ball-milled wood, both xylan and glucomannan became more reactive and degraded in the similar temperature range, which was lower than that of isolated glucomannan. This is explained by the action of uronic acid groups attached on xylan chain, which became accessible to glucomannan through the disruption of hemicellulose-lignin matrix, followed by the cleavage of the lignin β-ether linkages by ball milling. Some cellulose molecules degraded with hemicellulose at temperatures lower than 320°C. These changes in reactivity explained the changes in shape of the DTG curves due to ball milling.

REFERENCE

Adler, E. (1977). Lignin chemistry-past, present and future. *Wood Science and Technology*, *11*(3), 169–218.

Åkerholm, M., & Salmén, L. (2001). Interactions between wood polymers studied by dynamic FT-IR spectroscopy. *Polymer*, *42*(3), 963–969.

Akhtar, J., & Saidina Amin, N. (2012). A review on operating parameters for optimum liquid oil yield in biomass pyrolysis. *Renewable and Sustainable Energy Reviews*. 16(3), 5105-5109.

Alén, R., Kuoppala, E., & Oesch, P. (1996). Formation of the main degradation compound groups from wood and its components during pyrolysis. *Journal of Analytical and Applied Pyrolysis*, *36*(2), 137–148.

Asmadi, M., Kawamoto, H., & Saka, S. (2010). Pyrolysis reactions of Japanese cedar and Japanese beech woods in a closed ampoule reactor. *Journal of Wood Science*, *56*(4), 319–330.

Asmadi, M., Kawamoto, H., & Saka, S. (2011). Gas- and solid/liquid-phase reactions during pyrolysis of softwood and hardwood lignins. *Journal of Analytical and Applied Pyrolysis*, *92*(2), 417–425.

Asmadi, M., Kawamoto, H., & Saka, S. (2017). Characteristics of softwood and hardwood pyrolysis in an ampoule reactor. *Journal of Analytical and Applied Pyrolysis*, *124*, 523–535.

Awano, T., Takabe, K., & Fujita, M. (2001). Xylan and lignin deposition on the secondary wall of Fagus crenata fibers. *Progress in Biotechnology*, *18*, 137–142.

Aznar, M. P., Corella, J., Delgado, J., & Lahoz, J. (1993). Improved steam gasification of lignocellulosic residues in a fluidized bed with commercial steam reforming Catalysts. *Industrial and Engineering Chemistry Research*, *32*(1), 1–10.

Balakshin, M., Capanema, E., & Berlin, A. (2014). Isolation and analysis of lignin-carbohydrate complexes preparations with traditional and advanced methods: A review. *Studies in Natural Products Chemistry*. *42*, 83-115.

Balakshin, M., Capanema, E., Gracz, H., Chang, H. min, & Jameel, H. (2011). Quantification of lignin-carbohydrate linkages with high-resolution NMR spectroscopy. *Planta*, *233*(6), 1097–1110.

Bar-On, Y. M., Phillips, R., & Milo, R. (2018). The biomass distribution on Earth. *Proceedings of the National Academy of Sciences of the United States of America*, *115*(25), 6506–6511.

Bertaud, F., Sundberg, A., & Holmbom, B. (2002). Evaluation of acid methanolysis for analysis of wood hemicelluloses and pectins. *Carbohydrate Polymers*, *48*(3), 319–324.

Biswas, B., Pandey, N., Bisht, Y., Singh, R., Kumar, J., & Bhaskar, T. (2017). Pyrolysis of agricultural biomass residues: Comparative study of corn cob, wheat straw, rice straw and rice husk. *Bioresource Technology*. *237*, 57-63.

Bleton, J., Mejanelle, P., Sansoulet, J., Goursaud, S., & Tchapla, A. (1996). Characterization of neutral sugars and uronic acids after methanolysis and trimethylsilylation for recognition of plant gums. *Journal of Chromatography A*, *720*(1–2), 27–49.

Bond, Brian; Hamner, P. (2002). Wood identification for hardwood and softwood Species native to Tennessee. *Agricultural Extension Service*. pp. 15.

Bradbury, A. G. W., Sakai, Y., & Shafizadeh, F. (1979). A kinetic model for pyrolysis of cellulose. *Journal of Applied Polymer Science*, *23*(11), 3271–3280.

Branca, C., Di Blasi, C., & Galgano, A. (2016). Chemical characterization of volatile products of biomass pyrolysis under significant reaction-induced overheating. *Journal of Analytical and Applied Pyrolysis*, *119*, 8–17.

Bridgwater, A. V. (2012). Review of fast pyrolysis of biomass and product upgrading. *Biomass and Bioenergy*, *38*, 68–94.

Busse-Wicher, M., Gomes, T., Tryfona, T., Nikolovski, N., Stott, K., Grantham, N. J., Bolam DN, Skaf M., & Dupree, P. (2014). The pattern of xylan acetylation suggests xylan may interact with cellulose microfibrils as a twofold helical screw in the secondary plant cell wall of Arabidopsis thaliana. *Plant Journal*, *79*(3), 492–506.

Busse-Wicher, M., Li, A., Silveira, R. L., Pereira, C. S., Tryfona, T., Gomes, T. C. F., Skaf M.S., & Dupree, P. (2016). Evolution of xylan substitution patterns in gymnosperms and angiosperms: Implications for xylan interaction with cellulose. *Plant Physiology*, *171*(4), 2418–2431.

Caffall, K. H., & Mohnen, D. (2009). The structure, function, and biosynthesis of plant cell wall pectic polysaccharides. *Carbohydrate Research*, *344*(14), 1879–1900.

Candelier, K., Chaouch, M., Dumaray, S., Pétrissans, A., Pétrissans, M., & Gérardin, P. (2011). Utilization of thermodesorption coupled to GC-MS to study stability of different wood species to thermodegradation. *Journal of Analytical and Applied Pyrolysis*. *92*(2), 376-383.

Cavalier, D. M., Lerouxel, O., Neumetzler, L., Yamauchi, K., Reinecke, A., Freshour, G., Zabotina, O.A., Hahn, M. G., Burgert, I., Raikhel, N. V., & Keegstra, K. (2008). Disrupting two Arabidopsis thaliana xylosyltransferase genes results in plants deficient in xyloglucan, a major primary cell wall component. *Plant Cell*, *20*(6), 1519–1537.

Clawson, C. C., & Clawson, C. C. (1999). Speculations on the nature of mathematics. *Mathematical Sorcery*, *2*, 281–285.

Collard, F. X., & Blin, J. (2014). A review on pyrolysis of biomass constituents: Mechanisms and composition of the products obtained from the conversion of cellulose, hemicelluloses and lignin. *Renewable and Sustainable Energy Reviews*. 38, 594-608.

Cosgrove, D. J., & Jarvis, M. C. (2012). Comparative structure and biomechanics of plant primary and secondary cell walls. *Frontiers in Plant Science*. *3*, 204.

Crestini, C., Melone, F., Sette, M., & Saladino, R. (2011). Milled wood lignin: a linear oligomer. *Biomacromolecules*, *12*(11), 3928–3935.

Dammström, S., Salmén, L., & Gatenholm, P. (2009). On the interactions between cellulose and xylan, a biomimetic simulation of the hardwood cell wall. *BioResources*, *4*(1), 3–14.

DeGroot, W. F. (1985). Preliminary investigation of the association of inorganic cations with carboxylic acid groups in wood. *Carbohydrate Research*, *142*(1), 172–178.

Du, X., Gellerstedt, G., & Li, J. (2013). Universal fractionation of lignin-carbohydrate complexes (LCCs) from lignocellulosic biomass: an example using spruce wood. *Plant Journal*, *74*(2), 328–338.

Du, X., Pérez-Boada, M., Fernández, C., Rencoret, J., del Río, J. C., Jiménez-Barbero, J., Li, J., Gutiérrez, A, & Martínez, A. T. (2014). Analysis of lignin–carbohydrate and lignin–lignin linkages after hydrolase treatment of xylan–lignin, glucomannan–lignin and glucan–lignin complexes from spruce wood. *Planta*, *239*(5), 1079–1090.

Eom, I. Y., Kim, J. Y., Kim, T. S., Lee, S. M., Choi, D., Choi, I. G., & Choi, J. W. (2012). Effect of essential inorganic metals on primary thermal degradation of lignocellulosic biomass. *Bioresource Technology*, *104*, 687–694.

Eom, I. Y., Kim, K. H., Kim, J. Y., Lee, S. M., Yeo, H. M., Choi, I. G., & Choi, J. W. (2011). Characterization of primary thermal degradation features of lignocellulosic biomass after removal of inorganic metals by diverse solvents. *Bioresource Technology*, *102*(3), 3437–3444.

Evans, R. J., & Milne, T. A. (1987). Molecular characterization of the pyrolysis of biomass. *Energy and Fuels*, *1*(2), 123–137.

Fengel, D., & Wegener, G. (1979). Hydrolysis of polysaccharides with trifluoroacetic acid and its application to rapid wood and pulp analysis. *Hydrolysis of Cellulose: Mechanisms of Enzymatic and Acid Catalysis*, pp 145–158.

Fisher, T., Hajaligol, M., Waymack, B., & Kellogg, D. (2002). Pyrolysis behavior and kinetics of biomass derived materials. *Journal of Analytical and Applied Pyrolysis*, *62*(2), 331–349.

Forziati, F. H., Stone, W. K., Rowen, J. W., & Appel, W. D. (1950). Cotton powder for infrared transmission measurements. *Journal of Research of the National Bureau of Standards*, *45*(2), 109-113.

Fujimoto, A., Matsumoto, Y., Chang, H. M., & Meshitsuka, G. (2005). Quantitative evaluation of milling effects on lignin structure during the isolation process of milled wood lignin. *Journal of Wood Science*. *51*, 89-91.

Gabrielii, I., Gatenholm, P., Glasser, W. G., Jain, R. K., & Kenne, L. (2000). Separation, characterization and hydrogel-formation of hemicellulose from aspen wood. *Carbohydrate Polymers*, *43*(4), 367–374.

Gírio, F. M., Fonseca, C., Carvalheiro, F., Duarte, L. C., Marques, S., & Bogel-Łukasik, R. (2010). Hemicelluloses for fuel ethanol: a review. *Bioresource Technology*, *101*(13), 4775–4800.

Giudicianni, P., Gargiulo, V., Grottola, C. M., Alfè, M., & Ragucci, R. (2018). Effect of alkali metal ions presence on the products of xylan steam assisted slow pyrolysis. *Fuel*, *216*, 36–43.

Gralén, N., & Svedberg, T. (1943). Molecular weight of native cellulose. *Nature*. *152*, 625.

HA, Y. W., & Tomas, R. L. (1988). Simultaneous determination of neutral sugars and uronic acids in hydrocolloids. *Journal of Food Science*, *53*(2), 574–577.

Haraguchi, T. (1985). Hemicellulose. In *Wood Chemistry* (3rd ed., pp. 84–95). Tokyo: Buneido-shuppan.

Harris, J. F., Baker, A. J., Conner, A. H., Jeffries, T. W., Minor, J. L., Pettersen, R. C., Scott, R. W., Springer, E., I., Wegner, T., H., Zerbe, J. I. (1985). Two-stage, dilute sulfuric acid hydrolysis of wood : an investigation of fundamentals. *Gen. Tech. Rep. FPL-45. Madison, WI: U.S. Department of Agriculture, Forest Service, Forest Products Laboratory; 1985. 73 P.*, *45*, 1–73.

Hideno, A. (2016). Comparison of the thermal degradation properties of crystalline and amorphous cellulose, as well as treated lignocellulosic biomass. *BioResources*, *11*(3), 6309–6319.

Hideno, A., Kawashima, A., Anzoua, K. G., & Yamada, T. (2013). Comparison of the enzymatic digestibility of physically and chemically pretreated selected line of diploid-Miscanthus sinensis Shiozuka and triploid-M.×giganteus. *Bioresource Technology*, *146*, 393–399.

Holtman, K. M., Chang, H. M., Jameel, H., & Kadla, J. F. (2003). Elucidation of lignin structure through degradative methods: Comparison of modified DFRC and thioacidolysis. *Journal of Agricultural and Food Chemistry*, *51*(12), 3535–3540.

Hosoya, T., Kawamoto, H., & Saka, S. (2007a). Cellulose-hemicellulose and cellulose-lignin interactions in wood pyrolysis at gasification temperature. *Journal of Analytical and Applied Pyrolysis*, *80*(1), 118–125.

Hosoya, T., Kawamoto, H., & Saka, S. (2007b). Pyrolysis behaviors of wood and its constituent polymers at gasification temperature. *Journal of Analytical and Applied Pyrolysis*, *78*(2), 328–336.

Hosoya, Takashi, Kawamoto, H., & Saka, S. (2007). Influence of inorganic matter on wood pyrolysis at gasification temperature. *Journal of Wood Science*, *53*(4), 351–357.

Ikeda, T., Holtman, K., Kadla, J. F., Chang, H. M., & Jameel, H. (2002). Studies on the effect of ball milling on lignin structure using a modified DFRC method. *Journal of Agricultural and Food Chemistry*. *50*(1), 129-135.

International Monetary Fund (IMF). (2019). *World Economic Outlook: Global Manufacturing Downturn, Rising Trade Barriers*. *International Monetary Fund*.

International Energy Agency (IEA). (2019). *Global Energy & CO2 Status Report: The Latest Trends in Energy and Emissions in 2018*. *Iea*.

Jacobs, A., & Dahlman, O. (2001). Characterization of the molar masses of hemicelluloses from wood and pulps employing size exclusion chromatography and

matrix-assisted laser desorption lonization time-of-flight mass spectrometry. *Biomacromolecules*, *2*(3), 894–905.

Jakab, E., Faix, O., Till, F., & Székely, T. (1995). Thermogravimetry/mass spectrometry study of six lignins within the scope of an international round robin test. *Journal of Analytical and Applied Pyrolysis*. *35*(2), 167-179.

Jiang, J., Wang, J., Zhang, X., & Wolcott, M. (2017). Assessing multi-scale deconstruction of wood cell wall subjected to mechanical milling for enhancing enzymatic hydrolysis. *Industrial Crops and Products*, *109*, 498–508.

Jin, Z., Katsumata, K. S., Lam, T. B. T., & Iiyama, K. (2006). Covalent linkages between cellulose and lignin in cell walls of coniferous and nonconiferous woods. *Biopolymers*, *83*(2), 103–110.

Kamel, M. Y., & Hamed, R. R. (1975). Aerobacter aerogenes PRL R3 urease. Purification and properties. *Acta Biologica et Medica Germanica*, *34*(6), 971–979.

Kan, T., Strezov, V., & Evans, T. (2016). Effect of the heating rate on the thermochemical behavior and biofuel properties of sewage sludge pyrolysis. *Energy and Fuels*, *30*(3), 1564–1570.

Katō, K. (1967). Pyrolysis of cellulose. *Agricultural and Biological Chemistry*, *31*(6), 657–663.

Kawamoto, H., & Saka, S. (2006). Heterogeneity in cellulose pyrolysis indicated from the pyrolysis in sulfolane. *Journal of Analytical and Applied Pyrolysis*, *76*(1–2), 280–284.

Kawamoto, H., (2016). Review of reactions and molecular mechanisms in cellulose pyrolysis. *Current Organic Chemistry*, *20*(23), 2444–2457.

Kawamoto, H., (2017). Lignin pyrolysis reactions. *Journal of Wood Science*. 63, 117-132.

Kawamoto, H., Yamamoto, D., & Saka, S. (2008). Influence of neutral inorganic chlorides on primary and secondary char formation from cellulose. *Journal of Wood Science*, *54*(3), 242–246.

Kim, D. Y., Nishiyama, Y., Wada, M., Kuga, S., & Okano, T. (2001). Thermal decomposition of cellulose crystallites in wood. *Holzforschung*, *55*(5), 521–524.

Kim, H. S., Kim, S., Kim, H. J., & Yang, H. S. (2006). Thermal properties of bio-flour-filled polyolefin composites with different compatibilizing agent type and content. *Thermochimica Acta*, *451*(1–2), 181–188.

Kloss, S., Zehetner, F., Dellantonio, A., Hamid, R., Ottner, F., Liedtke, V., Schwanninger, M., Gerzabek, M. H., & Soja, G. (2012). Characterization of slow pyrolysis biochars: effects of feedstocks and pyrolysis temperature on biochar properties. *Journal of Environmental Quality*. *41*(4), 990-1000.

Kumagai, A., & Endo, T. (2018). Comparison of the surface constitutions of hemicelluloses on lignocellulosic nanofibers prepared from softwood and hardwood. *Cellulose*, *25*(7), 3885–3897.

Lange, J. P. (2007). Lignocellulose conversion: An introduction to chemistry, process and economics. *Biofuels, Bioproducts and Biorefining*. *1*, 39-48.

Lawoko, M., Henriksson, G., & Gellerstedt, G. (2005). Structural differences between the lignin-carbohydrate complexes present in wood and in chemical pulps. *Biomacromolecules*, *6*(6), 3467–3473.

Le Brech, Y., Jia, L., Cissé, S., Mauviel, G., Brosse, N., & Dufour, A. (2016). Mechanisms of biomass pyrolysis studied by combining a fixed bed reactor with advanced gas analysis. *Journal of Analytical and Applied Pyrolysis*, *117*, 334–346.

Li, J., Kisara, K., Danielsson, S., Lindström, M. E., & Gellerstedt, G. (2007). An improved methodology for the quantification of uronic acid units in xylans and other polysaccharides. *Carbohydrate Research*, *342*(11), 1442–1449.

Ling, Z., Wang, T., Makarem, M., Santiago Cintrón, M., Cheng, H. N., Kang, X., Bacher, M., Potthast, A., Rosenau, T., King, H., Delhom, C., D., Nam, S., Edwards., J. V., Kim, S., H., Xu, F., & French, A. D. (2019). Effects of ball milling on the structure of cotton cellulose. *Cellulose*. *26*, 305-328.

Lv, G., & Wu, S. (2012). Analytical pyrolysis studies of corn stalk and its three main components by TG-MS and Py-GC/MS. *Journal of Analytical and Applied Pyrolysis*. *97*, 11-18.

Maeda, Y., Awano, T., Takabe, K., & Fujita, M. (2000). Immunolocalization of glucomannans in the cell wall of differentiating tracheids in Chamaecyparis obtusa. *Protoplasma*, *213*(3–4), 148–156.

Matsuoka, S., Kawamoto, H., & Saka, S. (2011). Reducing end-group of cellulose as a reactive site for thermal discoloration. *Polymer Degradation and Stability*, *96*(7), 1242–1247.

Matsuoka, S., Kawamoto, H., & Saka, S. (2014). What is active cellulose in pyrolysis? An approach based on reactivity of cellulose reducing end. *Journal of Analytical and Applied Pyrolysis*, *106*, 138–146.

Mattonai, M., Pawcenis, D., del Seppia, S., Łojewska, J., & Ribechini, E. (2018). Effect of ball-milling on crystallinity index, degree of polymerization and thermal stability of cellulose. *Bioresource Technology*, *270*, 270–277.

McKendry, P. (2002). Energy production from biomass (part 1): Overview of biomass. *Bioresource Technology*, *83*(1), 37–46.

Meier, H., & Vangedal, S. (1961). Isolation and Characterisation of an Acetylated Glucomannan from Pine (*Pinus silvestris L.*). *Acta Chemica Scandinavica*, *15*, 1381–1385.

Mejanelle, P., Bleton, J., Tchapla, A., & Goursaud, S. (2002). Chapter 24 Gas chromatography-mass spectrometric analysis of monosaccharides after methanolysis and trimethylsilylation. Potential for the characterization of substances of vegetal origin: Application to the study of museum objects. *Journal of Chromatography Library*, *66*(C), 845–902.

Mian, A. J., & Timell, T. E. (1960). Isolation and Properties of a Glucomannan From the Wood of Red Maple (*Acer Rubrum L.*) . *Canadian Journal of Chemistry*, *38*(9), 1511–1517.

Mikkelsen, D., Flanagan, B. M., Wilson, S. M., Bacic, A., & Gidley, M. J. (2015). Interactions of arabinoxylan and (1,3)(1,4)-β-glucan with cellulose networks. *Biomacromolecules*, *16*(4), 1232–1239.

Miyazaki, K. (1975). A new compound, 4-hydroxy-5,6-dihydro-2H-pyran-2-one, from xylan on heating. *Mokuzai Gakkaishi*, *21*,120–121.

Mohnen, D. (2008). Pectin structure and biosynthesis. *Current Opinion in Plant Biology*. *11*(3), 266-277.

Moon, R. J., Martini, A., Nairn, J., Simonsen, J., & Youngblood, J. (2011). Cellulose nanomaterials review: Structure, properties and nanocomposites. *Chemical Society Reviews*. *40*, 3941-3994.

Mukarakate, C., Mittal, A., Ciesielski, P. N., Budhi, S., Thompson, L., Iisa, K., Nimlos, M., R., & Donohoe, B. S. (2016). Influence of crystal allomorph and crystallinity on the products and behavior of cellulose during fast pyrolysis. *ACS Sustainable Chemistry and Engineering*, *4*(9), 4662–4674.

Müller-Hagedorn, M., Bockhorn, H., Krebs, L., & Müller, U. (2003). A comparative kinetic study on the pyrolysis of three different wood species. *Journal of Analytical and Applied Pyrolysis*, *68–69*, 231–249.

Nair, S. S., & Yan, N. (2015). Effect of high residual lignin on the thermal stability of nanofibrils and its enhanced mechanical performance in aqueous environments. *Cellulose*, *22*(5), 3137–3150.

Nakamura, T., Kawamoto, H., & Saka, S. (2008). Pyrolysis behavior of Japanese cedar wood lignin studied with various model dimers. *Journal of Analytical and Applied Pyrolysis*. *81*(2), 173-182.

Nieduszynski, I., & Marchessault, R. H. (1971). Structure of β-d-(1→4′) xylan hydrate. *Nature*, *11*, 1335–1344.

Nishiyama, Y. (2009). Structure and properties of the cellulose microfibril. *Journal of Wood Science*. *55*, 241-249.

Nomura, T., Kawamoto, H., & Saka, S. (2017). Pyrolysis of cellulose in aromatic solvents: Reactivity, product yield, and char morphology. *Journal of Analytical and Applied Pyrolysis*, *126*, 209-217.

Norgren, M., & Edlund, H. (2014). Lignin: recent advances and emerging applications. *Current Opinion in Colloid and Interface Science*. *19*(5), 409-416.

Obst, J. R., & Kirk, T. K. (1988). Isolation of lignin. *Methods in Enzymology*, *161*(C), 3–12.

O'Sullivan, A. C. (1997). Cellulose: the structure slowly unravels. *Cellulose*, *4*(3), 173–207.

Ohnishi, A., Kato, K., & Takagi, E. (1977). Pyrolytic formation of 3-hydroxy-2-penteno-1,5-lactone from xylan, xylo-oligosaccharides, and methyl xylopyranosides. *Carbohydrate Research*, *58*(2), 387–395.

Pandey, M. P., & Kim, C. S. (2011). Lignin depolymerization and conversion: a review of thermochemical methods. *Chemical Engineering and Technology*. *34*(1), 29-41.

Patwardhan, P. R., Brown, R. C., & Shanks, B. H. (2011). Product distribution from the fast pyrolysis of hemicellulose. *ChemSusChem*, *4*(5), 636–643.

Patwardhan, P. R., Dalluge, D. L., Shanks, B. H., & Brown, R. C. (2011). Distinguishing primary and secondary reactions of cellulose pyrolysis. *Bioresource Technology*, *102*(8), 5265–5269.

Patwardhan, P. R., Satrio, J. A., Brown, R. C., & Shanks, B. H. (2009). Product distribution from fast pyrolysis of glucose-based carbohydrates. *Journal of Analytical and Applied Pyrolysis*, *86*(2), 323–330.

Peng, Y., & Wu, S. (2010). The structural and thermal characteristics of wheat straw hemicellulose. *Journal of Analytical and Applied Pyrolysis*. *88*(2), 134-139.

Pereira, C. S., Silveira, R. L., Dupree, P., & Skaf, M. S. (2017). Effects of xylan side-chain substitutions on xylan-cellulose interactions and implications for thermal pretreatment of cellulosic biomass. *Biomacromolecules*, *18*(4), 1311–1321.

Pettersen, R. C. (1984). The chemical composition of wood. *The Chemistry of Solid wood*, 57–126.

Piras, C. C., Fernández-Prieto, S., & De Borggraeve, W. M. (2019). Ball milling: a green technology for the preparation and functionalisation of nanocellulose derivatives. *Nanoscale Advances*. *1*, 937-947.

Plomion, C., Leprovost, G., & Stokes, A. (2001). Wood formation in trees. *Plant Physiology*. *127*, 1513-1523.

Poletto, M. (2016). Thermal degradation and morphological aspects of four wood species used in lumber industry. *Revista Árvore, 40*(5), 941–948.

Poletto, M., Zattera, A. J., Forte, M. M. C., & Santana, R. M. C. (2012). Thermal decomposition of wood: Influence of wood components and cellulose crystallite size. *Bioresource Technology, 109*, 148–153.

Ponder, G. R., & Richards, G. N. (1991). Thermal synthesis and pyrolysis of a xylan. *Carbohydrate Research, 218*(C), 143–155.

Pouwels, A. D., Tom, A., Eijkel, G. B., & Boon, J. J. (1987). Characterisation of beech wood and its holocellulose and xylan fractions by pyrolysis-gas chromatography-mass spectrometry. *Journal of Analytical and Applied Pyrolysis, 11*, 417–436.

Puig-Arnavat, M., Bruno, J. C., & Coronas, A. (2010). Review and analysis of biomass gasification models. *Renewable and Sustainable Energy Reviews*. *14*(9), 2841-2851.

Rabemanolontsoa, H., & Saka, S. (2013). Comparative study on chemical composition of various biomass species. *RSC Advances, 3*(12), 3946–3956.

Radotić, K., Mićić, M., & Jeremić, M. (2005). New insights into the structural organization of the plant polymer lignin. In *Annals of the New York Academy of Sciences, 1048*, 215-229.

Räisänen, U., Pitkänen, I., Halttunen, H., & Hurtta, M. (2003). Formation of the main degradation compounds from arabinose, xylose, mannose and arabinitol during pyrolysis. *Journal of Thermal Analysis and Calorimetry, 72*(2), 481–488.

Ralph, J., & Hatfield, R. D. (1991). Pyrolysis-gc-ms characterization of forage materials. *Journal of Agricultural and Food Chemistry*, *39*(8), 1426–1437.

Reis, D., & Vian, B. (2004). Helicoidal pattern in secondary cell walls and possible role of xylans in their construction. *Comptes Rendus - Biologies*, *327*(9–10), 785–790.

Reis, D., Vian, B., & Roland, J. C. (1994). Cellulose-glucuronoxylans and plant cell wall structure. *Micron*, *25*(2), 171–187.

Ridley, B. L., O'Neill, M. A., & Mohnen, D. (2001). Pectins: structure, biosynthesis, and oligogalacturonide-related signaling. *Phytochemistry*, *57*, 929–967.

Rolando, C., Monties, B., & Lapierre, C. (1992). Thioacidolysis, In: Methods in lignin chemistry, Springer Series in Wood Science, pp. 335-349.

Ruiz, J. A., Juárez, M. C., Morales, M. P., Muñoz, P., & Mendívil, M. A. (2013). Biomass gasification for electricity generation: Review of current technology barriers. *Renewable and Sustainable Energy Reviews*. *18*, 174-183.

Saha, B. C. (2003). Hemicellulose bioconversion. In *Journal of Industrial Microbiology and Biotechnology*. *30*(5), 279-291.

Saka, S., & Mimori, R. (1994). The distribution of inorganic constituents in white birch wood as determined by SEM-EDXA. *Mokuzai Gakkaishi*, *40*, 88–94.

Salmén, L., & Burgert, I. (2009). Cell wall features with regard to mechanical performance. A review. COST Action E35 2004-2008: Wood machining - Micromechanics and fracture. *Holzforschung*, *63*(2), 121–129.

Sanchez-Silva, L., López-González, D., Villaseñor, J., Sánchez, P., & Valverde, J. L. (2012). Thermogravimetric-mass spectrometric analysis of lignocellulosic and marine biomass pyrolysis. *Bioresource Technology*, *109*, 163–172.

Scheller, H. V., & Ulvskov, P. (2010). Hemicelluloses. *Annual Review of Plant Biology*, *61*, 263–289.

Schill, S. R. (2013). IEA Task40: Biomass provides 10 percent of global energy use. *BIOMASS Magazine*, 18–21.

Schwanninger, M., Rodrigues, J. C., Pereira, H., & Hinterstoisser, B. (2004). Effects of short-time vibratory ball milling on the shape of FT-IR spectra of wood and cellulose. *Vibrational Spectroscopy*, *36*(1), 23–40.

Segal, L., Creely, J. J., Martin, A. E., & Conrad, C. M. (1959). An empirical method for estimating the degree of crystallinity of native cellulose using the X-Ray diffractometer. *Textile Research Journal*, *29*(10), 786–794.

Shafizadeh, F., McGinnis, G. D., & Philpot, C. W. (1972). Thermal degradation of xylan and related model compounds. *Carbohydrate Research*, *25*(1), 23–33.

Shen, D. K., & Gu, S. (2009). The mechanism for thermal decomposition of cellulose and its main products. *Bioresource Technology*, *100*(24), 6496–6504.

Shen, D. K., Gu, S., & Bridgwater, A. V. (2010a). Study on the pyrolytic behaviour of xylan-based hemicellulose using TG-FTIR and Py-GC-FTIR. *Journal of Analytical and Applied Pyrolysis*. *87*(2), 199-206.

Shen, D. K., Gu, S., & Bridgwater, A. V. (2010b). The thermal performance of the polysaccharides extracted from hardwood: Cellulose and hemicellulose. *Carbohydrate Polymers*, *82*(1), 39–45.

Shen, D. K., Gu, S., Luo, K. H., Wang, S. R., & Fang, M. X. (2010). The pyrolytic degradation of wood-derived lignin from pulping process. *Bioresource Technology*, *101*(15), 6136-6146.

Shimada, N., Kawamoto, H., & Saka, S. (2008). Different action of alkali/alkaline earth metal chlorides on cellulose pyrolysis. *Journal of Analytical and Applied Pyrolysis*, *81*(1), 80–87.

Šimkovic, I., Varhegyi, G., Antal, M. J., Ebringerová, A., Szekely, T., & Szabo, P. (1988). Thermogravimetric/mass spectrometric characterization of the thermal decomposition of (4-*O*-methyl-D-glucurono)-D-xylan. *Journal of Applied Polymer Science*, *36*(3), 721–728.

Simmons, T. J., Mortimer, J. C., Bernardinelli, O. D., Pöppler, A. C., Brown, S. P., DeAzevedo, E. R., Dupree, R., & Dupree, P. (2016). Folding of xylan onto cellulose fibrils in plant cell walls revealed by solid-state NMR. *Nature Communications*, *7*, 1–9.

Sims, I. M., Craik, D. J., & Bacic, A. (1997). Structural characterisation of galactoglucomannan secreted by suspension-cultured cells of Nicotiana plumbaginifolia. *Carbohydrate Research*, *303*(1), 79–92.

Sims, I. M., Munro, S. L. A., Currie, G., Craik, D., & Bacic, A. (1996). Structural characterisation of xyloglucan secreted by suspension-cultured cells of *Nicotiana plumbaginifolia*. *Carbohydrate Research*, *293*(2), 147–172.

Sipponen, M. H., Laakso, S., & Baumberger, S. (2014). Impact of ball milling on maize (*Zea mays L.*) stem structural components and on enzymatic hydrolysis of carbohydrates. *Industrial Crops and Products*, *61*, 130–136.

Siró, I., & Plackett, D. (2010). Microfibrillated cellulose and new nanocomposite materials: a review. *Cellulose*. *17*, 459-494.

Sjöström, E., Janson, T., Haglund, P., & Enström, B. (1965). The acidic groups in wood and pulp as measured by ion exchange. *Journal of Polymer Science Part C: Polymer Symposia*, *11*(1), 221–241.

Sundberg, A., Sundberg, K., Lillandt, C., & Holmbom, B. (1996). Determination of hemicelluloses and pectins in wood and pulp fibres by acid methanolysis and gas chromatography. *Nordic Pulp and Paper Research Journal*, *11*(4), 216-219.

Sun, Y., & Cheng, J. (2002). Hydrolysis of lignocellulosic materials for ethanol production: A review. *Bioresource Technology*, *83*(1), 1–11.

Takahashi, N., & Koshijima, T. (1988a). Ester linkages between lignin and glucuronoxylan in a lignin-carbohydrate complex from beech (*Fagus crenata*) wood. *Wood Science and Technology*, *22*(3), 231–241.

Takahashi, N., & Koshijima, T. (1988b). Molecular properties of lignin-carbohydrate complexes from beech (*Fagus crenata*) and pine (*Pinus densiflora*) woods. *Wood Science and Technology*, *22*(2), 177–189.

Tarasov, D., Leitch, M., & Fatehi, P. (2018). Lignin-carbohydrate complexes: properties, applications, analyses, and methods of extraction: a review. *Biotechnology for Biofuels*. BioMed Central. *11*, 269.

Terashima, N., Kitano, K., Kojima, M., Yoshida, M., Yamamoto, H., & Westermark, U. (2009). Nanostructural assembly of cellulose, hemicellulose, and lignin in the middle layer of secondary wall of ginkgo tracheid. *Journal of Wood Science*, *55*(6), 409–416.

Terrett, O. M., Lyczakowski, J. J., Yu, L., Iuga, D., Franks, W. T., Brown, S. P., Dupree, R., & Dupree, P. (2019). Molecular architecture of softwood revealed by solid-state NMR. *Nature Communications*, *10*, 4978.

Thakur, B. R., Singh, R. K., & Handa, A. K. (1997). Chemistry and uses of pectin - a review. *Critical Reviews in Food Science and Nutrition*, *37*(1), 47–73.

Thomas, H. (2015). Cellulose: structure and properties. In *Cellulose Chemistry and Properties: Fibers, Nanocelluloses and Advanced Materials in Polymer Science*, Springer, Cham, pp. 1-52.

Timell, T. E. (1961). Isolation of galactoglucomannans from the wood of gymnosperms. *Tappi*, *44*, 88–96.

Timell, T. E. (1967). Recent progress in the chemistry of wood hemicelluloses. *Wood Science and Technology*, *1*(1), 45–70.

Tsuchiya, Y., & Sumi, K. (1970). Thermal decomposition products of cellulose. *Journal of Applied Polymer Science*, *14*(8), 2003–2013.

Tyminski, A., & Timell, T. E. (1960). The Constitution of a Glucomannan from White Spruce (*Picea glauca*). *Journal of the American Chemical Society*, *82*(11), 2823–2827.

United Nations Development Programme. (2000). *World Energy Assessment. Energy and the challenge of Sustainability*. *World Energy Assessment*.

Vamvuka, D. (2011). Bio-oil, solid and gaseous biofuels from biomass pyrolysis processes-an overview. *International Journal of Energy Research*. *35*, 835-862.

Varhegyi, G., Antal, M. J., Szekely, T., Till, F., Jakab, E., & Varhegyi, G. (1988). Simultaneous thermogravimetric-mass spectrometric studies of the thermal decomposition of biopolymers. *Energy and Fuels*, *2*(3), 267–272.

Vian, B., Roland, J.-C., Reis, D., & Mosiniak, M. (2014). Distribution and possible morphogenetic role of the xylans within the secondary vessel wall of linden wood. *IAWA Journal*, *13*(3), 269–282.

Voragen, A. G. J., Coenen, G. J., Verhoef, R. P., & Schols, H. A. (2009). Pectin, a versatile polysaccharide present in plant cell walls. *Structural Chemistry*, *20*(2), 263–275.

Wang, J., Asmadi, M., & Kawamoto, H. (2018). The effect of uronic acid moieties on xylan pyrolysis. *Journal of Analytical and Applied Pyrolysis*, 136, 215–221.

Wang, J., Minami, E., & Kawamoto, H. (2020). Thermal reactivity of hemicellulose and cellulose in cedar and beech wood cell walls. *Journal of Wood Science*, *66*, 41.

Wang, J., Asmadi, M., Minami, E., & Kawamoto, H. (2021). Location of uronic acid group in Japanese cedar and Japanese beech wood cell walls as evaluated by the influences of minerals on thermal reactivity. *Journal of Wood Science*, *67*, 3.

Wang, J., Asmadi, M., Minami, E., & Kawamoto, H. (2021). Effect of delignification on thermal degradation reactivities of hemicellulose and cellulose in wood cell walls. *Journal of Wood Science*, 67, 19.

Wang, S., Liang, T., Ru, B., & Guo, X. juan. (2013). Mechanism of xylan pyrolysis by Py-GC/MS. *Chemical Research in Chinese Universities*, *29*(4), 782–787.

Wang, S., Dai, G., Yang, H., & Luo, Z. (2017). Lignocellulosic biomass pyrolysis mechanism: a state-of-the-art review. *Progress in Energy and Combustion Science*, *62*, 33–86.

Wang, S., Guo, X., Liang, T., Zhou, Y., & Luo, Z. (2012). Mechanism research on cellulose pyrolysis by Py-GC/MS and subsequent density functional theory studies. *Bioresource Technology*, *104*, 722–728.

Wang, S., Ru, B., Lin, H., & Luo, Z. (2013). Degradation mechanism of monosaccharides and xylan under pyrolytic conditions with theoretic modeling on the energy profiles. *Bioresource Technology*, *143*, 378–383.

Wang, S., Ru, B., Lin, H., & Sun, W. (2015). Pyrolysis behaviors of four *O*-acetyl-preserved hemicelluloses isolated from hardwoods and softwoods. *Fuel*, *150*, 243–251.

Wang, S., Wang, K., Liu, Q., Gu, Y., Luo, Z., Cen, K., & Fransson, T. (2009). Comparison of the pyrolysis behavior of lignins from different tree species. *Biotechnology Advances*. *27*(5), 562-567.

Wang, Z., Cao, J., & Wang, J. (2009). Pyrolytic characteristics of pine wood in a slowly heating and gas sweeping fixed-bed reactor. *Journal of Analytical and Applied Pyrolysis*. *84*(2), 179-184.

Werner, K., Pommer, L., & Broström, M. (2014). Thermal decomposition of hemicelluloses. *Journal of Analytical and Applied Pyrolysis*, *110*(1), 130–137.

Wise, L. E., Murphy, M., & D'Addieco, A. A. (1946). Chlorite holocellulose, its fractionation and bearing on summative wood analysis and on studies on the hemicelluloses. *Paper trade Journal*, *122*, 35-43.

Worasuwannarak, N., Sonobe, T., & Tanthapanichakoon, W. (2007). Pyrolysis behaviors of rice straw, rice husk, and corncob by TG-MS technique. *Journal of Analytical and Applied Pyrolysis*. *78*(2), 265-271.

Yang, H., Yan, R., Chen, H., Lee, D. H., & Zheng, C. (2007). Characteristics of hemicellulose, cellulose and lignin pyrolysis. *Fuel*, *86*(12–13), 1781–1788.

Yang, H., Yan, R., Chen, H., Zheng, C., Lee, D. H., & Liang, D. T. (2006). In-depth investigation of biomass pyrolysis based on three major components: hemicellulose, cellulose and lignin. *Energy and Fuels*. *20*(1), 388-393.

Huang Y., Indrarti, L., Azuma, J. I, & Okamura, K. (1992). Simultaneous determination of xylose and uronic acid in beech xylan by methanolysis. *Mokuzai Gakkaishi*, *38*, 1167–1171.

Yuan, T. Q., Sun, S. N., Xu, F., & Sun, R. C. (2011). Characterization of lignin structures and lignin-carbohydrate complex (LCC) linkages by quantitative 13C and 2D HSQC NMR spectroscopy. *Journal of Agricultural and Food Chemistry*, *59*(19), 10604–10614.

Zhang, J, Choi, Y. S., Yoo, C. G., Kim, T. H., Brown, R. C., & Shanks, B. H. (2015). Cellulose-hemicellulose and cellulose-lignin interactions during fast pyrolysis. *ACS Sustainable Chemistry and Engineering*, *3*(2), 293–301.

Zhang, J, Chen, T., Wu, J., & Wu, J. (2014). A novel Gaussian-DAEM-reaction model for the pyrolysis of cellulose, hemicellulose and lignin. *RSC Advances*, *4*(34), 17513–17520.

Zhou, H., Long, Y., Meng, A., Chen, S., Li, Q., & Zhang, Y. (2015). A novel method for kinetics analysis of pyrolysis of hemicellulose, cellulose, and lignin in TGA and macro-TGA. *RSC Advances*, *5*(34), 26509–26516.

Zhou, X., Li, W., Mabon, R., & Broadbelt, L. J. (2017). A critical review on hemicellulose pyrolysis. *Energy Technology*, *5*(1), 52–79.

Zhou, X., Li, W., Mabon, R., & Broadbelt, L. J. (2018). A mechanistic model of fast pyrolysis of hemicellulose. *Energy and Environmental Science*, *11*(5), 1240–1260.

Zickler, G. A., Wagermaier, W., Funari, S. S., Burghammer, M., & Paris, O. (2007). In situ X-ray diffraction investigation of thermal decomposition of wood cellulose. *Journal of Analytical and Applied Pyrolysis*, *80*(1), 134–140.

ACKNOWLEDGEMENT

The author would like to express his sincerest gratitude to Professor Haruo Kawamoto, Department of Socio-Environment Energy Science, Graduate School of Energy Science, Kyoto University, for his suggestion and continuous direction for this research. His patient guidance towards students and serious attitude towards research deeply influences the author not only in research but in the life.

The author is very grateful to Assistant Professor Eiji Minami for his helpful comments and discussion, especially on the way to express accurate information simply and beautifully through graphs and tables.

The author is deeply grateful to Professor Takayuki Kameda, Department of Socio-Environment Energy Science, Graduate School of Energy Science, Kyoto University and Professor Junji Sugiyama, Division of Forest and Biomaterial Science, Graduate School of Agriculture, Kyoto University, for the valuable suggestion and critical reading of this manuscript.

This research was made possible by the cooperation and assistance of the members in the Laboratory for Energy Ecosystems, Kyoto University.

The author is grateful to Dr. Asmadi, Department of Chemical Engineering, Universiti Teknologi Malaysia, for preparation of the samples and helpful suggestion of the research and teach the author a lot about the experiment.

The author is grateful Ms. Rie Nakanishi, secretary of Laboratory of Energy Ecosystem, Kyoto University, for her kind help and support to the daily life in the laboratory.

Finally, the author would like to express his sincere thanks to his parents and beloved wife for the support and encouragement.

LIST OF PUBLICATIONS

Original papers

1. Wang, J, Asmadi M, and Kawamoto H. 2018. The effect of uronic acid moieties on xylan pyrolysis. *Journal of Analytical and Applied Pyrolysis* 136: 215–21. (Chapter 2)

2. Wang, J, Minami E, and Kawamoto H. 2020. Thermal reactivity of hemicellulose and cellulose in cedar and beech wood cell walls. *Journal of Wood Science* 66: 41. (Chapter 3)

3. Wang, J, Minami E, and Kawamoto H. 2021. Location of uronic acid group in Japanese cedar and Japanese beech wood cell walls as evaluated by the influences of minerals on thermal reactivity. *Journal of wood Science* 67: 3. (Chapter 4)

4. Wang, J, Minami E, Asmadi M, Kawamoto H. 2021. Effect of delignification on thermal degradation reactivities of hemicellulose in wood cell walls. *Journal of wood Science* 67: 19. (Chapter 5)

5. Wang, J, Minami E, Asmadi M, Kawamoto H. 2021 Thermal degradation reactivity of hemicellulose and cellulose in ball-milled cedar and beech wood. *Journal of wood Science* 67: 32. (Chapter 6)

International Conferences

1. Wang J.W. Asmadi M., Kawamoto H. 2018 Influence of metal cation on pyrolysis of beech wood xylan. Poster, the 22nd International symposium on analytical and applied pyrolysis. Jun, 3-8 (5), 2018. Kyoto, Japan. P4-22A.

2. Wang J, Asmadi M, Minami, E, Kawamoto H. 2019 Influence of wood cell wall ultrastructure on thermal reactivities of polysaccharides. Poster, the 20th

International symposium on wood, fiber and pulping chemistry. Sep. 9-11 (11), 2019. Tokyo, Japan. P-73.

Domestic Conferences

1. Wang J, Asmadi M, Kawamoto H. 2018 Influence of metal cation on pyrolysis of beech wood xylan. Oral, the 68th Annual Meeting of the Japan Wood Research Society, Mar. 14-16 (14), 2018, Kyoto, Japan. P14-08-1315.

2. Wang J, Asmadi M, Kawamoto H. 2018 Role of uronic acid moiety in xylan pyrolysis in wood, Oral, 2018 Celllulose R&D, the 25th Annual Meeting of the Cellulose Society of Japan, June 5-6 (5), 2018, Uji, Japan. K03, pp. 7-8.

3. Wang J, Asmadi M, Kawamoto H. 2018 Effect of uronic acid moiety in xylan pyrolysis, Oral, the 27th Annual Meeting of the Energy Society of Japan, Aug 8-9 (9), 2018, Tokyo, Japan. 3-5-2, pp. 108-109.

4. Wang J, Asmadi M, Kawamoto H. 2018 Thermal reactivities of xylan and other polysaccharides in beech wood. Oral, the 69th Annual Meeting of the Japan Wood Research Society, Mar. 14-16 (14), 2019, Hakotate, Japan. P14-06-1315.

5. Wang J, Minami Eiji, Asmadi M, Kawamoto H. 2019 Thermal reactivities of polysaccharides in beech and cedar wood cell wall, Poster, the 26th Annual Meeting of the Cellulose Society of Japan, July 11-12 (11), 2019, Fukuoka, Japan. P035, pp. 90-91.

6. Wang J, Asmadi M, Minami E, Kawamoto H. 2019 Thermal reactivities of hemicellulose and cellulose in beech and cedar wood cell wall, Poster, the 28th Annual Meeting of the Energy Society of Japan, Aug 8-9 (9), 2019, Suita, Japan. 3-4-4, pp. 94-94.

7. Wang J, Asmadi M, Minami E, Kawamoto H. 2020 Influences of delignification and ball milling on thermal reactivity of hemicellulose and cellulose. Oral, the 70th Annual Meeting of the Japan Wood Research Society, Mar. 16-18 (16), 2020, Tottori, Japan. P16-02-1515